The role of downslope versus alongslope sediment transport over the last glacial

cycle on the Scotian Rise

By
Jeremy Bentley

A Thesis Submitted to
Saint Mary's University, Halifax Nova Scotia
In Partial Fulfilment of the Requirements for a
Bachelor of Science Honours Degree in Geology

April 2016, Halifax, Nova Scotia

| Approved: | Dr. David Piper |
| | External supervisor |

| Approved: | Dr. Georgia Pe-Piper |
| | Internal supervisor |

| Approved: | Dr. Calvin Campbell |
| | External reader |

Date: April 4th, 2016

Certification

I certify that this thesis was submitted by Jeremy Bentley in fulfilment of the honours degree requirement for the Bachelors of Science Honours degree in Geology at Saint Mary's University, Halifax, Nova Scotia. This thesis truly represents the original work carried out by Mr. Bentley under our supervision

Dr. Georgia Pe-Piper

Professor of Geology

Saint Mary's University

Dr. David Piper

Research Scientist

Geological Survey of Canada

The role of downslope versus alongslope sediment transport over the last glacial cycle on the Scotian Rise

By Jeremy N. Bentley

Abstract

Little work has been done on the Scotian Rise to identify the mode of sediment transportation. Specifically, identifying to what extent the Western Boundary Undercurrent (WBUC) influences the Scotian Rise and how previous ice advances and retreats may have played a role in this sediment transport.

The physical properties of two piston cores located on the Central Scotian Rise south of Western Bank were analysed to identify the sources of six recognized sediment units. The overall framework for age was established by C-14 dating and the recognition of Heinrich events (H-events). The age model corresponding to the units could then be linked to stadial and interstadial times via marine isotopic stages (MIS). The sources of sediments were mostly from glacial supply from the Appalachians and erosion of the Scotian Shelf, as indicated by numerous physical properties, such as clay mineralogy, Nd isotopes, pXRF and spectrophotometry data.

The sources and the corresponding ages of the units developed in this study indicate the Scotian Rise typically experienced downslope transport during stadial periods (units II, III, V, VI), and alongslope transport during interstadials in unit I (MIS I) and IV (early MIS 3). The data confirm that a major glacial advance (Caledonia phase) took place in Nova Scotia in MIS 4, reaching the edge of the shelf.

Preface

This study involved many different methods completed by different people to investigate the question proposed. The majority of the data collected was done so by the staff at the core lab and sediment lab at the Geological Survey of Canada Atlantic Division (GSCA) at the Bedford Institute of Oceanography (BIO) (Owen Brown and Jenna Higgins). These methods used in the core lab included: X-Radiography, portable X-Ray Fluorescence (pXRF) and multisensor core logging (magnetic susceptibility, P-wave velocity, and bulk density along with spectrophotometry.) The methods used in the sediment lab, with the additional help from myself, were the preparation of < 2 μm separates for X-ray diffraction (XRD) and grain size analysis. The analysis of the clay mineralogy via XRD was done by Lori Campbell at BIO. Gravel counts were done by Heidi McKee in 2006, during her time as a co-op student at the GSCA. O-isotope data was obtained from Dr. H. Rashid, while Sm/Nd isotope data was obtained from a third party consulting firm (GeoSpec Consultants Ltd.).

Acknowledgements

Table of Contents

List of Figures

List of Tables

1. Introduction

The Western Boundary Undercurrent (WBUC) is a deep southerly flowing bottom current associated with the thermohaline circulation (THC) in the North Atlantic Ocean. The WBUC travels along the foot of the Scotian Slope; this region is known as the Scotian Rise and the current is strongest below 4000 m (Tuckolke et al., 1985). The WBUC is the main contributor to the lower branch of the THC in the Atlantic, while its more northern equivalent, the East Greenland current is responsible for global redistribution of heat and fresh water (Mueller-Michaelis, and Uenzelmann-Neben, 2013). The relative current strength coincides with climate change. This potential influx in current strength could play a role in the sediment transportation along the Scotian Rise. By using numerous methods this thesis will attempt to trace sediment provenance to understand the extent that the Scotian Rise is influenced by the WBUC over the last glacial cycle and last glacial maximum (LGM).

2. Geological Setting and Previous work

2.1. Geological history of the Scotian Margin

Rifting and sea-floor spreading of the eastern Canadian margin has occurred in three phases (Louden et al. 2004). The first phase was Triassic rifting and Early Jurassic sea-floor spreading off Nova Scotia. This was followed by sea-floor spreading off the eastern Grand Banks in the Early Cretaceous, followed by spreading in the Labrador Sea and Baffin Bay in the Paleogene. Thick Mesozoic – Cenozoic sediments accumulated on the margin of the Scotian Basin.

The continental shelf of eastern Canada has been glaciated numerous times from the Mid to Late Pleistocene, and these prior glaciations have resulted in various morphologies consisting of banks and intervening transverse troughs (Piper, 1988). These previous glaciations delivered large amounts of sediments to the continental slope and rise (Piper, 2005). Although there is evidence for neotectonic activity in the Quaternary, mainly on the eastern Scotian and the southwestern Grand Banks margin, there is also a large amount of salt tectonic deformation (Shimeld, 2004), which locally offsets Quaternary strata (Piper & Gould, 2004).

2.2 Bathymetry

There have been numerous studies on the Scotian Slope and Rise, but for this section the details will be based on Emery and Uchupi (1984), as it provides a relatively basic and general background of the regional setting to understand the context of this study. The concept of a continental rise was introduced by Heezen et al. (1959) and the distinction between the slope and rise was based on the angle of the slope. The slope typically has an angle of 1.4 degrees, while the rise is typically 0.08 degrees. In general the slope is irregular in bathymetry caused by and slumping and also by salt and mud diapirs, which happen when low density salt or mud starts to thrust upwards through higher density overlying sediment.

The slope also has numerous submarine canyons. The turbidity current hypothesis for the origin of canyons was proposed by Daly (1936). This hypothesis states that canyons all trend downslope or diagonally downslope and can transport masses of sediment-laden water that can flow at high velocities through the canyon, beyond the adjacent continental rise onto the abyssal plain. At the transition from continental slope to continental rise there is often a transition from canyon into deep sea channel due to the diminished gradient. It is also significant to note that the

locations of these canyons are highly influenced by the former extent of ice sheets. Regions that have wider continental shelves have typically experienced farther ice extents during times of glaciation. The ramification of this is that canyons also appear farther offshore.

Mass movement occurs on the slope in a few different ways. The first being slumping of sediments in which a section of sediment slowly creeps downslope, but does not fully dislodge, thus moving a short distance. In contrast, being transported over a larger distance is considered a slide or mass transport deposit (MTD). Sometimes slides can remain as a unit or mound downslope, while the upslope is left with a cavity and often scouring. This is not always the case. Often the downslope portion of this event dissipates into a thin mud flow or turbidity flow; in this case there is only a cavity upslope that is recognizable.

The surface of the Scotian Rise is a relatively smooth region, which has a width range up to 240 km but is on average 110 km. The top of the rise, where it meets the slope, is between 2000 - 3000 m deep and at the bottom of the rise, adjacent to abyssal plains or abyssal apron, is approximately between 3500 - 6000 m deep. This region often contains bathymetric details which may be deemed significant. The transition from continental slope to rise is marked by the mouth of submarine canyons where deep sea channels start to develop. Slumping structures are also present, but are often restricted to debris piles at the base of the slope or on small slides at the edge of deep ocean channels. These slumping structures on the rise are much smaller and not as common as once believed (Emery & Uchupi, 1984). Another notable structure are sediment drifts, which are exceptionally large masses of sediments that appear to have been deposited by swift moving bottom currents such as the WBUC. Essentially, the morphology of the continental rise is due to turbidity and bottom currents, not specifically gravitational tectonics (Uchupi et al., 1977, Uchupi & Austin, 1979).

2.3. Oceanic circulation

The general water circulation of the study area is complex, but as described by Smith et al. (2014), the study region is under the influence of two main surface currents, the Gulf Stream and the Labrador Current. The Labrador Current is a colder, denser water than its warmer saltier counterpart of the Gulf Stream. Oxygen isotopes of the shelf water as far south as the Middle Atlantic Bight, show that one of the main components of the Labrador Current is glacial melt water and river runoff, which come from the Hudson Strait and the Baffin Bay, driving the current based on the buoyancy of the fresh water. The Labrador Current (Fig. 1) is subdivided into an offshore and an inshore current. The inshore current hugs the coast, eventually branching off near the eastern tip of Labrador. A portion of this current begins cutting towards the south west through the Strait of Belle Isle and the other circling Newfoundland clockwise and branching off in various directions such as towards the Flemish Pass, eventually meeting back up with the portion of the current traveling south west. This south west trending current eventually feeds into Cabot Strait outflow and the Gulf of St. Lawrence. This mixes and ends up in the Nova Scotia current in addition to the outer current that cuts around the Grand Banks margin.

The area is also affected by a north to south deep under current referred to as the Western boundary undercurrent (WBUC). This undercurrent is the dominant lateral transporting agent carrying a suspended load along the North Atlantic Bottom (Eittreim & Ewing, 1972). The water that feeds the WBUC is derived from sources in the Labrador, Norwegian and Mediterranean seas. There have been studies done to quantify the strength of this current. Its velocity is variable but it is characteristically flowing southwestwardly at 10 to 20 cm/sec with some speeds reaching upwards of 30 cm/sec (Tuckolke et al., 1985).

Annually the water influx is dictated by seasons; with the warmer months providing more

4

melt water from the winter snow and ice. In comparison, this annual fluctuation can be similar to glacial (stadial) and interglacial (interstadial) periods. Both the Labrador Current and bottom water circulation were the strongest were during interglacial periods (Hillaire Marcel et al., 1994). This change in circulation strength may play a role in the transportation of sediments.
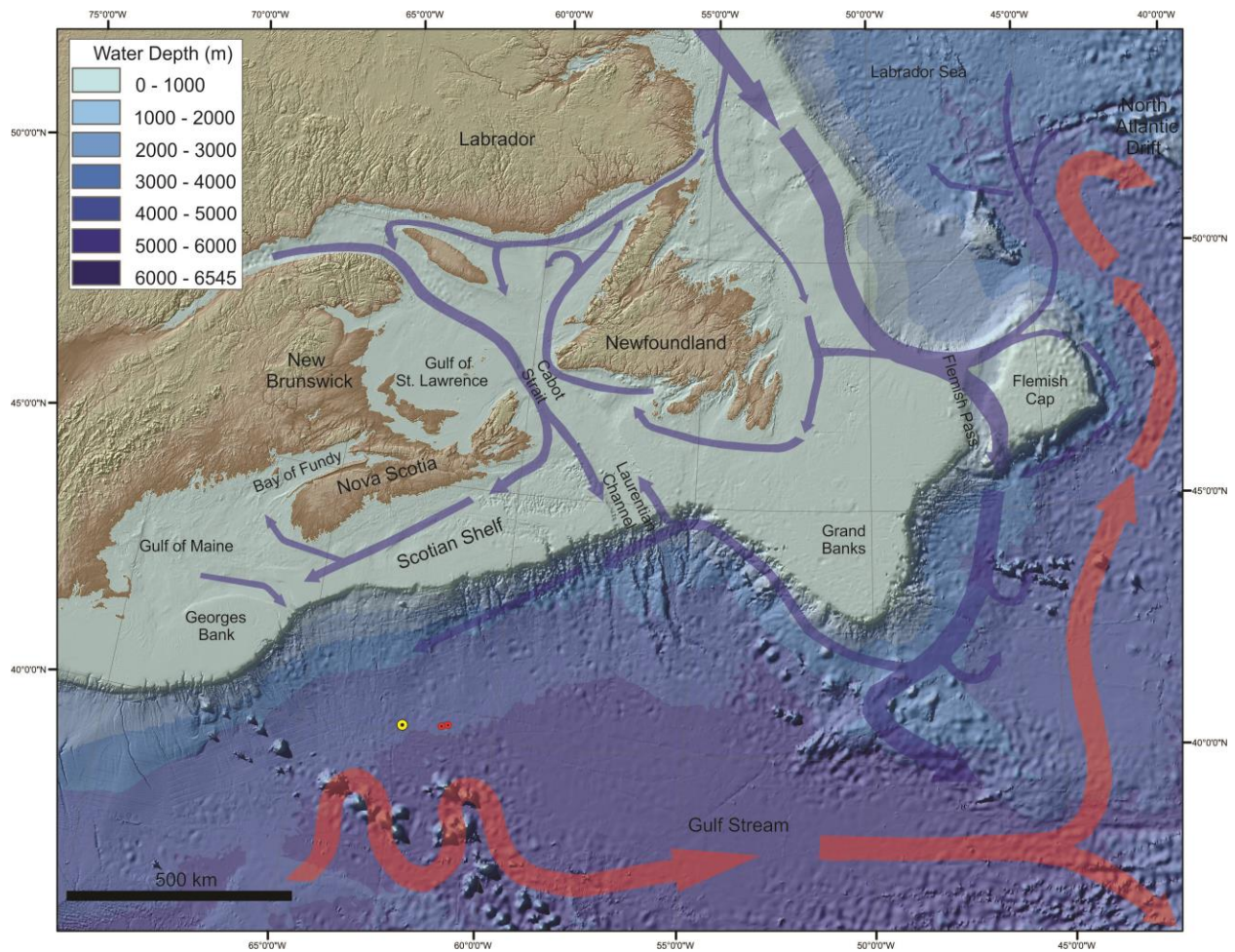
Fig. 1 – Map of the north Atlantic with ocean currents (ocean currents after Smith et al. 2014). Blue being cooler currents and red being warmer currents. Small red dots between Scotian Shelf and Gulf Stream are core locations, while yellow is the HEBBLE site.

2.4. HEBBLE

The High Energy Benthic Boundary Layer Experiment (HEBBLE) (Nowell & Hollister, 1985) was a seabed experiment on the Scotian Rise to quantify the magnitude of deep-ocean currents and their impact on sedimentation. The site chosen for the study was one with low slope, and lack of bedding, which showed evidence for recent erosion or deposition. It was located at 4820 m on the Scotian Rise (40°27'N, 62°20'W) in the path of the WBUC (Fig. 1). The main HEBBLE occurred in 1985 and 1986. It measured seafloor currents and sediment transportation and was used to predict sediment entrainment and flux rates of imposed fluid shear stress. This experiment revealed that there are occasional abyssal storms that transport silt and clay along rise. It has been suggested that these abyssal storms are due to Gulf Stream rings as they passed over the study area that even led to flow reversals.

2.5. Distinction of contourites from turbidites

Contourites and turbidites may be extremely similar in terms of their sedimentary structures (Rebesco et al., 2014) but they do have one subtle difference: their orientation. Turbidites are downslope features, while contourites are alongslope features. This distinction is especially difficult in sediment cores as the original sediment orientation is not preserved. One potential way to sort out the confusion around this issue is to find the source of sediments. This can indicate the direction in which these sediments were moving. Another potentially helpful means of understanding this discrepancy is seafloor mapping in the form of multibeam bathymetry and seismic profiles. Both of these may exhibit structures which can then be extrapolated to the cores that have been taken. Davies & Laughton (1972) characterized the distinction between contourites and turbidites in echograms and seismic profiles. Turbidites

show high reflectivity with sea-bed multiples and strong stratification, while contourites are relatively transparent with hyperbolic or prolonged patchy echos indicative of a wavy upper surface.

2.6. Glacial history of the Scotian Shelf and upper slope

In the past glacial ice has completely crossed most of the eastern Canadian continental shelf, during the last glacial maximum (Shaw et al., 2006), and during marine isotope stage (MIS) 6 (~130 ka) and deposited till on the Scotian Shelf and till tongues on the upper slope. The till tongues form a series of interfingered, wedge shaped, massive incoherent seismic units (Mosher et al., 1989, 1991).

The last major glacial cycle has been described as four particular phases in which ice was present on Nova Scotia and in most cases extended to the Scotian Shelf (Stea et al., 1998). The Caledonia phase (75 - 41 ka) was a time of ice sheet advance from the Appalachian Ice Sheet and the Laurentide Ice Sheet in a south east direction. This phase is suggested to have experienced a retreat during the Mid-Wisconsinan, as radiometric dating of a mollusk shell revealed that during this time the outer regions of the Gulf of Maine were free of ice (Stea et al., 1998). The Late Wisconsinan ice flow (MIS Late 3 -2), or phase two, is known as the Escuminac Phase (26 - 21 ka) or simply the last glacial maximum (LGM). This Late Wisconsinan glaciation transported large quantities of local red-bed material south onto the shelf and slope (Stea et al., 1998). This was not recognized until this ice began to retreat and divide, which marks the start of the Scotian Phase (21-18 ka), a period of glacial retreat. Between 16 and 14 ka there was a reestablishment of the ice margin from terrestrial ice in the more northern parts of Nova Scotia into the Bay of Fundy and just beyond the modern day Atlantic coast. This phase is called the Chignecto Phase

(Stea et al., 1998).

An important topic to consider is the presence of till tongues at ~130, ~75, ~28, ~23, ~18 ka, as described in Mosher et al., (2004), between Mohican Channel and Verrill Canyon. This is important because the study area lies just south of this section.

2.7. Previous work on the Scotian Rise

Previous work on the Scotian Rise has been limited. As previously discussed, HEBBLE took place during the mid-1980's and investigated sea floor currents and sediment transportation on the seafloor. One of the first studies that were conducted was by Zimmerman (1972), who investigated sediments of the New England continental rise (south west of this study area). Specifically, clay minerals were examined to find potential origin, which would indicate the transportation method. Zimmerman (1972) found that the continental margin is affected by downslope processes but can be reworked by alongslope bottom currents. Similar principles will be applied in this study.

Another study was by Shor et al., (1984) which used anisotropy of magnetic susceptibility (AMS) to identify current-deposited sediments. This method targeted preferential alignments or fabrics of magnetic grains in a clay matrix. The orientations of these magnetic fabrics could be used to quantify a vector of sediment transportation. Shor et al. (1984) identified only their Holocene sediments as retaining a magnetic fabric which corresponded to alongslope, while the rest of the fabrics found in their sediments we related to downslope. Minimal work has been done to link paleoclimate to the direction of sediment transportation on the Scotian Rise.

2.8. Tracing sediment sources using petrology

The two principal orientations of sediment transportation are downslope and alongslope, and the magnitude of these directions will be discussed in this paper. To identify which vector is dominant in a specific stratigraphic unit within the two studied piston cores, the most intuitive method is tracing sediment sources using petrology. The two main criteria used to investigate the sourcing are gravel fraction and clay mineralogy. The provenance of the ice rafted detritus (IRD) gravel fraction can be identified according to its lithology and compared to rock lithologies in the surrounding region, potentially indicating its origin. The initial petrographic investigation can then be coupled with Sm/Nd isotope ratios which will then confirm or deny the probability of the source, based on relative age as outlined in Farmer et al. (2003).

The other method as briefly described was clay mineralogy. The variation in clay minerals may provide some insight to the orientation of sediment transportation. As stated in Fagel et al. (1996), the abundance of smectites along the margins of Labrador Sea provides strong evidence for a link to the WBUC as the transportation method. This increase in smectites may also be linkable to this study area, which may indicate that the source of smectites from adjacent continents is unlikely.

2.9. Sortable silt as a proxy for current strength

Fine grained sediments, particular below 10 μm, are dominantly cohesive in nature. This is suggested by the dynamics of sediment erosion, deposition and aggregate break up (McCave et al., 1995). Sediments greater than 10 μm respond to hydrodynamic processes and allow size sorting. The sortable silt is the 10-63 μm fraction and can be used to infer relative current strength (McCave et al., 1995). Thus higher sortable silt and fine grained sand may suggest

greater current velocity (Marshall et al., 2014).

3. Materials and Methods

3.1. Location of study area

This study area is based on two piston cores that were collected in 1999. The two piston cores as depicted in the bathymetric map (Fig. 2) are located on the Central Scotian Rise south of Western Bank. Piston core 99036-0035 is located at 40.217968N and 61.365445W at a water depth of 4792 meters. Piston core 99036-0037 is located at 40.154572N and 61.117798W at a water depth of 4791 meters. These two cores are located on an apparently featureless area on the Scotian Rise.

Several canyons and valleys cut the continental slope upslope from the piston cores. These include Mohican Channel, the small Acadia Valley, Verrill Canyon and Dawson Canyon. None of these valleys can be traced with confidence to the Scotian Rise, but any of them may have played a role in transporting sediment to the Rise near the core sites.
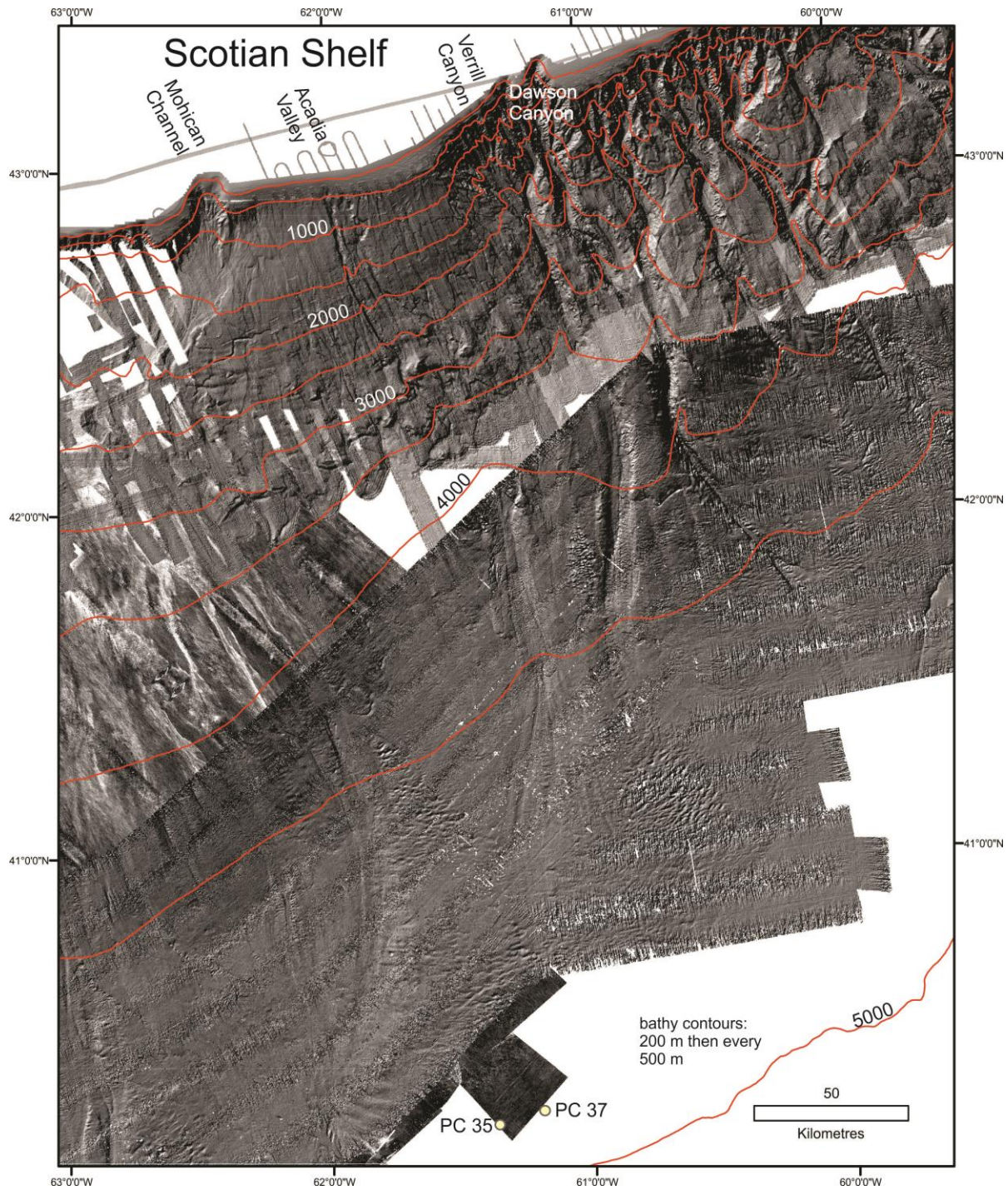
Fig. 2 – Location of studied cores (PC 035 and PC 037) on a map of backscatter from multibeam bathymetry surveys of the central Scotian Slope and Rise. Selected bathymetric contours and major physiographic features are also shown. (Base map provided by Dr. Calvin Campbell.)

3.2. Seismic profile from the study area

As described in the 99036 cruise report, NRCan's DeepTow Seismic (DTS) system, originally manufactured by Huntec Limited, was used to record high resolution sub-bottom profiles. The seismic profiles show good penetration to 75 ms (55 m) subbottom. Several reflections (numbered 1–5 in Fig. 3) can be traced from one core site to the other. Most intervals between these reflections thin eastward. These intervals show subparallel continuous reflections. Reflection 4 overlies an interval with hummocky and incoherent reflections, characteristic of either a channelled horizon or of mass-transport deposits (debris flows). There also appears to be a poorly imaged interval of similar character beneath reflection 7. Core 35 intersects reflector 1 at about 0.6 metres subbottom, whereas at core site 37 the same reflection cannot be resolved with certainty, but is no more than 0.55 metres subbottom.
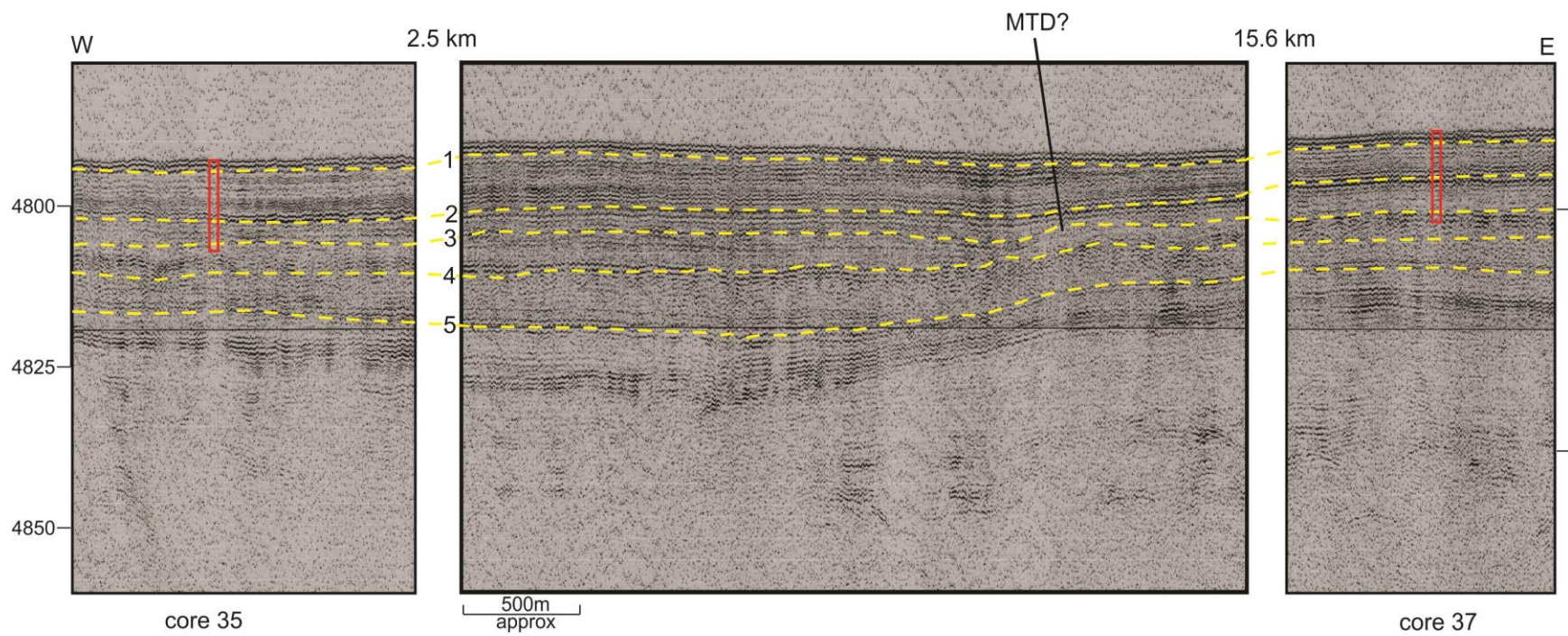
Fig. 3 – Huntec profile showing traced reflectors correlation of seismic stratigraphy between the two core sites. Please note that cores are not to scale horizontally. The central seismic profile shows a potential mass transport deposit (MTD). 1-5 are reflections described in text.

13

3.3 Collection of cores

3.3.1 Piston core & Trigger weight core

Piston coring is a method in retrieving a sample of marine sediments in which the succession of sediments is preserved. This system is comprised of a large core head on the piston corer to provide weight for penetration power. Attached to this head are 4 or 5 steel barrels (99.2 mm in diameter), each 10 ft (3m) long. A transparent plastic core liner is inserted into the steel barrels to aid in the collection and transportation. A tightly fitting piston is then placed in the liner just above the core catcher. The core catcher fits inside the liner with metal fingers pointing upward. This allows for sediment to pass through but not fall back out (Bouma, 1969). At the end of the barrel there is a core cutter or nosepiece which is a tapered edge to help facilitate penetration.

The trigger weight corer is a similar set up, but it is much shorter, only a 1.5 m barrel with the same diameter. The trigger weight corer differs in that there is no piston that moves up through the core liner. Instead there is a plunger at the top of the barrel by the core head that allows water to flow out as it penetrates the sediments, but closes and provides pressure when retrieving, to keep the sediments in the barrel. This trigger weight corer is attached to the trigger arm. As it is lowered to the seafloor the trigger weight core hits the bottom, this releases the piston core, which allows freefall, for greater momentum and deeper penetration. From this point, the whole system is retrieved from the seafloor and disassembled. Cores are generally cut on deck into more manageable 1.5 m lengths (Bennett et al., 2008).

14

3.4. Core Analysis

3.4.1 Multisensor Core Logging (MSCL)

Cores that are collected at sea are brought back to the core lab at the Geological Survey of Canada Atlantic Division at the Bedford Institute of Oceanography, where they are analysed by the Geotek multisensor core logger. The measured physical properties are: magnetic susceptibility, P-Wave velocity, bulk density and colour. These physical properties are used to understand the history of the sediments and often used to correlate to other cores in the region to get a regional perspective of the sedimentological environment.

3.4.1.1. Magnetic Susceptibility

Magnetic susceptibility is the degree of magnetization of a material in response to an applied magnetic field. A positive magnetic susceptibility indicates the presence of a mineral that is paramagnetic, ferrimagnetic, ferromagnetic or antiferromagnetic. Such minerals will strengthen the magnetic field and a positive reading will be recorded. In contrast if the magnetic susceptibility reading is negative, diamagnetic minerals predominate and weaken the magnetic field. The operating principle for the Geotek is that an oscillator circuit in the sensor produces a low intensity, non-saturated, alternating magnetic field at 2 kHz. Any material that passes through the vicinity of the sensor will interrupt and change the oscillator frequency, the electronics convert the pulsed frequency into magnetic susceptibility.

3.4.1.2. P-Wave Velocity

P-waves, or primary waves, are compressional or longitudinal waves. By measuring this parameter we are able to potentially link contrasting layers with higher or lower acoustic impedance to the Huntec seismic profiles. The operating principle for the Geotek is that a short P-wave pulse is introduced through a transmitter into the core and this pulse propagates through the core and it is detected by a receiver. This pulse is timed by pulse timing software and a resolution of 50 ns is achieved. The distance travelled is measured by the outside core diameter, and, after calibration, has been conducted to maintain accuracy. The final resolution of these measurements are within 3 m/s. The accuracy often depends on the thickness of the core liner walls.

3.4.1.3 Spectrophotometer

Distinct colour changes over a short interval are easy to spot but transitional changes are not. In these cases it is easier to see a graphical representation of colour intensities to quantify changes in colour. Quantifying colour is not the easiest thing for humans to do with the naked eye so a spectrophotometer mounted on the Geotek Multi Sensor Core Logger was used to quantify colour. Some objects reflect light, where as others transmit or even emit light, all of these contribute to colour. Values are created by measuring colour by gathering and filtering different wavelengths of reflected lights from the samples and their corresponding relative intensities. These colours are reported as spectral data in 10 nm increments from 360 nm to 740 nm. These spectral data can be seen in the CIE (La Commission Internationale de l'Eclairage) L* a* and b* colour system. L* is the lightness component of the system, low values represent black, whereas higher values represent white. This study looked at the a* and b* which are the

16

chroma portion of the system, with a* representing green (low) to red (high) and b* representing yellow (low) to blue (high) (Debret et al., 2011).

3.4.2. Splitting cores

Core splitting is done after a whole core analysis is performed. The plastic liner is cut longitudinally using the GSC Duits splitter. The sediments are then cut using a fine piece of wire which is pulled through the sediments along the cuts made by the splitter. The two core halves are designated as either working or archive, metre tape is placed on the plastic liner. The cores are then covered by plastic wrap and slid into a plastic sleeves, labelled and put into plastic D-tubes and stored at 4°C in the GSC Core Repository.

3.4.3. Clay Mineralogy

To determine clay mineralogy by X-ray diffraction, the less than 2 micron separates must be put on glass slides. The process of making less than 2 micron separates on glass slides starts with the separation process. The first step was to add 40 mℓ of sodium hexametaphosphate to a 1000 mℓ graduated cylinder. The main purpose of the first step is to have a deflocculating agent to keep the sample in suspension so it will differentiate and the larger particles will settle out. The samples were mixed in a separate beaker and were put into an ultrasonic bath to make sure there were minimal to no clumping of the sediments. The newly agitated sample was added to the graduated cylinder and was topped up with water to the 1000 mℓ line. The cylinder was then shaken vigorously and left to settle for 16 hours. This allows for the sediments that are larger than 2 microns to settle. The top 800 mℓ of the graduated cylinder was decanted into a centrifuge bottle with 2 mℓ of magnesium chloride which combats the action of the hexametaphosphate and

allows the sediments to settle. These samples were then centrifuged for an hour. Once the spin was completed the samples were decanted again. These samples were then added into a 500 mℓ graduated cylinder and were topped up to 500 mℓ. To get the representative proportion of material, 20 mℓ from each sample was withdrawn using a fixed volume pipette. The 20 mℓ was added to an aluminium dish and was placed into an oven to dry. Once the drying was complete and there was only sediment left, the dishes with sediments were weighted and recorded and added to a spreadsheet to determine the amount of zinc oxide that needed to be added. The zinc oxide is added because it is a standard to which the X-ray diffraction (XRD) results will be compared against. Once the amount of zinc oxide was determined, it was added to the sample and shaken up and was centrifuged down again, only to be decanted and transferred into 50 mℓ tubes. The transfer is done by introducing more water, and it would need to be centrifuged in the 50 mℓ tubes and decanted. Once this was completed a small amount of sample was spread onto a 1"x1" slide with a piece of plastic.

3.4.4. X-Ray Diffractometer (XRD)

The eight samples that were produced using the method described in the previous section were studied using X-ray diffraction. XRD is a rapid analytical method that is used to identify crystalline material and can provide information on crystal structure and atomic spacing. The operating principle behind XRD is that there is interaction of incident rays with the sample which produces constructive interference when conditions are right and Bragg's law is satisfied. This law relates the wavelength of electromagnetic radiation and diffraction and lattice spacing in the crystalline structure. The diffracted X-rays are detected and counted and diffraction peaks are converted to d-spacing which allow for the mineral identification. Each mineral has a unique

set of d-spacing, and these diffractograms are compared to standard reference peaks which have been archived. The samples were also glycolated, which allows for expandable clays such as smectites to be more easily identified as they produce sharper peaks in the diffractograms. To obtain the diffractograms from the raw data, the Siemens Evaluation Software (diffractplus EVA) was used for both the normal air-dried and the glycolated samples and the results were overlaid for better comparison.

3.4.5. Grain size

Grain size was analyzed on the Beckman Coulter LS 230 Laser Diffraction Particle Size Analyser. This instrument measures grain size from 0.04–2000 μm. The first step of the cycle was to allow for the instrument to perform its preliminary functions which include measuring the electrical offset measurement, the background measurement and laser beam alignment. For each sub sample, a small amount of sample from the sub sample was added to a small beaker and water was added. Once the sample was prepared the sample was added to the sample vessel and an obscuration value would be presented. This value had to be between 8% and 12% which corresponds to concentration that is at the optimal levels for the machine. When the sample is run, a polarized light beam illuminates the dispersed sample. The particles scatter the light, and depending on the dispersion pattern, it determines the sizes of the grains. The scattered light is detected and measured on an array of photodetectors. The photodectors are then scanned and their output is converted to digital values and are sent to the computer where a graph is produced showing the distribution of grain sizes, and the raw values are stored.

There was a section in the piston core 99036-037, from 600-750 cm, that showed high total carbon in the form of carbonate. This carbonate was removed by adding approximately 15

ml of 10% HCl to the samples, which were shaken vigorously using a Vortex-Genie mixer and were left under the fume hood till the reaction was complete. Then the tubes were filled with water and centrifuged down, to be decanted later. This process was done a few times and the sample was then run on the LS 230, and the decarbonated data was substituted for the original data at the corresponding depths

3.4.6. X-radiography

Whole core X-radiographs were made as described in Weitzman et al., (2014). It is a non-destructive analytical method that allows for the evaluation and potential interpretation of sediment structures and their composition.

3.4.7. Portable X-Ray fluorescence (pXRF)

XRF is a non-destructive method that uses high energy X-ray photons which strike the sample. These photons interact with the electrons from the elements present and it is this interaction which produces a secondary X-ray photons. This occurs because the photon that strikes the sample knocks electrons from the innermost orbitals of that element and are replaced with electrons from the outer orbitals to maintain a stable electronic configuration. This movement from outer to inner orbitals creates the secondary X-rays. This emitted radiation is different for each element and thus characteristic as well. The Innov-X system Delta Premium XRF spectrometer was used to measure: Al, Si, Ti, P, Fe, Mn, V, Cr, Ni, Cu, Zn, Sn, Ca, K, Zr, and Cl. This particular pXRF instrument has two modes: Mining Plus Mode and Soil Mode. For this study Mining Mode plus with two beams was selected due to the larger number of elements that were needed to be scanned for this study. The XRF was calibrated for each element

individually by the device itself, and are normalized to the Compton scattering peak to account for the loss of photons in the matrix. Following the collection of this data, the values were tabulated in Excel and ratios of Al/Si, Fe/Ti, Mn/Fe, V/Fe, Cr/Ti, Ni/Ti, Cu/Ti, Zn/Ti, Sn/Ti, Ca/Ti, K/Ti and Zr/Ti were calculated. For this study there will be a focus on Ca/Ti, K/Ti and Zr/Ti ratios. Ca/Ti typically indicates the presence of carbonate mineral, such as calcite but also foraminifera. K/Ti can be used to indicate clays, such as illite, as potassium is part of its chemical structure. Lastly Zr/Ti can act as a proxy for sand as they tend to contain a heavy mineral fraction and zircon is a mineral that is often concentrated in the sands in such a fraction.

3.4.8. O-isotopes

Oxygen isotopes in foraminifera are used to determine the ratio of heavy (^{18}O) to light oxygen (^{16}O) isotopes in seawater at the time of their formation. Ocean waters are richer in heavy oxygen during periods of glaciation because the lighter oxygen isotopes are locked up in the ice during this time. Stable oxygen and carbon isotopes were measured on the polar planktonic foram *Neogloboquadrina pachyderma* (sinistral) in the 150-250 μm size fraction. This data was obtained by Dr. H. Rashid using the isotope ratio mass-spectrometer in the Stable Isotope Biogeochemistry Laboratory at the School of Earth Sciences (Ohio State University). The analytical reproducibility was determined by taking replicate measurements on the standard material routinely and the reproducibility is better than ±0.05‰ for both δ^{18}O and δ^{13}C.

3.4.9. Nd-isotopes

Sm and Nd isotopes were measured on bulk samples of > 2mm ice rafted grains at two stratigraphic levels and from a turbidite granule gravel bed. Rock powders are weighed and a known amount of ^{150}Nd - ^{149}Sm tracer solution was added. A vessel containing both the rock powder and the tracer are sealed and heated to 160^OC for 5 days. From here the fluoride residue is then converted to chloride with HCl. The Nd and Sm are then separated by conventional cation and HDEHP based chromatography. The isotopic composition of Nd is then determined by ICPMS and the ratios of ^{143}Nd / ^{144}Nd are compared. The ^{150}Nd - ^{149}Sm tracer solution is used to calibrate the Caltech mixed Sm/Nd and it is this tracer that is used to measure ^{147}Sm/ ^{144}Nd.

3.4.10. Smear slide

A series of 7 smears slides were made from unit IV in PC 37 and one from unit I in PC 35 (Table 2), and were analysed under a petrographic microscope. Smear slides are made by taking a small amount of sediment and placing it on a glass slide. A few drops of water are added to the sediment to allow for it to be spread around. A cover slip with permount is then placed over the sediment and it is left on a hotplate to dry.

4. Core description and stratigraphy

Variations downcore in lithology and physical properties are indicative of a change in sediment properties which is often caused by a change in an event such as stadial to interstadial. This section will outline the downcore descriptions which include lithology, structures, along with multiple physical properties such as colour, magnetic susceptibility isotope dates and even relative age. All of these stated properties can be found on Figures 4 B, C and D.

4.1. Correlating the TWC with the PC

Piston cores (PC) commonly poorly sample the uppermost sediment at the seafloor, and the trigger weight core (TWC) usually obtains a better sample of the upper few tens of centimetres of the seabed. The TWC is commonly compacted compared with the PC. The 99036 cruise report noted that TWC 35 was overfilled and the uppermost sediment was therefore probably lost in the weightstand. When attempting to match downcore data such as element analysis by pXRF and colour by spectrophotometer, the correlation between the TWC and the PC did not appear simple. First, there is a missing section at the top of TWC 35 which may be due to this over filling and the top was lost in retrieval. Second, the bottom half of the TWC below 100 cm appeared to be compacted which makes the XRF curves not match with the PC. To solve this issue the plot of the bottom half of TWC 35 was expanded 125%, bulk shifted, and over laid on top of the PC element curves to get a good match (Fig. 5A). TWC 37 appeared to be intact but still compressed, thus this TWC was expanded 110% to match the PC and the same process of overlaying was performed (Fig. 4C).
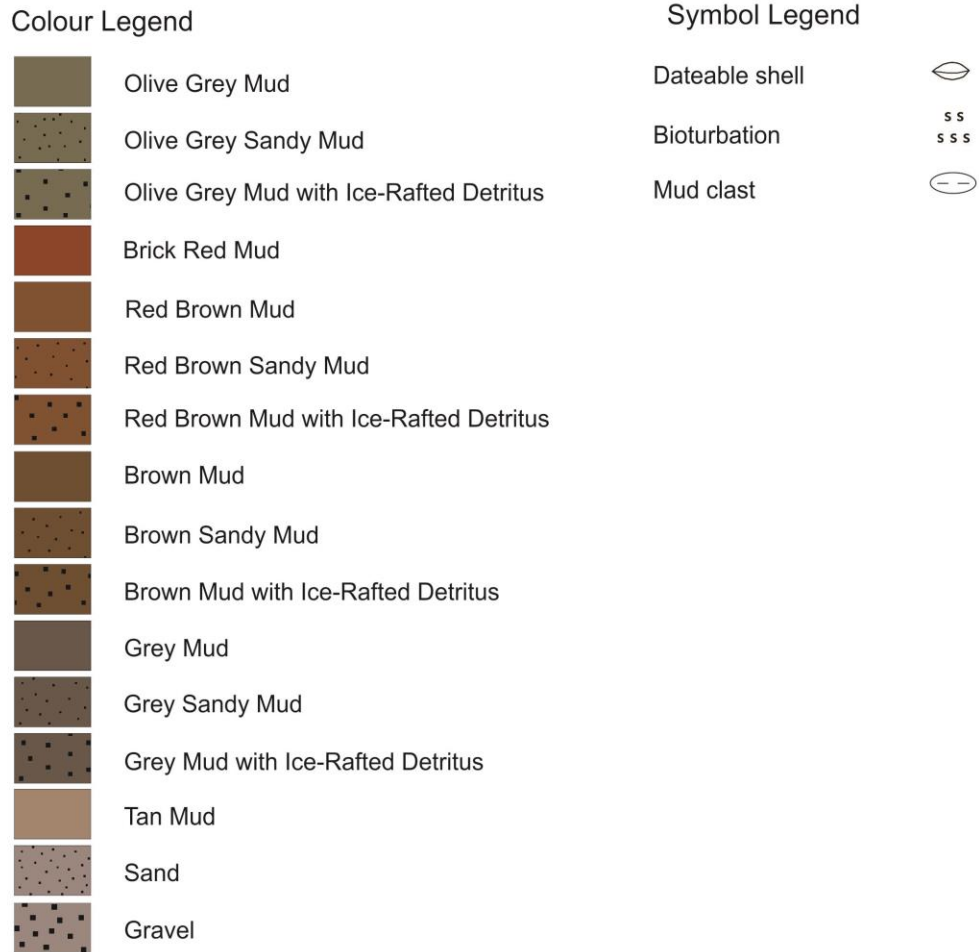
Scotian Rise Core Plot Summary Legend

Colour Legend

▦	Olive Grey Mud
▦	Olive Grey Sandy Mud
▦	Olive Grey Mud with Ice-Rafted Detritus
▦	Brick Red Mud
▦	Red Brown Mud
▦	Red Brown Sandy Mud
▦	Red Brown Mud with Ice-Rafted Detritus
▦	Brown Mud
▦	Brown Sandy Mud
▦	Brown Mud with Ice-Rafted Detritus
▦	Grey Mud
▦	Grey Sandy Mud
▦	Grey Mud with Ice-Rafted Detritus
▦	Tan Mud
▦	Sand
▦	Gravel

Symbol Legend

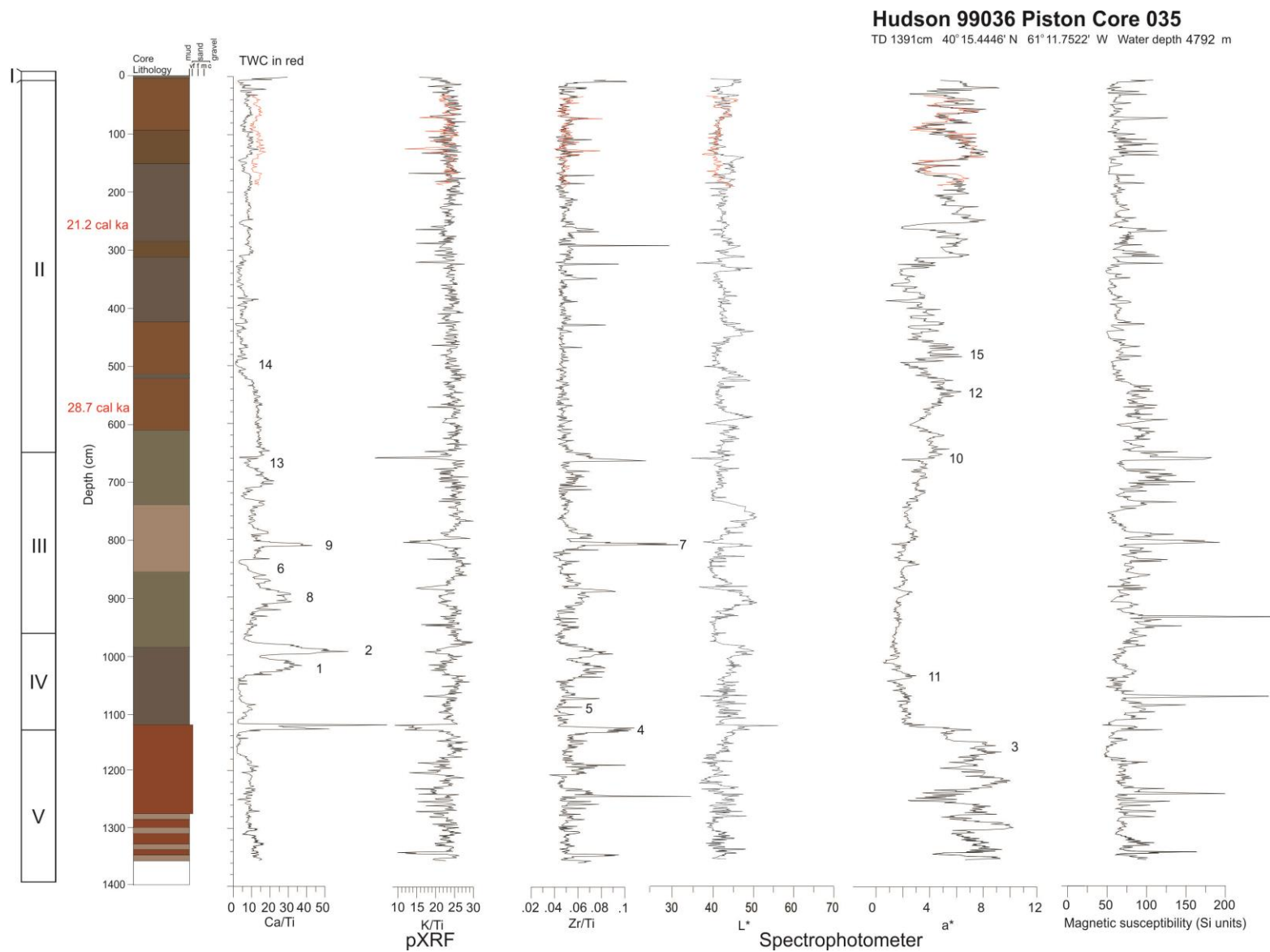|	
Dateable shell	⬯
Bioturbation	s s / s s s
Mud clast	⬭

Fig. 4 A – Core plot legend (Provided by the GSC)

24

Fig. 4 B – Downcore summary plots of PC 35 showing pXRF, Spectrophotometer and Magnetic susceptibility, C-14 dates, correlation numbers. TWC are over laid in red, modified as described in the text.
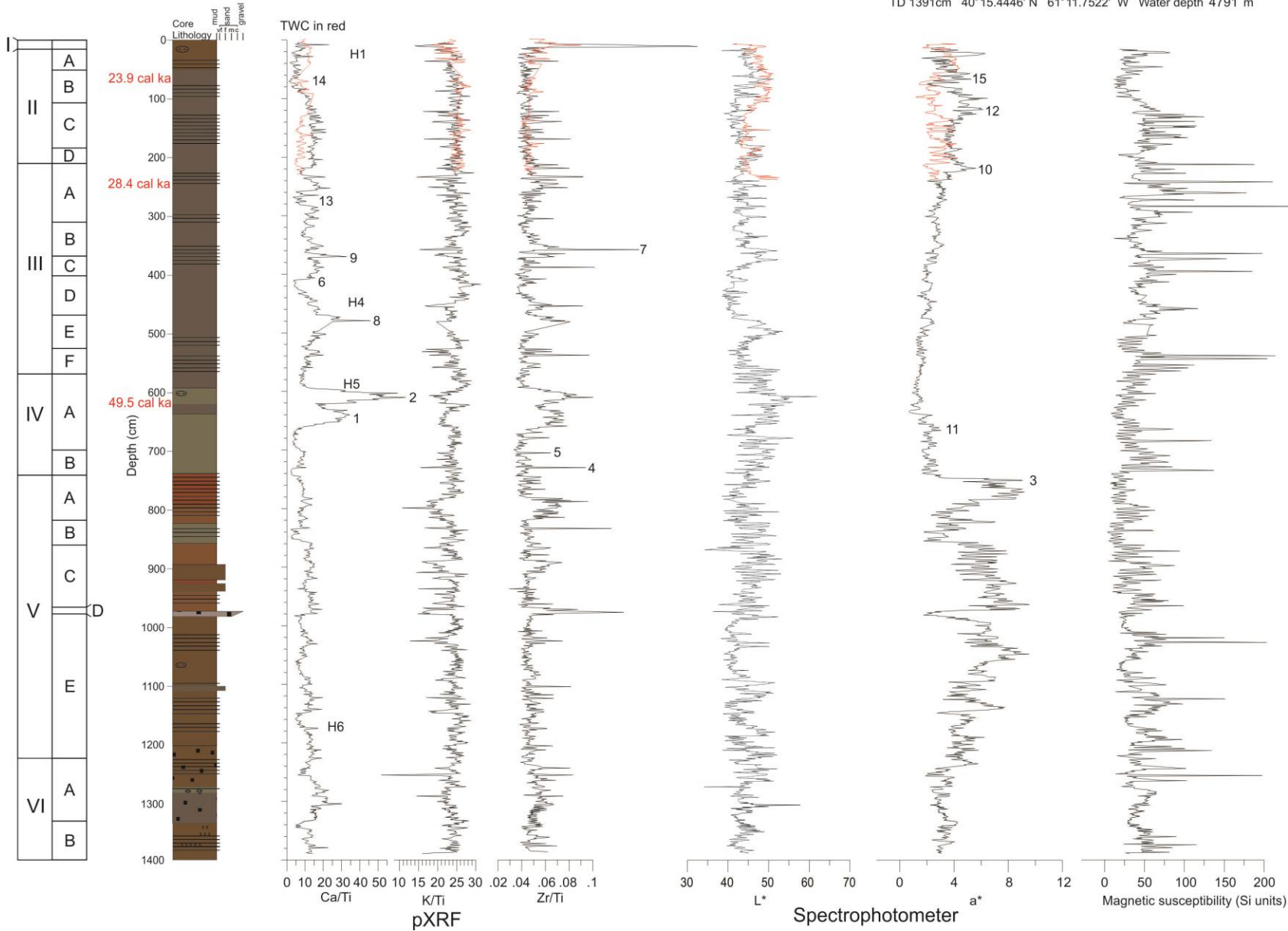
Fig. 4 C – Downcore summary plots of PC 37 showing pXRF, Spectrophotometer and Magnetic susceptibility, C-14 dates, correlation numbers. TWC are over laid in red, modified as described in the text.
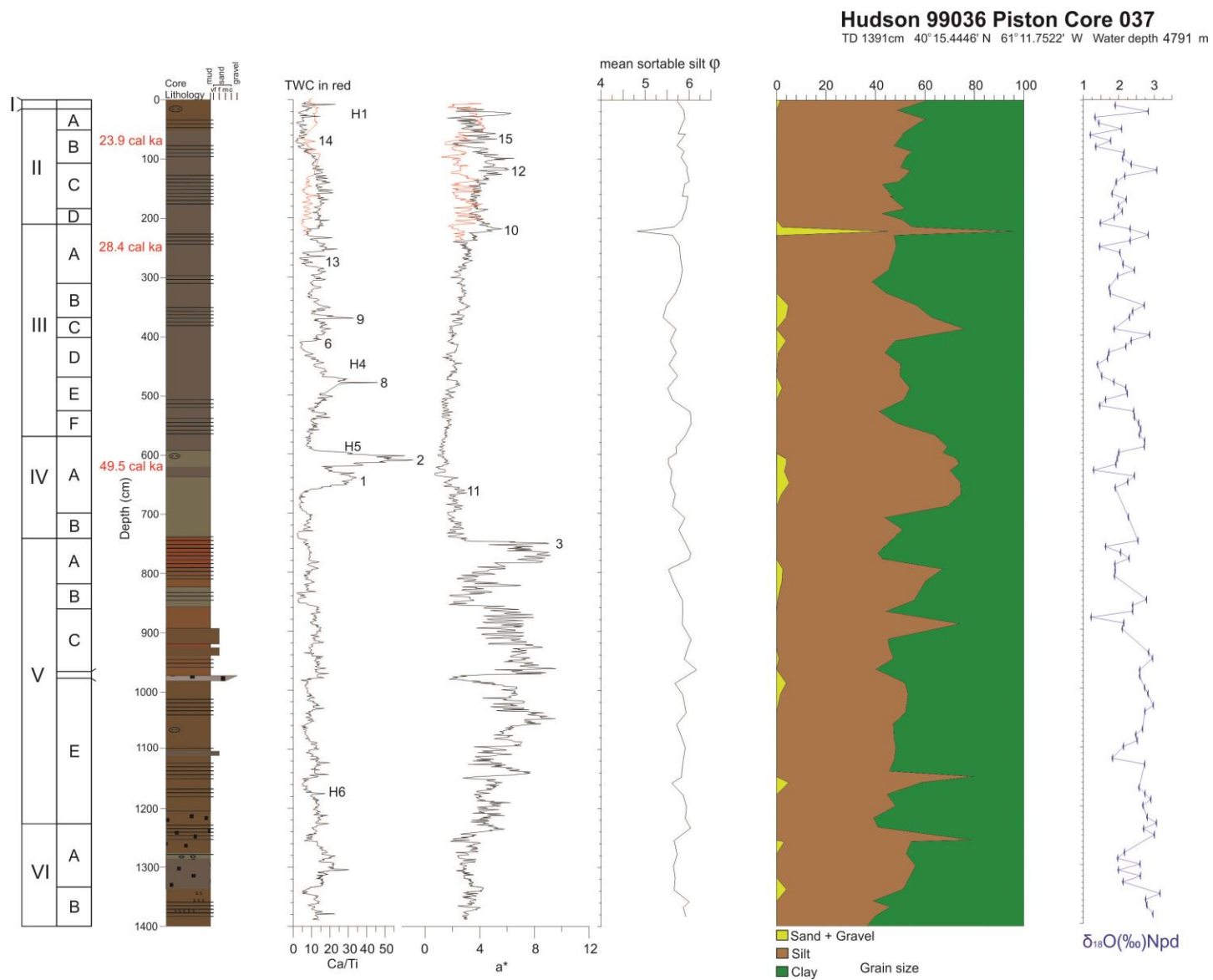
Fig. 4 D – Downcore summary plots of PC 37 showing Ca/Ti, a*, mean sortable silt, grainsize and Oxygen isotopes, C-14 dates, correlation numbers. TWC are over laid in red, modified as described in the text.

27

4.2. Lithology of PC 37

For this study PC 37 was subdivided on the basis of structures present in the X-radiographs, such as sediment type, visible bedding structures, bioturbation, and granules. Core photos were also used to distinguish variation in colour. Other properties such as the a* and XRF curves for Ca/TI, K/TI and Zr/Ti were also used in some intervals to signify a petrographic change which may not have visible to the eye. This helped to facilitate the divisions of certain units. Even though these properties were helpful in dividing this core into units, the precise boundaries were placed based on the X-radiographs. These units have also been subdivided based on subtle differences and these subunits will be referred to with letters, for example unit II A, B, C, and D.

4.2.1. Unit I

Unit I was classified as the top 15 cm of the core (Fig. 4C). This interval is considered to be a carbonate rich foram ooze which is analogous to the modern day sea floor. It is absent from the TWC, suggesting that the TWC was slightly overfilled.

4.2.2. Unit II

Unit II is a red brown mud with alternating silt laminae that starts at 15 cm and extends to 210 cm (Fig. 4C). Four subdivisions are recognized. Subunit II-A is from 15-50 cm and has sharp based silt laminae with a gradational top, which is also bioturbated (Appendix B, Fig. B-15). Subunit II-B is the interval from 50-105 cm and has less bioturbation than subunit A, but contains a few granules which are absent in subunit A. It also has iron monosulphides filling burrows which are concentrated towards the middle of this subunit. These iron monosulphides

appear as bright string-like objects in the X-radiograph due to their higher relative density (Appendix B, Fig. B-16). Subunit II-C is marked by alternating silt and clay layers which span from 105 cm to 185 cm and appear to have little to no bioturbation. The degree of alternation from silt to clay varies in this subunit. The top of the subunit has a tighter alternating pattern (laminae a few millimetres thick) which appears to have more gradual transitions, compared to the silt laminae between 115 and 170 cm which are much larger at approximately 2 cm thick with sharp tops. Subunit II-D is from 185-210 cm and has fewer silt laminae and it also appears to have moderate bioturbation, where some of the silt laminae are disrupted and discontinuous.

4.2.3. Unit III

Unit III is an interval of brown muds with silt laminae and granules which begins at 210 cm and ends at 570 cm (Fig. 4C). This unit has been subdivided into 6 subunits, A-F. Unit III-A is from 210-315 cm, where there are common silt laminae which are more than 5 cm thick in places; there are also some scattered granules throughout this subunit. Unit III-B is an interval from 315-375 cm and has fewer silt laminae than subunit A but has common bioturbation, and a larger number of dispersed granules. Unit III-C is an interval from 375-400 cm which has very sharp continuous silt laminae that are typically a few millimetres in thickness. This subunit appears to have little bioturbation. Unit III-D is a more bioturbated interval from 400-470 cm with minimal silt laminae. The base of this subunit is marked by a 5 cm mud bed with silt laminae at the base. Unit III-E spans from 470-528 cm and is a moderately bioturbated lighter mud, which may be caused by the higher carbonate present. This subunit also does not appear to have any silt present, but there are still common granules present. Unit III F is from 528-570 cm, with silt laminae and a slight increase in the amount of bioturbation and larger burrows present.

4.2.4. Unit IV

Unit IV is a light brown carbonate-rich mud which starts at 570 cm and ends at 744 cm (Fig. 4C). This unit appears to be relatively uniform but was subdivided into 2 subunits. The first, Unit IV-A is an interval from 570-700 cm. It is moderately bioturbated with larger patches of bioturbation present. It appears to have very few or no silt laminae, and granules are present in concentrated areas such as at 585 cm, where there are numerous granules in a 5-10 cm interval. Unit IV-B is from 700-744 cm and there is much less bioturbated silt and laminae are present. These silt laminae appear to be gradational in nature, and are approximately 0.5-1 cm in thickness, with the exception of the bottom two silts which are approximately 2-3 cm thick.

4.2.5. Unit V

Unit V is a bright red mud which starts at 744 cm and ends at 1223 cm (Fig. 4C). This unit was divided into 5 subunits. Unit V-A is from 744-820 cm, with packets of silt laminae and slight bioturbation only in the interbedded muds. Unit V-B is a heavily bioturbated muddy subunit from 820-863 cm, where silt laminae become indistinguishable and monosulphide strings are present throughout. This subunit also experienced some core disturbance near the bottom of the unit. Unit V-C is from 863-970 cm and is very similar to V-A, with packets of silt laminae and some interbedded bioturbated clay. Monosulphide strings are also present at the bottom of this subunit. Unit V-D is a beautifully preserved, well sorted granule gravel bed with a sharp basal contact. The base of this bed is composed of fine sand which is overlaid by 6 cm of granule gravel bed that has no particular grading pattern. Above this gravel bed there is normal grading from fine sand into silt. This subunit is from 970-980 cm (Appendix B, Fig. B-12). Unit V-E is from 980-1223 cm, and has alternating silt laminae with mud beds. These mud beds are slightly

bioturbated with the exception of a large concentration of monosulphide strings which occur around 1160cm. This subunit also has common granules irregular distributed throughout.

4.2.6. Unit VI

Unit VI is a brown red mud which starts from 1223 cm and ends at 1391 cm (Fig. 4C). This unit is divided into two subunits. Unit VI-A is from 1223-1335 cm and lacks prominent stratified silt laminae (Fig. B-13). The silt laminae that are present are rare, possibly due to the heavy bioturbation. There are also rare granules that are disturbed randomly. Unit VI-B is from 1335-1391 cm, and contains common granules along with common silt laminae, with less bioturbation than VI-A (Fig. B-14).

4.3. Downcore Colour Variation

4.3.1. a*

Down-core from unit I into unit II there is a gradual but slight increase of a* until approximately half way though unit II around 100 cm (correlation 12) (Fig. 4C). From this half way point in the unit a* then gradually decreases towards the base of Unit II (210 cm) but, there is an abrupt peak in a* at the base (correlation number 10). Throughout unit III there is a gradual decrease in a*. This is followed by a gradually increases of a* to the base of unit IV with an abrupt increase at the top of unit V (correlation 3) and then decreases for 150 cm. This is followed by a sharp spike in a* and then a gradual decrease to the base of the core.

31

4.3.2. L*

   Down-core from unit I into unit II there is a gradual but slight increase of both L* and a*

until approximately half way though unit II around 100 cm, from this point L* gradually

decreases. L* then experiences some variations within unit III, oscillating over 10 (units of L*)

from 350 cm to the uppermost part of unit IV (620 cm) where L* increases to a core high of 60

(units of L*). L* then gradually decreases to the base of unit IV and then it continues to

gradually decrease through unit V from 744 - 1100 cm. L* then again gradually increases to the

base of unit V. At this point there is an abrupt increase of L* which marks the transition between

unit V and unit VI. L* then gradually decreases to the bottom of unit VI.

4.4. Downcore Variation in Elements

4.4.1. Ca/Ti

   Ca/Ti was plotted to act as a proxy for carbonates. From the top of unit I into unit II there

is gradual decrease to 80 cm, where it then begins a gradual increase only to decrease slightly

before the base of unit II (Fig. 4C). Ca/Ti is fairly consistent throughout unit III except for two

peaks: one at 370 cm and the other at 480 cm. Unit IV is characterized by abundant carbonates.

The top of unit IV is marked by a gradual increase for 20 cm which is followed by an abrupt

spike in Ca/Ti around 600 cm. This peak signifies the most carbonate rich section in the core.

This 25 cm interval is followed by an abrupt decrease of Ca/Ti only to be followed by another

increase. Another 20 cm carbonate rich section which is again followed by another abrupt

decrease. The general trend from the middle of unit IV to the bottom of unit VI is a slight gradual

increase.

4.4.2. K/Ti

K/Ti is a proxy for clays such as illite. There is a trend that is constant from unit I through to the top of unit III, at which there is a gradual decrease at 320 cm down to 550 cm (Fig. 4C). There is a slight peak at the contact between units III and unit IV, followed by a constant trend until the top of unit V. This is preceded by a dip in K/Ti at 800 cm. The values then re-stabilize to the previous consistent general trend and this trend is followed to the bottom of the unit VI.

4.4.3. Zr/Ti

Zr/Ti acts as a proxy for sands particularly those of polycyclic origin, because zircon, which contains zirconium, often gets concentrated in the heavier sand fractions. From the top of the unit I to the base of unit II a gradual increase is followed by a slight increase at the top of unit III (Fig. 4C). This increase is followed by a gradual decrease. This decrease occurs until about 360 cm then there is an abrupt spike for a short 10-15 cm interval (correlation 7), followed by a gradual decrease until the next spike at 480 cm, which again is followed by a gradual decrease to the base of unit III. The curve for Zr/Ti for the carbonate rich unit IV follows the same trend as Ca/Ti. The top of unit IV is marked by a gradual increase for 25 cm which is followed by an abrupt spike in Zr/Ti around 600 cm for 20 cm. This 20 cm interval is followed by a rather abrupt decrease only to be followed by another increase to a Zr/Ti rich interval of 20 cm. It abruptly decreases around 680 cm and then gradually increases to the middle of unit VI. This gradual increase is also accompanied by several spikes at 780, 830, 900, 970 and 1100 cm.

4.5. Downcore variation in grain size and mean sortable silt

Grain size is an important parameter for interpreting the history of the sediments. The grain size may indicate the transport and depositional history of the sediment. Grain size was analysed on the Beckman coulter LS 230 Laser Diffraction Particle Size Analyser as described in the materials and methods section. Two downcore plots were produced to indicate variation of mean sortable silt (mean of 10-63 μm fraction), along with percent gravel + sand, percent silt, and percent clay (grain size) (Fig. 4D). The grain size and sortable silt are consistent through unit I and unit II, until the base of unit II where there is a 10 cm interval with a peak in the sand and mud fractions and thus a decrease in silt and mean sortable silt. The top of unit III is very similar to the constant trend at the top of the core until 330 cm, where there are two smaller peaks in the sand fraction both approximately 40 cm thick, although there is only one peak for the silt fraction which encompasses these two sand peaks. There is one smaller peak in the sand fraction at 480 cm with a thickness of 40 cm again. This smaller sand peak is again encompassed by a larger more dominant mud peak. At the base of unit III there is a peak in mean sortable silt and also a peak in silt grain size itself. As unit IV becomes deeper there is a decrease in mean sortable silt and an increase in sand and mud grain size. At the base of unit IV and the top of unit V there is an increase in the silt fraction and thus mean sortable silt increases again. From 800 cm down the mean sortable silt seems rather constant to the base of unit VI. From the top of unit V to the bottom of unit VI the same trends of periodic increase in sand and silt.

4.6. Downcore variation in ice rafted detritus

The first appearance of ice rafted detritus (IRD) occurs in the top of unit II at 20 cm. In this interval the granules are 100 % carbonate rocks (Fig. 5A). Towards the bottom of unit II the IRD consists principally of volcanic rocks and granites. These lithologies continue to dominate until half way through unit III where carbonate grains are abundant at 440 cm, although volcanics and granites are also present, in contrast to the carbonate-dominated IRD at the top of unit II. This is followed by a sharp decrease in carbonate grains at 530 cm, but an increase in volcanics and granites. At the base of unit III there is an increase in the proportion of carbonate grains. Below this point there is a gradual increase in carbonate grains to the bottom of unit V and a gradual decrease in volcanics and granites. The bottom of the core and the last recorded interval of IRD show a spike in both carbonates and volcanics/granites.

4.7. Correlation of units from core 37 to core 35

Cores 35 and 37 were correlated by identifying similar peaks in multiple different properties (Figs. 4B, C and D) (correlations seen on core photography in appendix A). Correlations within units II from 37 to 35 were based on a* and are represented as correlations peaks numbers 10, 12 and 15 along with the Ca/Ti correlation peak number 14. Unit III is confirmed by Ca/Ti peaks 6, 8, 9 and 13 along with Zr/Ti, peak number 7. Unit IV can be confirmed by Ca/Ti peak numbers 1 and 2 which show drastic increases in Ca/Ti, along with increases in Zr/Ti at peak numbers 4 and 5. Lastly it can confirm this unit based on a* peak number 11. The top of unit V is marked by an abrupt shift in a* which is marked by correlation number 3. A summary of these correlations can be found on Figure 4E.
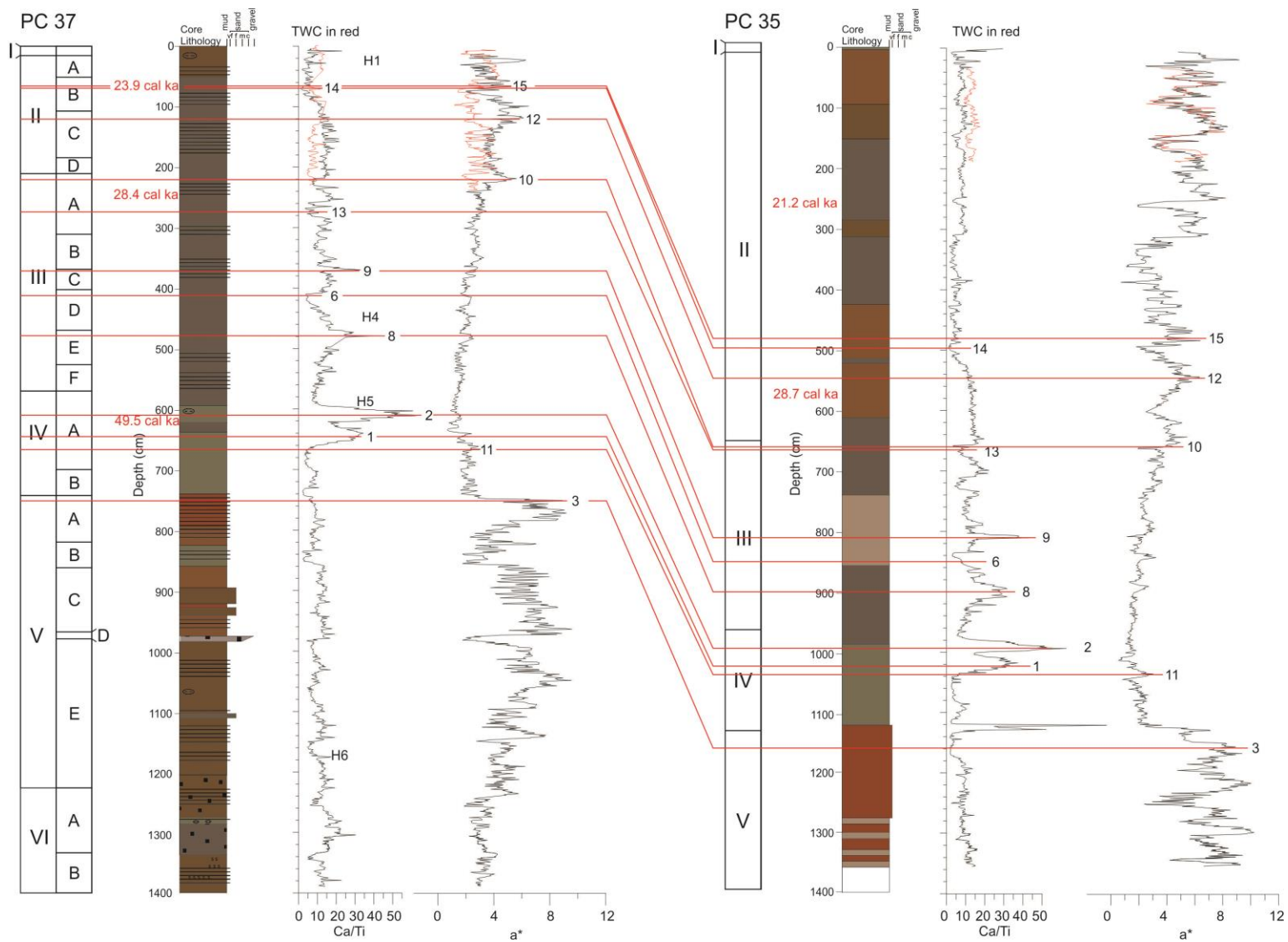
Fig. 4 E – A summary of correlations between core 35 and 37 excluding Zr/Ti

36

4.8. Variation between 35 and 37

There are a few main differences when comparing the two cores. First, PC 35 has a much thicker unit II than PC 37. Further investigation appears to show that PC 37 is missing a larger portion of these sediments. The locations of the C-14 dates in PC 37 alone indicate thinning of sediments in PC 37 as 23.9 ka is towards the top of unit II. The other noticeable difference is that there is a much thinner unit V and no unit VI in PC 35. If it were possible to recover a longer core it may have been possible to correlate the bottom section of PC 37 to PC 35.

4.9. C-14 dates

Carbon-14 dating was used in this study to give absolute ages of the sediments by dating forams. Three samples were dated in piston core 37 along with two in piston core 35. The table below indicates the dates corresponding to the depths. These radiocarbon ages are based on accelerator mass spectrometry (AMS).

Core and Depth	Lab Number	Material dated	Weight of material (mg)	^{14}C age	±	Calibrated MARINE13 (1 Sigma)
99036-35pc; 258-261 cm	TO9548	Globorotalia puncticulata	11.9	18100	230	21070 - 21337
99036-35pc; 688-693 cm	UCI167204	N. pachyderma	10.1	25220	120	28605 - 28805
99036-37twc; 60 cm	UCI167205	N. pachyderma	3.7	20470	80	23863 - 24087
99036-37pc; 250-252 cm	UCI167206	N. pachyderma	11.2	24910	100	28299 - 28555
99036-37pc; 600-602 cm	UCI167207	N. pachyderma	8.7	46500	1300	49218 - 49793

Table 1 – C-14 data: including depths, lab number, amount and species of foram and calibrated dates, with error

Calibrations of the marine radiocarbon dates were made using the Calib 7.1 program (Stuiver & Reimer, 1993) and the MARINE 13 calibration dataset (Reimer et al., 2013). The standard deviations of present marine radiocarbon corrections (ΔR) from McNeely (2006) were applied and values from Newfoundland Shelves and upper slope waters (144 ± 38 years) were used as this is the closest data set to the study area.

5. Grain size analysis

Piston core 99036-0037 was subsampled approximately every 20 cm for grain size analysis. This section will describe the finer details of individual intervals, based on 14 representative samples which were chosen to illustrate the variation in grain size with bedding structures as seen in the X-radiographs (Appendix B). For these samples, distribution curves (in φ units) were produced to show the contrast in grain size among these samples. In these plots 0-4 φ is the sand range with particles ranging from 1000 μm to 62 μm, 4-8 φ is the silt range with particles ranging from 62 μm to 4 μm and lastly the range between 8 and 12 φ represents clay, which is anything less than 4 μm.

There were five subsamples chosen to represent the silt layers in this core. Their corresponding depths are at 138, 388, 708, 816 and 888 cm. In addition the silt layers present in this study were subdivided into two groups (A and B). Silt A is represented by samples 388 and 888, which both appear to have a bimodal size distribution, but with much larger concentrations of silt near the 6 φ range compared to clay mode which is around the 10 φ (80 % silt – 20 % clay). Silt B is represented by 138, 708 and 816; these silt layers have a higher concentration of clays in them, but still preserve a bimodal distribution with peaks at 7 φ and 10 φ. There is an exception in this group; sample 816 is the only sample to include some material in the sand

38

range.

Five representative mud samples were chosen: 143, 508, 848, 1257, and 1358 cm; each sample shows considerable differences. For example: 508 is the only sample that appears to have no sand fraction present, whereas sand is present in all the other samples. Also concentrations of clay and silt vary, depending on the sample interval and the bioturbation structures that are present. Sample 143 is a mud bed that occurs between silt laminae. When comparing these five representative plots it is easy to see that there is an absence of silt (6 φ) in contrast to silt samples 388 and 888. The muddy sample at 222.5 cm (Appendix B Fig. B -3) has almost no clay, but it has a somewhat bimodal distribution between 2 and 6 φ showing that it is a well sorted sandy silt.

There are three other important features in these cores which may reflect in grain size distribution are: bioturbation, chemical composition (the carbonate rich interval) and the sorted granule gravel bed. The sample at 648 cm (Appendix B Fig. B -7) appears bioturbated in the X-radiograph with no original bedding preserved and shows a relatively uniform grain size distribution around 6.8-7 φ. There is some concentration of material in the sand range, which is present in bioturbated sandy patches. Lastly, a sample was taken directly under a sorted granule gravel bed at 988 cm (Appendix B Fig. B - 12). This sample has an unusually high sand fraction, probably due to the sample including some of the base of the granule bed.

6. Sedimentary petrology and sources

6.1. Sedimentary sources in the < 2 µm size fraction

A key part to this study is to make correlations between the two cores, but these correlations are merely just an exercise if we do not attempt to put these cores in context of the regional setting. The source petrology and clay mineral sources give us an indication of the direction of material transfer and how it may have changed or been influenced through periods of glaciation or interglacial periods. It also provides us with a more detailed story of which factors may be influencing the sourcing of these sediments, such as ice sheet erosion on the shelf and mass transport deposits. This section will attempt to provide some insight on the history of these sediments. This region is influenced by five major sources (Piper & Slatt, 1977). Those on land and the continental shelf were deemed principally by glacial erosion and transport; (1) Low grade metamorphic rocks from the Appalachians, primarily chlorite schists and muscovite schists. The erosion of these rocks introduced illite and Mg-rich chlorite, along with quartz and feldspar glacial rock flour. (2) Carboniferous-Permian shales from the Maritimes Basin which provided illite into the system. (3) The Cretaceous sediments onshore from the Chaswood Formation and offshore from Scotian Basin both provided illite and kaolinite, but the offshore, may also have supplied iron-rich chlorite. (4) Tertiary sediments of the Scotian Basin which may be eroded by glaciers on the shelf, or transported by slumping, turbidity flows or as mass transport events and they are bringing illite and smectite. (5) The Western Boundary Undercurrent which introduced smectites from seafloor weathering of basalt and rock flour from high grade metamorphic rocks including amphibole along with quartz and feldspar.

6.2. Gravel petrology

The petrology of ice rafted detritus data (IRD) was another tool which was used to interpret the sourcing of the sediments. Piston core 99036-0037 had 16 intervals investigated and 888 grains (coarser than 2 mm) in total identified and tabulated into Excel. All grains are interpreted as IRD, except the 980 cm sample which is from a granule bed. For these tabulated values a down core plot with the percentage of grain types was created (Fig. 5A). There is no systematic correlation between depths in the core and grain types, but there are some localized patterns that may shed some light on the story, for example the bottom seven intervals show a somewhat constant pattern of carbonate-rich clasts, volcanics and granites. Higher in the core there appears to be a lower percentage of carbonate grains with the exception of around 440 cm which has a slight increase and 20 cm which comprises only six beige and brown carbonate grains. There may be some statistical bias as most of the intervals towards the top of the core have fewer grains which gives more influence on the grains present.
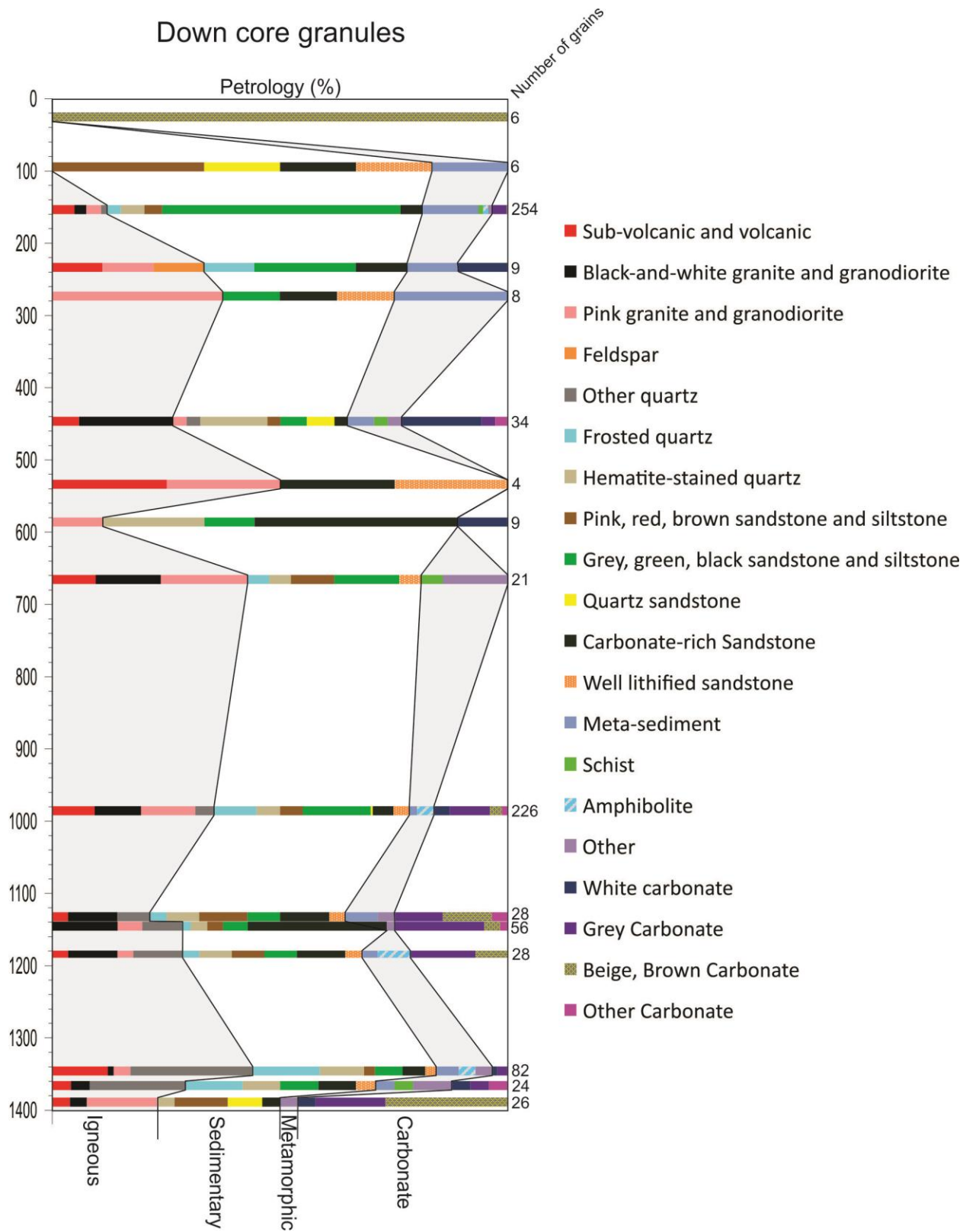
Fig. 5 A – Downcore Granule petrography counts divided into 4 categories.

Depth (cm)	20	90	150	230	270	440	530	580	660	980	1130	1140	1180	1340 A	1340 B	1360	1385	
Sub-volcanic and volcanic	0	0	12	1	0	2	1	0	2	21	1	0	1	10	4	1	1	
Black-and-white granite and granodiorite	0	0	7	0	0	7	0	0	3	23	3	8	3	1	1	1	1	
Pink granite and granodiorite	0	0	8	1	3	1	1	1	4	27	0	3	1	3	4	0	4	
Feldspar	0	0	0	1	0	0	0	0	0	0	0	0	0	0	0	0	0	
Other quartz	0	0	3	0	0	1	0	0	0	9	2	5	3	22	4	5	0	
Frosted quartz	0	0	8	1	0	0	0	0	1	21	1	1	1	12	10	3	0	
Hematite-stained quartz	0	0	13	0	0	5	0	2	1	12	2	2	2	8	24	2	1	
Pink, red, brown sandstone and siltstone	0	2	10	0	0	1	0	0	2	11	3	2	2	2	2	0	3	
Grey, green, black sandstone and siltstone	0	0	133	2	1	2	0	1	3	34	2	3	2	5	1	2	0	
Quartz sandstone	0	1	0	0	0	2	0	0	0	1	0	0	0	0	1	0	2	
Carbonate-rich Sandstone	0	1	12	1	1	1	1	4	0	10	3	17	3	4	2	2	1	
Well lithified sandstone	0	1	0	0	1	0	1	0	1	8	1	0	1	2	5	1	0	
Meta-sediment	0	1	31	1	2	2	0	0	0	4	2	0	1	4	3	1	0	
Schist	0	0	3	0	0	1	0	0	1	0	0	0	0	0	0	1	0	
Amphibolite	0	0	3	0	0	0	0	0	0	8	0	0	2	3	1	0	0	
Other	0	0	2	0	0	1	0	0	3	0	1	1	0	3	3	2	1	
White carbonate	0	0	0	1	0	6	0	1	0	8	0	0	0	1	0	1	1	
Grey Carbonate	0	0	8	0	0	1	0	0	0	20	3	11	4	2	2	1	4	
Beige, Brown Carbonate	6	0	1	0	0	0	0	0	0	6	3	2	2	0	0	0	7	
Other Carbonate	0	0	0	0	0	1	0	0	0	3	1	1	0	0	0	1	0	
Total grains	6	6	254	9	8	34	4	9	21	226	28	56	28	82	67	24	26	888

Table 2 – Downcore granule counts for specific lithologies for piston core 37 (completed by Heidi McKee)

Granules from three intervals (150, 980 and 1340 cm) were sampled and sent to Geospec

Consultants Limited for Sm/Nd isotopic analyses. Our values of $^{147}Sm/^{144}Nd$ and εNd were

plotted in the figure created by Farmer et al. (2003) to show comparative age of our grains. This

figure was primarily developed for the Norwegian Sea, so values for areas closer to our study

area such as the Gulf of St. Lawrence, Cartwright, Hudson Strait and Baffin Bay were added

(Farmer et al., 2003). As seen in Figure 5B the two submitted samples of IRD in red plot high

and to the right, with slightly higher εNd than Mesoproterozoic sources, suggesting a possible

Appalachian source. The granule bed at 980 cm falls within the Mesoproterozoic field suggesting

a significant source contribution from the Canadian Shield.
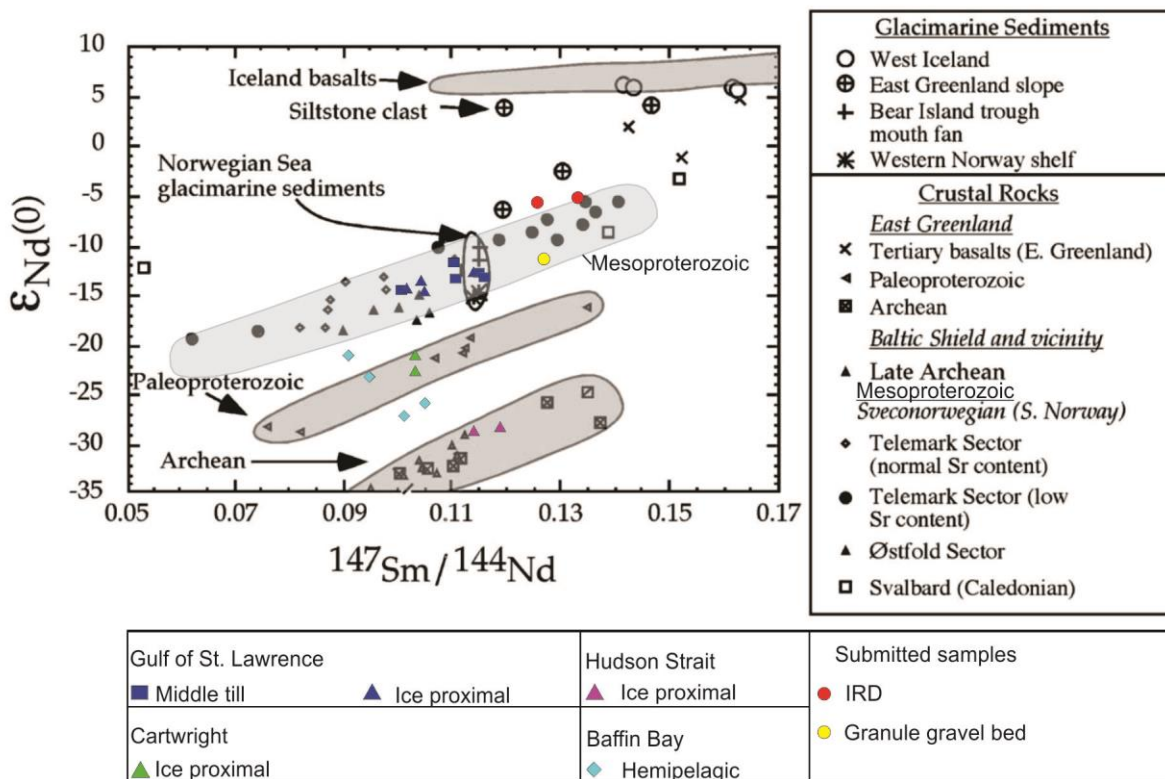
Fig. 5 B – εNd vs $^{147}Sm/^{144}Nd$ for glacimarine sediments (modified from Farmer et al. 2003)

6.3. Clay Mineral Identification

The method of X-ray diffraction allows us to analyze variations in diffraction intensity from the principal crystallographic planes in clay minerals and displays this variation of intensity against the spacing of the crystallographic planes (Carroll, 1970). The distance between the planes of the mineral structure is called the d-spacing and this is measured in angstroms (Å). Each mineral has its own specific set of d-spacing and diffraction peak intensities. The d-spacing is also influenced by the orientation of the mineral or in other terms its Miller indices. The angstrom value of a clay mineral may be expressed differently by its orientation (Carroll, 1970), for example Chlorite 001 has a peak at 14 Å, while Chlorite 002 is at 7 Å and Chlorite 003 is at 4.7 Å. There are a couple considerations to take into account when interpreting diffractograms. First, mixed layer clays have complex diffraction patterns at high d-spacings. These mixed layer clays often overprint simpler clays making the simple clays often overlooked. Second, peaks often appear so close to one another that it is almost impossible to distinguish them from one another. A possible way to combat this is to run the XRD at a slower rate that will produce better resolution and subsequently a cleaner separation between peaks, if one is present. For this study, four main clay assemblages (types) have been identified and types 1-4 will be referenced when discussing minerals present (Figs. 6 A-D). Type I is represented by clays 106-108, 277-279, 437-439 and 577-579. Type II is represented by 604-608. Type III is represented by 677-679 and type IV is represented by 791-793, 903-905 and 1281-1283.

Minerals present

In this section minerals are listed in order of decreasing d-spacing, based on Carroll (1970) and White (2014), to systematically describe the minerals present in the diffractograms (Figs. 6 A - D). These diffractograms have been used to describe four clay assemblage types in this study but will be discussed in the next section.

Smectite:

Smectite is present by itself in all the clay assemblage types and it forms a peak at 16.5 Å. Smectite is recognized between 14-16 Å in air-dried samples but when the sample is glycolated it shows a shift towards 17 Å but in this study it appears to be closer to 16.5 Å. Smectites was used as one of the first diagnostic difference between the clay assemblage types. Type I has the least amount of smectites, type III has the next lowest amount, while type IV has the second highest and type II has the highest amount of smectite present. This can be easily seen with the visible gap between the nonglycolated and glycolated sample: type I (Fig. 6 A) having the smallest gap and type II (Fig. 6 B) having the largest.

Chlorite:

Chlorite has characteristic diffractions at 14, 7, 4.7, and 3.54 Å. Chlorite overlaps with kaolinite in two spots since its peaks are so close to 7 and 3.54 Å. Chlorites can have varying contents of iron and magnesium and thus they have peaks of different strength. For example Fe-rich chlorites tend to have stronger 002 and 004 diffractions, while Mg-rich tend to have stronger 001 and 003 diffractions. All four types of clay assemblage (Figs. 6 A-D) have 001/004 ratios (high 004 and low 001) indicating predominance of Mg-rich Chlorite.

46

Illite:

There are three main peaks in which illite can occur in oriented mounts. Illite 001 is found at 10.1 Å and is not overlapped by any other common mineral. The illite 002 peak occurs at 5 Å while illite 003 occurs at 3.35 Å, overlapping with quartz.

Amphibole:

Amphibole is present in all four clay assemblage types at a d-spacing of 8.4 Å.

Kaolinite:

A Kaolinite 001 overlapped with the Chlorite 002 peak occurs at 7.1 Å, and is found in all the samples. The 3.58 Å kaolinite 002 peak can generally be separated from the chlorite 004 peak at 3.54 Å (e.g. Fig. 6 B).

Mixed Layer Clays (MLC):

There are two mixed layer peaks that appear in this study at 11 Å and 5.5 Å. These spacings suggest that the two peaks represent the same MLC. White (2014) interpreted peaks in these positions to represent illite-chlorite (I-C) mixed layer clays (Figs. 6 A – D).

Quartz:

Quartz is present in all four types of clay assemblage and its diagnostic peak positions occur at 4.26 Å by itself and at 3.19 Å overlapping with illite.

Feldspar:

Plagioclase occurs in all the samples at 4.04 and 3.27 Å. Alkali feldspar occurs in all the samples at d-spacings of 3.78, 3.7 and 3.13 Å.

Zincite:

Zincite was used as a standard in this study and it is found in all the samples at d-spacings 2.8, 2.72, 2.6, 2.48 and 1.7 Å.

Calcite:

Calcite only appears in clay assemblage type II. It occurs in sample 604-608 (Fig. 6 B) at a d-spacing of 3.05 Å. Calcite is the diagnostic difference setting type II apart from the other types.

Unknown:

Unknown peaks occur in both the glycolated and unglycolated at 7.9 Å (unknown 2) and 3.9-4.0 Å (unknown 3). The same unknown peaks were also found by White (2014) in the Scotian Basin

6.3.1. Clay assemblage types

These diffractograms have been divided in four types (I - IV) (Figs. 6 A – D) each being slightly different. Additional clay samples were analyzed and can be found in appendix C as they also fall under one of the types. Clay assemblage Type I (Fig. 6 A) is characterized by having; (1) low smectite content (small gap between air dried and glycolated curves): (2) a high chlorite

48

004/001 chlorite ratio: (3) a sharp peak at unknown 2: and (4) a less obvious peak of kaolinite (3.58 Å). This clay assemblage also occurs at the intervals of 277 – 279, 437 – 439 and 577 – 579 cm (Appendix C, Figs. C-1, C-2 & C-3)

Type II only has one representative sample at 604 – 608 cm (Fig. 6 B). This clay assemblage is recognized on the following criteria; (1) it contains the highest smectite content (largest gap between air dried and glycolated curves): (2) it is the only sample to contain calcite at 3.05 Å: (3) a low 004/001 chlorite ratio: (4) a low value of unknown 2.

Type III (Fig. 6 C) is similar to type II but the first noticeable difference is that it lacks the unknown at mineral at 3.05 Å. This clay assemblage type is found only at the 677 – 679 cm interval and is recognized by the following criteria: (1) high amphibole content at 8.4 Å: (2) a low 004/001 chlorite ratio: (3) a low value of unknown 2: (4) moderate smectite: (5) larger concentration of 3.

Type IV is found in the intervals 791 – 793 cm (Fig. 6 D), 903 - 905 and 1281 - 1283 cm (Appendix C, Figs. C 4 &5). This clay is recognized on the following criteria: (1) a high 004/001 chlorite ratio: (2) a sharp peak at unknown 2: (3) moderate smectite content.
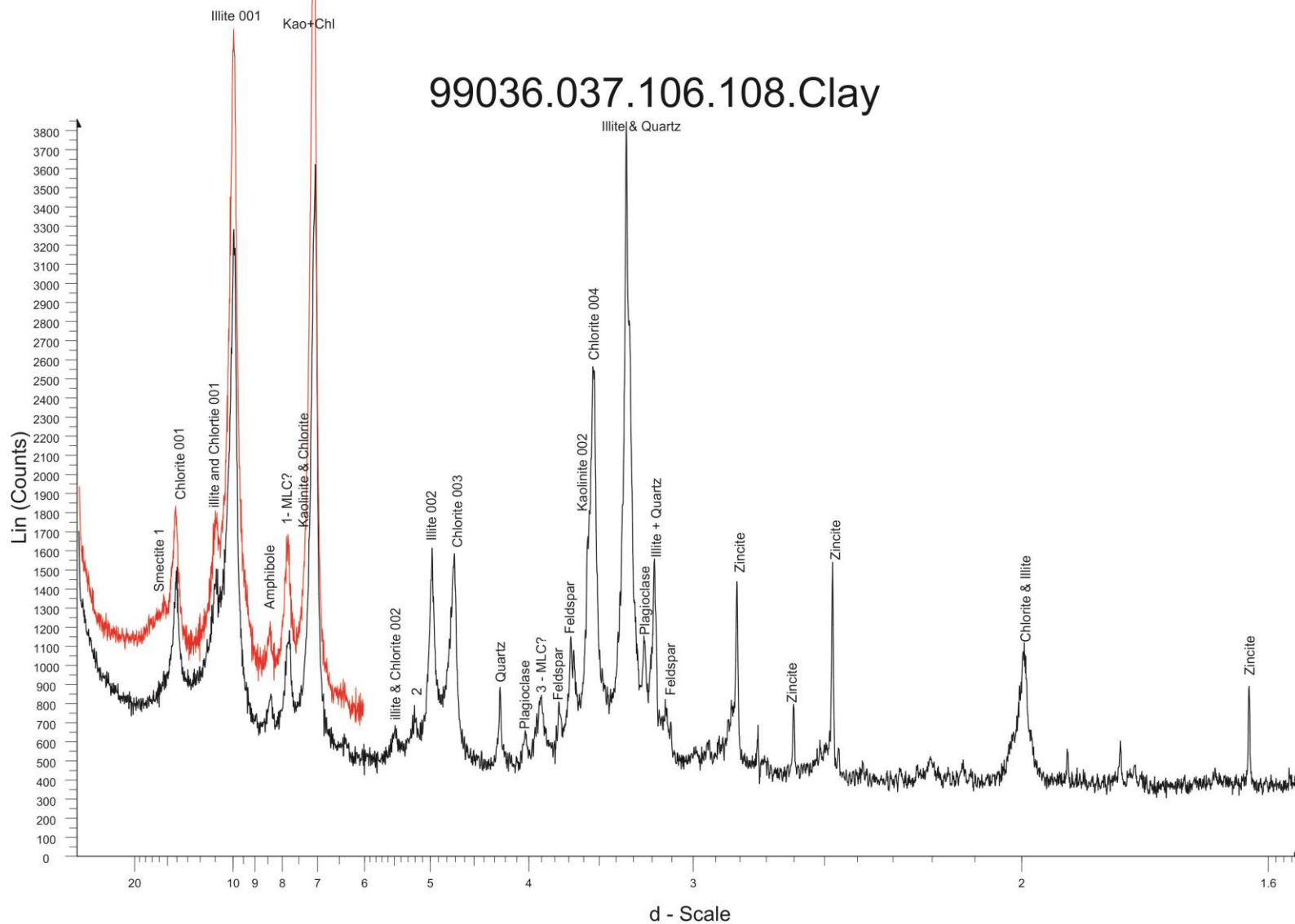
Fig. 6 A – Diffractogram of air dried (black) and glycolated (red) clay at 106 - 108 cm (Type I clay assemblage)
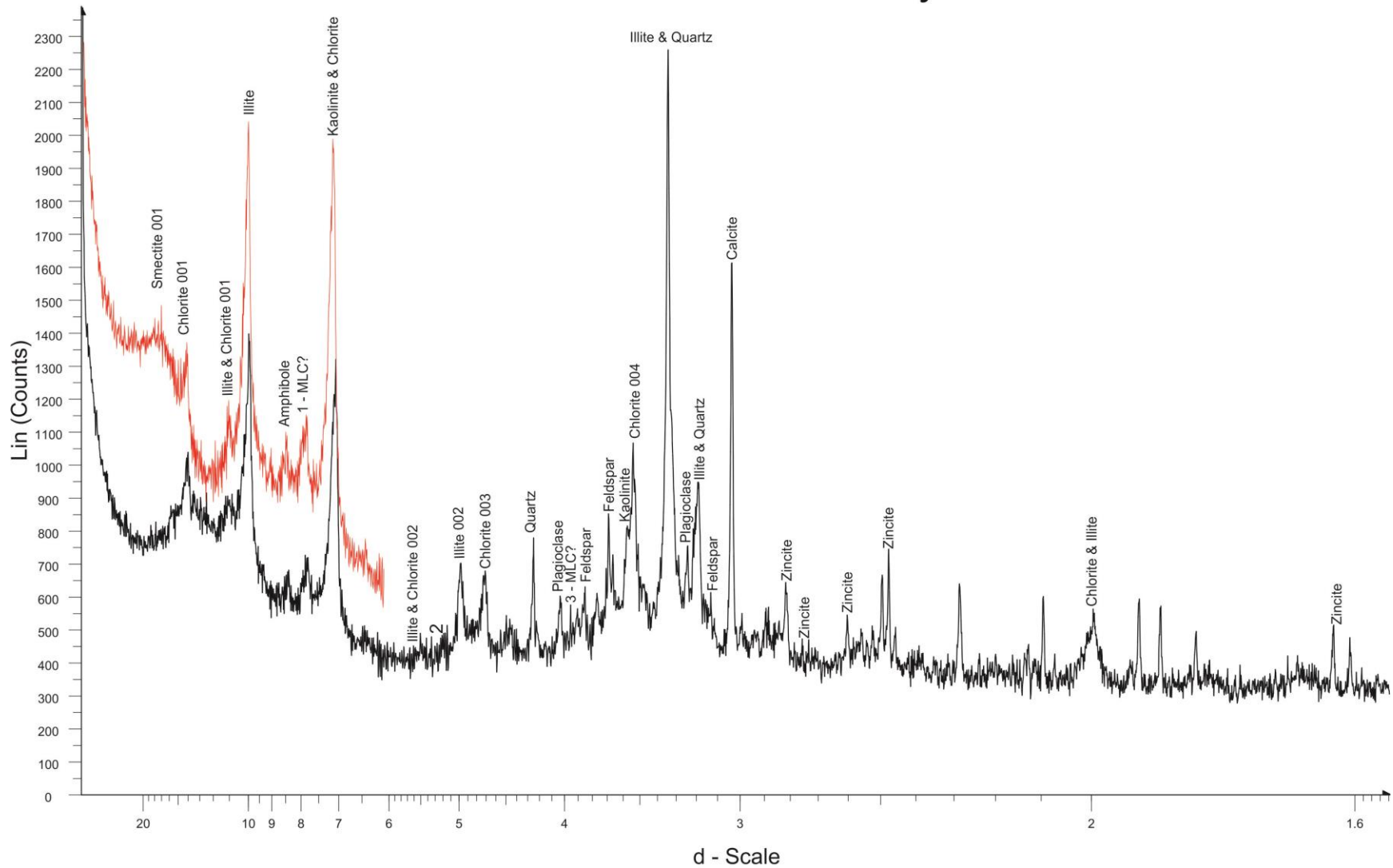
Fig. 6 B – Diffractogram of air dried (black) and glycolated (red) clay at 604 - 608 cm (Type II clay assemblage)
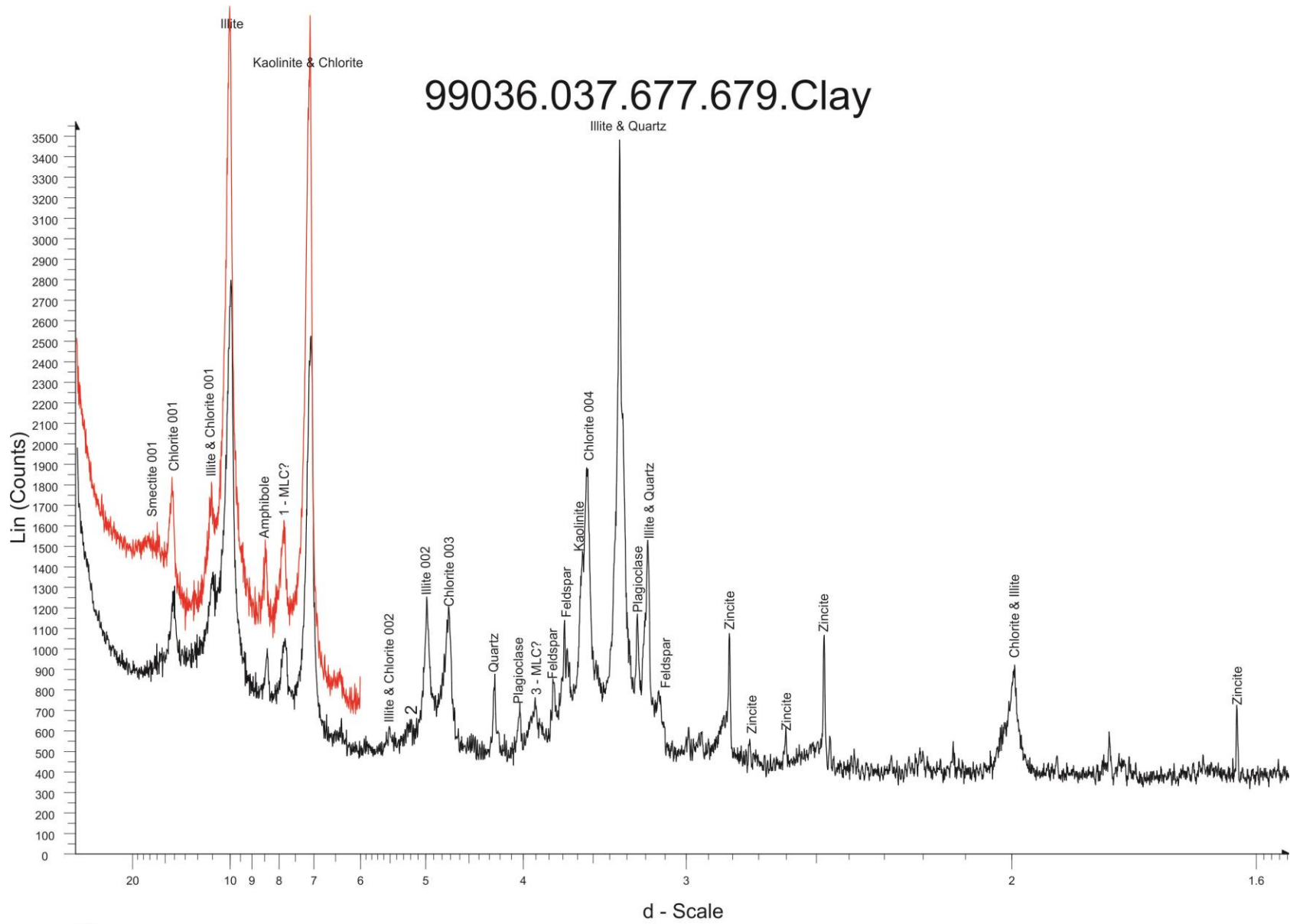
Fig. 6 C – Diffractogram of air dried (black) and glycolated (red) clay at 677 - 679 cm (Type III clay assemblage)
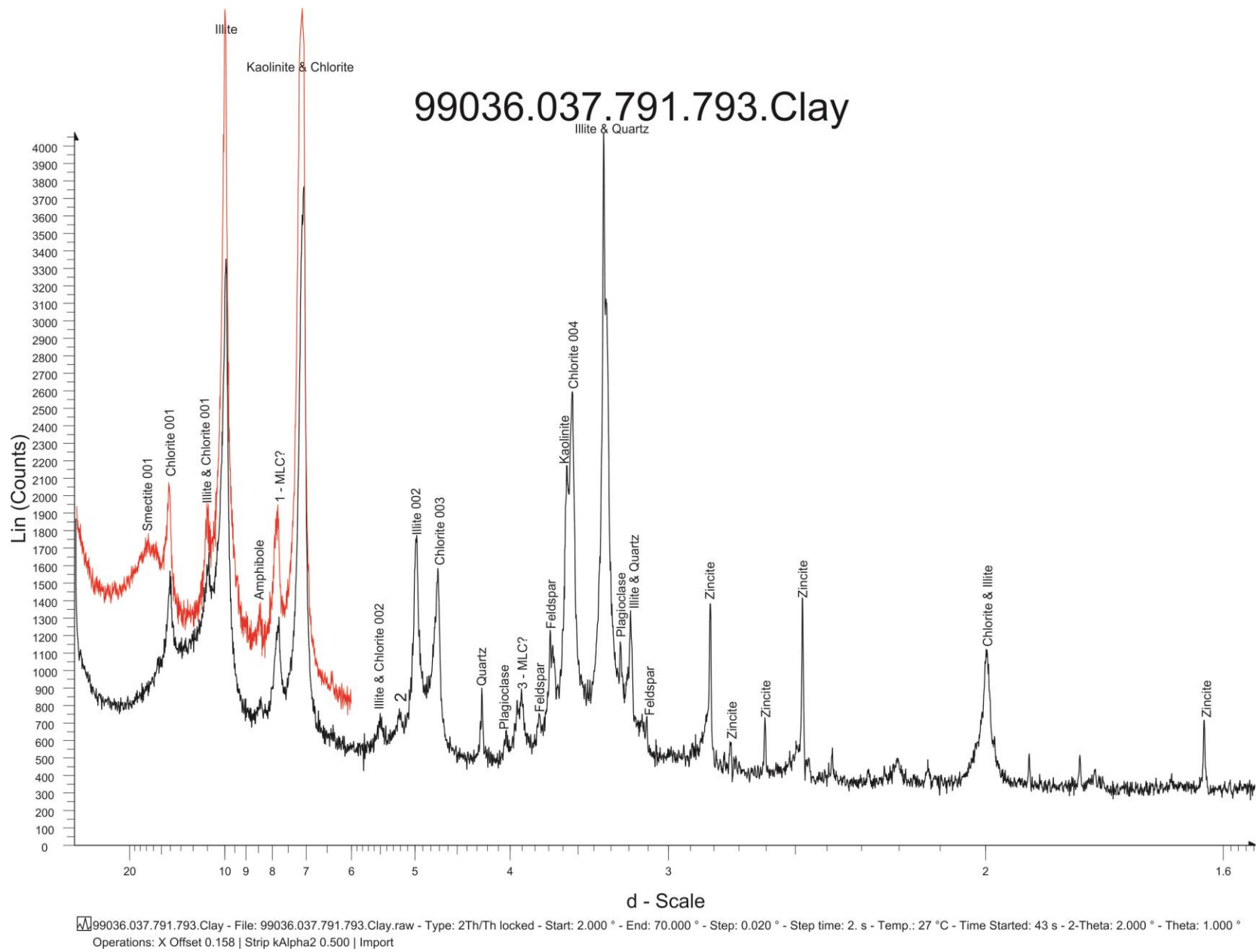
Fig. 6 D – Diffractogram of air dried (black) and glycolated (red) clay at 791 - 793 cm (Type IV clay assemblage)

6.4. Petrological analysis via smear slides

This technique was done to rapidly identify abundances of terrigenous (lithic carbonate grains) and biogenic sources of carbonate such as forams and coccoliths. The variation may indicate differences in sedimentation conditions. The values of abundance are as followed: 0 indicates there is no presence of that particular material. 1 indicates that there are very few grains present; 2 indicates that there is a moderate amount present; 3 represents that the material present is in abundance; while 4 indicates that material dominates the sample.

Depth (cm)	Forams	Lithic Carbonate grains	Coccolith	Sponge spicules	Quartz	Other
1 (PC35)	2	1	3	1	2	(Glauconite) 2
475 (PC 37)	3	1	3	2	2	(Diatoms) 2
555 (PC 37)	1	3	2	1	2	-
605 (PC 37)	3	1	3	2	2	(Diatoms) 2
615 (PC 37)	2	2	3	2	2	(Glauconite) 3
640 (PC 37)	2	2	3	3	2	(Opaques) 3
680 (PC 37)	1	2	1	2	3	(Radiolarians) 2
710 (PC 37)	1	3	2	2	3	(silicoflagellates) 2

Table 3 – Smear slide abundances numbers represent relative amount present

7. Discussion

7.1. Chronology

The overall framework for age is set by C-14 dates (Fig. 7) but is supported by the correlations of the physical properties of the cores (Fig. 4 E). According to the dates obtained (section 4.9) the 23.9 ka date found in the upper interval of unit II indicates that the last glacial maximum (~21 ka) is in unit II. The 28.4 ka date occurs at the top of unit III in core 37 suggests that unit III predates the LGM. The two lower dates also provides a mean sedimentation rate of 16.6 cm/ka for unit III. Extrapolating this sedimentation rate below the 49.5 ka date suggests that the boundary between unit IV and V is approximately in the range of 57 ka. Further extrapolation becomes problematic, assuming constant sedimentation would make the bottom of the core around 100 ka. There is evidence that will be discussed that disproves this constant sedimentation rate for unit V and VI will be discussed below.

Taking this overall framework and attempting to identify the corresponding marine isotopic stages (MIS) is paramount in understanding the paleoclimate. The paleoclimate may be indicative of sediment influx and thus is a good link to the regional context over the past glacial cycle.
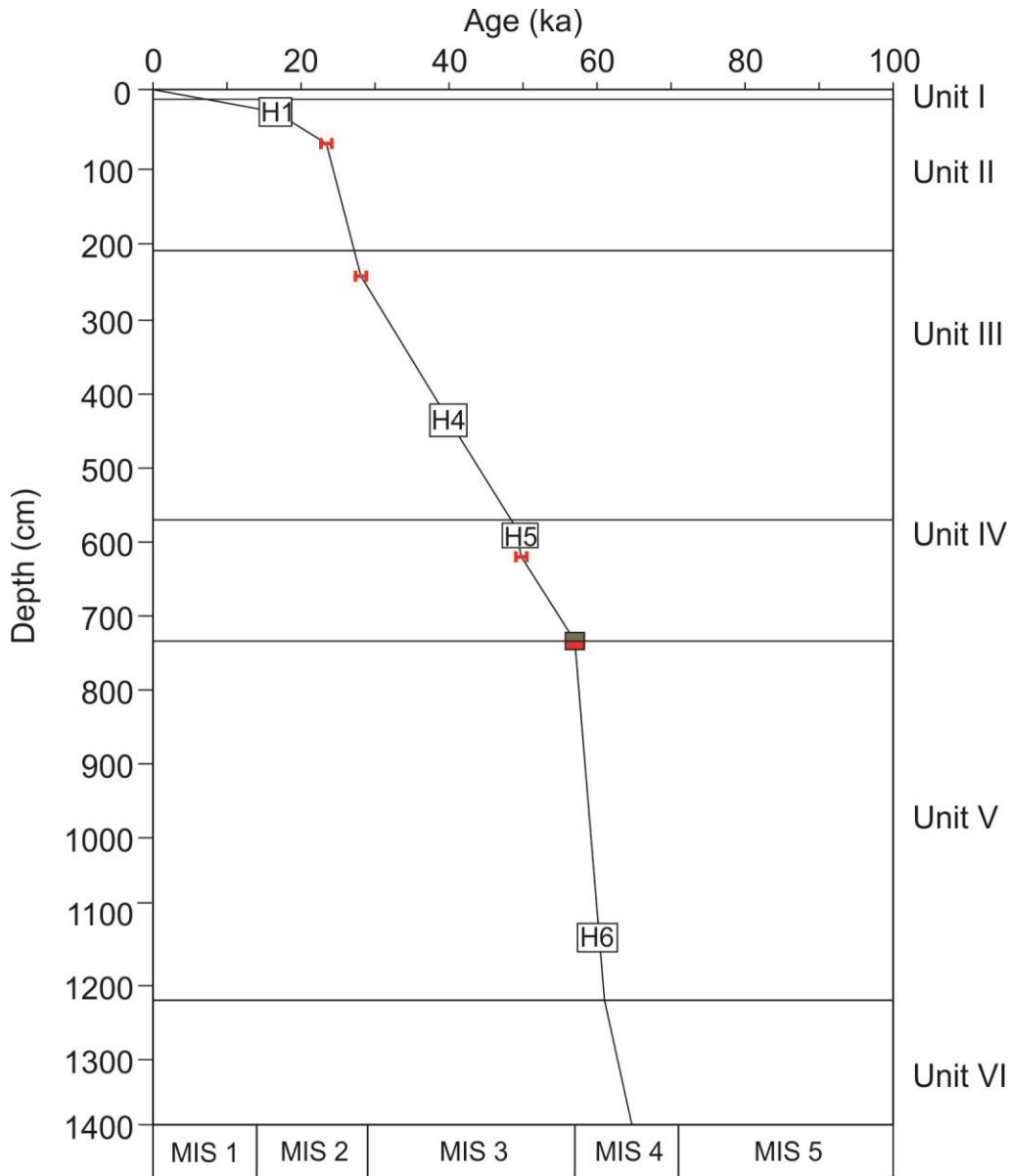
Fig. 7 – Age vs. Depth in piston core 99036-037. H-layers are labelled to their corresponding number and red bars represent C-14 dates with error. The straight line represents a hypothetical constant sedimentation between dated points. Age of MIS and H events from Channell et al. (2012), the brown to red box represents the sedimentological change observed in 37 between MIS 3 and 4

The chronology of PC 37 confirms the correlations between the two cores proposed in Figure 4 E. Piston core 35 has two dates, the first at 259 cm and the other at 690 cm. Correlations 12 and 10 constrain the 28.4 ka date on PC 37 and 28.7 ka on PC 35 to an interval that is reasonable

with expected error on C-14 age dating. The other dates can be confirmed simply on the position once again. The date on PC 35 (21.2 ka) is a younger date and lies above the correlations and age (23.9 ka) on PC 37, this once again is reasonable.

7.2. Recognition of H-events

Heinrich events occur when there is rapid break up and retreat of floating ice sheets, producing numerous icebergs which are then transported farther offshore. These icebergs contain rock mass which was eroded by the ice sheets as they moved across the land. As these icebergs melt, they release the rock mass and it is deposited on the sea floor as ice rafted debris. These events typically take place, but are not limited to, periods of glaciation. In the NW Atlantic, they have been documented as being intervals with high detrital carbonate IRD (Heinrich, 1988), as a result of the dominant supply from the Hudson Strait ice stream. Heinrich Layers can thus be recognized from high Ca/Ti and L* (unless carbonate sources are biogenic in origin) and by abundant carbonate IRD.

This study uses with the standard Heinrich layers labelling scheme of H1 − H6 (youngest to oldest). Heinrich events do in fact occur in older sediments (H7, H7A…), but are often hard to identify, as the signatures become weak and are often overprinted by other processes. When attempting to recognize Heinrich layers in piston core 37 (Fig. 4 C) there are some indicators that Heinrich 1 (H1) is located at the top of the core. The presence of 100% IRD carbonate grains at 90 cm (Fig. 5 A) provides some evidence, but with the number of grains being limited lessens the confidence level of this interval. However the C-14 date at 60 cm of 23.9 ka suggests that this indeed is a possibility. There is no evidence to strongly support the occurrence of H2 and H3 in piston core 37. This location is fairly far offshore and thus these Heinrich layers may not extend enough laterally. A Heinrich layer (H4) occurs between our C-14 dates of 28.4 and 49.5 ka. This

57

interval contains the presence of 8 carbonate grains at 440 cm (Fig. 5A) and based on reasonable

sedimentation rate, extrapolated between the two dates, matches the timing of H4 at 40 ka

(Hemming 2004). H5 is based on the higher presence of carbonate grains in the smear slide at

555 cm (Table 3). This smear slide may be misleading due to the small amount of material

needed along with the moderate concentration of quartz which is a terrigenous source. Thus this

cannot be confidently interpreted. H6 is another layer that cannot be placed with certainty.

However we can compare our downcore to an up flow equivalent by Channell et al. (2012),

which is a robust data set from a location seaward of Orphan Knoll. This area is affected by the

WBUC and the Labrador Current, which effectively simulate this study area. Based on this

comparison, it provides evidence that H6 should be towards the bottom of the core since the

boundary between MIS 4 and MIS 5 occurs at 71 ka. H6 is essentially in the middle of MIS 4

and occurs at approximately 60 ka. This is reasonable based on our inferred 57 ka contact

between units IV and V.
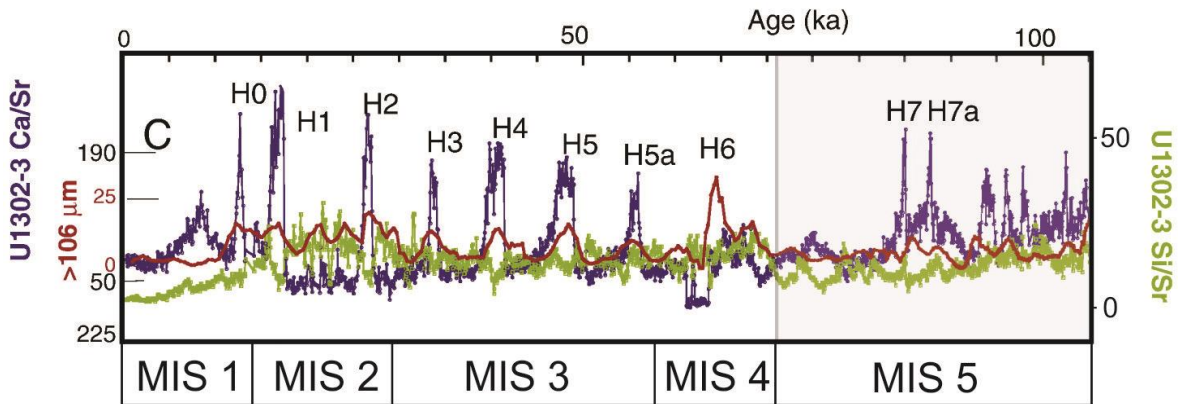
Fig. 8 – XRF scanning ratios depicting age correspondence of H-layers in comparison to Marine
Isotopic stages at 10DP hole U1302-3 near Orphan Knoll (modified from Channell et al. 2012)

7.3. Downcore variation in sources

A number of methods were used to attempt to understand the variations in sources, specifically: IRD data, grain size data, clay mineral data, colour data and Nd isotopes. Unit I is likely the modern sea floor as it is a carbonate rich foram ooze interval as described in HEBBLE (Nowell &Hollister, 1985). Unit II contains red-brown muds like those on the upper slope (Jenner et al., 2010) indicating that they have travelled down the slope. As previously presented in section 6.2, Nd isotopes reveals that IRD was probably derived from the Appalachians and not from Precambrian terranes further north such as Greenland (Fig. 5B). This confirms that unit II involves downslope transport. Unit III is similar to unit II in clay minerals and primary sedimentary structures, although it is less red in colour, and it is highly probable that this unit also involves downslope transport. Unit IV is a unit which contains higher smectite content (Fig. 6 B). The distribution of smectites is primarily on the outer continental shelf from Labrador to Nova Scotia (Piper & Slatt, 1977) and from deep marine basalts (Fagel et al,. 1996). In addition unit IV is characterized by having a lower ratio of chlorite 004/001, indicating that low grade metamorphic detritus from the Appalachians is less abundant. This evidence allows for the possibility of sediment being reworked by the WBUC laterally alongslope. This reworking of sediments can be seen in the grain size (Fig. 4D), where unit IV shows an abundant concentration of silt (Appendix B, Figs. B5- B8). This concentration around the silt range indicates that there is bottom current activity which is depositing sediment of this size fraction and preferentially winnowing finer clays. In addition the other units in this core have higher values of a*. This evidence of this unit has a lower value of a* or red material which suggests that it is unlike the more red brown material which is derived from the slope as previously discussed, once again suggesting that it has been reworked by the WBUC. The last contributor to

the potential of alongslope transport is the presence of a Heinrich event. Heinrich events

introduce cooler waters which can be analogous of stronger cold water currents, supporting the

idea of greater current strength but also stronger surface currents as well. Unit V is like unit II

but there is more evidence for downslope transportation. Nd isotope from 980 cm (Fig. 5 B)

suggests that the material was also derived from the Appalachians or Grenville Province,

deposited as a turbidite rather than IRD. When looking at the lithologies of these grains in this

bed it is predominantly sandstones which may indicate that it is Appalachian in origin. The

relative age of the material rules out the possibility of alternative more northern sources. Unit VI

has Nd isotopes from IRD at 1340 cm also indicate that this unit has Appalachian material in it.

This unit also has similar characteristics as unit V.

7.4. Downcore variation in sedimentary processes

Sedimentary processes contribute to the development of the sediments history. The use of

X-radiographs, grain size (Appendix B), and the sediment source information discussed in the

previous section are used to construct the history of the sediments described in this section. Unit

I is likely modern sea floor as described in HEBBLE (section 2.4). Unit II is composed of many silt

to mud laminae which are indicative of turbidites. This suggests that this unit is downslope as

proposed. Unit III lacks information to classify it as a specific sedimentary process; however it is

similar to unit II in most regard and thus is likely downslope but just lacks structure in the core.

Unit III will be addressed in the next section to possibly identify its origin. However if these

cores were analysed to obtain orientations of magnetic fabrics as described in Shor et al., (1984)

any uncertainty could potentially be resolved. Unit IV has more bioturbation, this suggests a

slower sedimentation rate. The grain size shows a mode in the silt range that probably implies

bottom currents. This unit also has a significant amount of forams and coccoliths. This carbonate rich interval composed of the biogenic material suggests a slow terrigenous sediment supply. Unit V is like unit II but contains more downslope/turbidity current characteristics. Specifically the granule gravel bed which is presumed to be a turbidite with an underlying sand bed presumably a sharp base, but it is not clear if it was being winnowed. Unit VI is important but not completely understood. The sediment record for this area has not typically gone back to this extent. In term of unit by unit sediment transportation, it appears to be mostly downslope, however something different is occurring in unit IV, probably alongslope by analogy with HEBBLE sediment descriptions of Unit 1.

Units V and VI appear to have a higher sedimentation rate, but due to the occurrence of turbidites and other structures that influence a larger potential influx of sediments. The consistent rate of sedimentation that would place the bottom of the core at approximately 100 ka cannot be implied. This suggests that in fact H6 does fit our model at a depth approximately 1150 cm. This places an age of approximately 67 - 70 ka at the bottom of core 37.

7.5. Link to glacial history of the shelf

Interstadial stages represents warmer climates during which rapid temperature oscillation events, Dansgaard-Oeschger (D-O) events, occurred in Greenland and the North Atlantic regions (Meerbeeck, 2009). These events are believed to be in association with the resurgence of the thermohaline circulation (THC) from a weak state to a stronger state. This strengthening of the THC is a potential factor in why there is evidence for a stronger alongslope sediment transportation influence during unit IV. The abrupt sedimentological change from unit IV to V may correspond to changes observed in the NW Atlantic between MIS 3 and MIS 4 (Channell et

al., 2012).

Unit III is approximately interstadial in Nova Scotia (Fig. 10), which is problematic for understanding its origin. Unit III could have occurred from three possible events; (1) rare submarine landslides of older sediments. (2) Sediment plumes from the Laurentian Channel which are being reworked alongslope, or (3) from residual ice on Nova Scotia. This ice would create melt water and sediment plumes may have been deposited and reworked or crossed the shelf then deposited. Figure 10(**2**) shows uncertainty in the ice extent, this uncertainty derives from other records on land that show evidence of mastodons roaming during this time (Dredge & Thorleifson, 1987). This means that there must have been sufficient deglaciation to allow for the roaming of mastodons. The most likely of the three proposed hypotheses is (3), as unit III is characterized by having lower values of a*. Both (1) and (2) would likely introduce red sediments into the system thus producing higher values of a*.
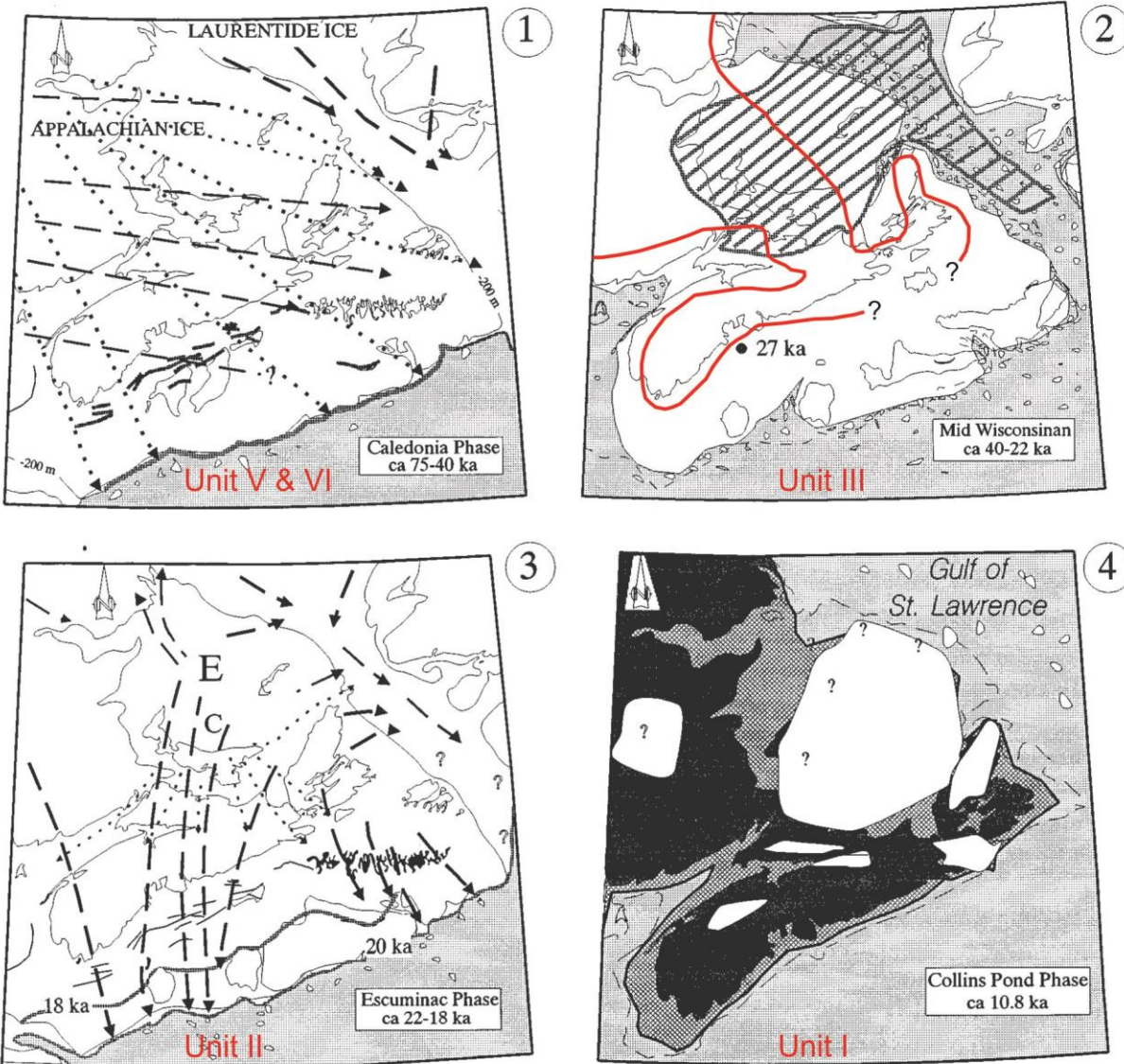
Fig. 9 – Previous ice extents over the Atlantic Canada modified from Stea et al. (1998.) Ice is represented by white (**1**) Caledonia Phase unit V and VI (**2**) Middle Wisconsinan ice retreat, maximum based on Stea et al. (1998), minimum (red line) based on Dredge and Thorleifson (1987) (unit III) (**3**) Escuminac phase (unit II) (**4**) Collins pond phase (unit I)

Stadials in contrast are colder times which can allow for shelf crossing ice. This ice can transported large quantities of local red-bed material south onto the shelf and slope (Stea et al 1998) and also deposits till tongues on the upper slope (Fig. 11). Figure 11 shows $\delta^{18}O$ which represent stadial and interstadial times. Stadial times are characterized by higher values of $\delta^{18}O$,

for example on Figure 11 at ~ 18 ka (LGM) there are higher values. While the top of the δ^{18}O

plot represents the Holocene (interstadial) and shows lower values.
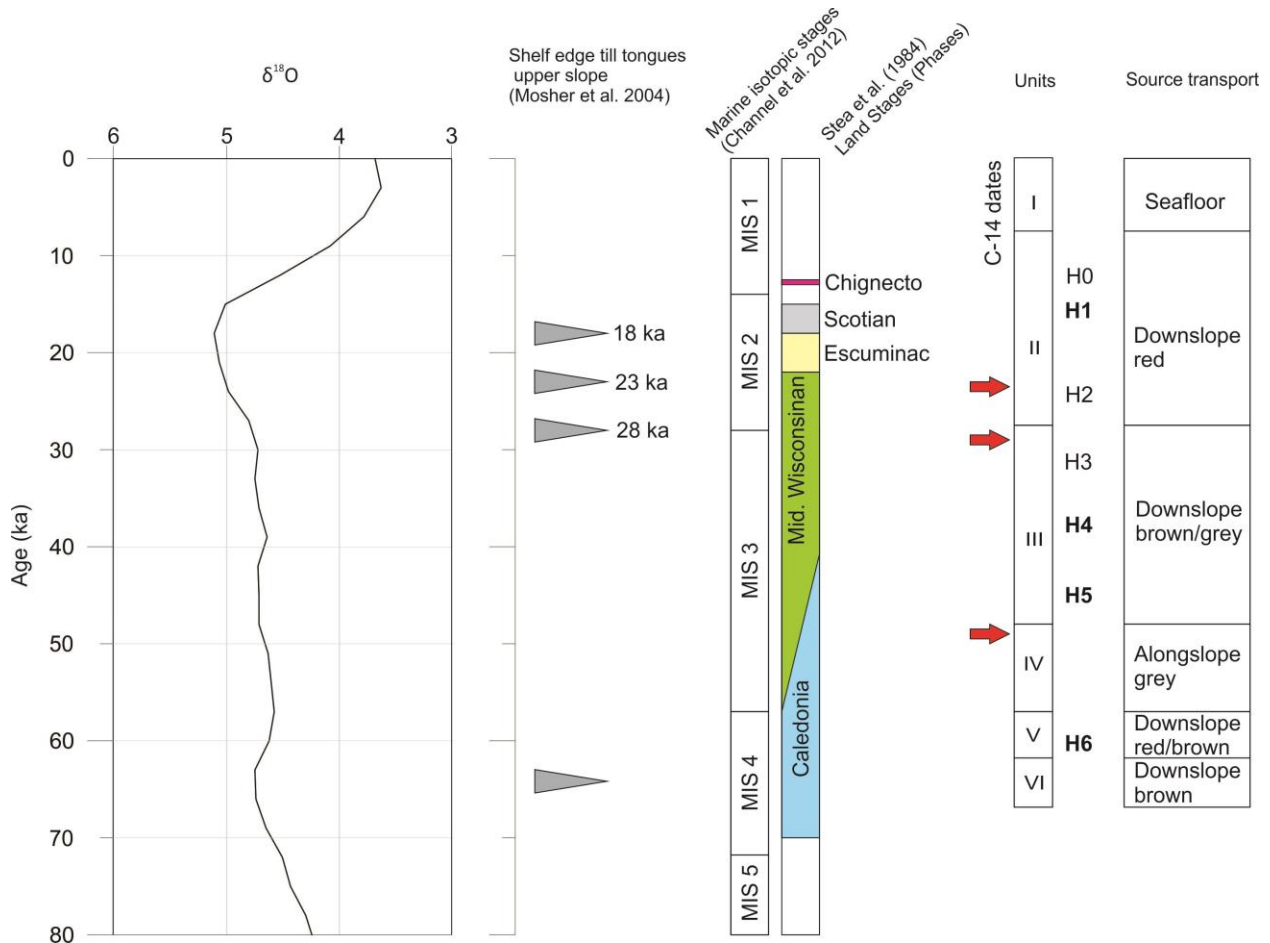
Fig. 10 – Ice phases/extent compared to units, red arrows indicates C-14 dates from PC 37 and H-events that are bold are been identified in core 37 from the study area. Ages from Mosher et al. (2004) have been corrected to calibrated ages, and the position of the deepest till tongue is shown in the middle of MIS 4. Ages of phases from Stea et al. (1998) have also been calibrated. Global benthic isotope curve from Heslop et al. (2002).

The glacial cycle seems to some a moderate to strong correlation between downslope and stadial times, specifically unit II, V and VI. However unit IV seems problematic in this approach as it appears to be alongslope, this unit appears to be during an intermediate stage of δ^{18}O (Fig. 11). The C-14 date of 49.5 ka falls in unit IV which validates that unit IV is within the early part

of MIS 3 (Fig. 7). This interstadial time corresponds to the lightest part of the isotope curve in MIS 3 (Fig. 11), potentially providing some evidence that that there were ice fluctuations in the mid Wisconsinan ice retreat.

The older relative age of the granule bed from Nd isotope (Fig. 5 B) may be explained by the corresponding glacial phase for unit V (Fig. 11). The source of the Caledonia phase glacier is not well known due to the lack of striations and erratics on land but it is believed to have originated in the Canadian Shield and flowed across the North and Central regions of New Brunswick (Stea et al., 1998). Erratics offshore are found in reworked younger sediments which indicated that the ice extended out to the Scotian Shelf end moraine complex or beyond (Stea et al., 1998). This provides evidence that sources of sediments are directly linked to glaciation advances and retreats.

8. Conclusions

The purpose of this thesis was to identify the role of downslope versus alongslope sediment transportation over the last glacial cycle. The goal was to use the physical properties of piston core 35 and 37 to identify the sourcing of the sediments.

1) Validates the statement by Emery & Uchupi (1984), "physiographic evidence supported by sedimentology indicates that the continental rises are due mainly to deposition by turbidity currents, although geostrophic bottom currents and pelagic depositions of organic sediments contribute"

2) This study has developed a robust age model back to 70 ka controlled by C-14 dates and recognition of H1, H4, H5, H6 from IRD and/or high Ca/Ti.

3) All of the units described appear to involve predominant downslope transportation with the exception of Unit I (Holocene) and unit IV. This unit has the strongest case for alongslope transportation, having a higher concentration of smectites as seen in the diffractograms (Fig. 6B), along with the abundance of coccoliths which indicates a slow terrigenous sediment supply.

4) The relative comparison of depth to age indicates sedimentation rate was not constant and was highest in stadials when glacial ice crossed the Scotian Shelf.

References

Bennett, R., A., Schell, T., Bartlett, J., Blasco, S., Hughes-Clarke, J., Scott, D., MacDonald, A., Rainey, W. 2008. Cruise Report Amundsen 2004-804: Beaufort Sea / Amundsen Gulf / Northwest Passage, June 23 - August 27, 2004. Geological Survey of Canada, Open File 5798. Natural Resources Canada.

Bouma, A. H., 1969. Methods for the study of sedimentary structures (pp. 140-244). New York: Wiley-Interscience.

Carroll, D., 1970. Clay minerals: A guide to their X-ray identification Vol. 126. Geological society of America.

Channell, J. E. T., D. A. Hodell, O. Romero, C. Hillaire-Marcel, A. de Vernal, J. S. Stoner, A. Mazaud, & U. Röhl., 2012. A 750-kyr detrital-layer stratigraphy for the North Atlantic (IODP Sites U1302–U1303, Orphan Knoll, Labrador Sea). Earth and Planetary Science Letters 317:218-230.

Daly, R. A. ,1936. Origin of submarine canyons. American Journal of Science, **186**: 401-420.

Davies, T.A., & Laughton, A.S., 1972. Sedimentary processes in the north Atlantic. In: Initial reports of the D.S.D.P. (Ed. By A. Laughton, W.A. Berggren et al.), **12**: 905-934

Debret, M., Sebag, D., Desmet, M., Balsam, W., Copard, Y., Mourier, B., Susperrigui, A.S., Arnaud, F., Bentaleb, I., Chapron, E. & Lallier-Vergès, E., 2011. Spectrocolorimetric interpretation of sedimentary dynamics: The new Q7/4 diagram. Earth-Science Reviews **109**(1): 1-19.

Dredge, L., & Thorleifson, L. H., 1987. The Middle Wisconsinan history of the Laurentide ice sheet. Géographie physique et Quaternaire, **41**(2): 215-235.

Eittreim, S. & Ewing, M., 1972. Suspended particulate matter in the deep waters of the North American basin. Studies in Physical Oceanography. New York, **2**: 123-167.

Emery, K. O., & Uchupi, E., 2012. The geology of the Atlantic Ocean. Springer Science & Business Media.

Fagel, N., Robert, C., & Hillaire-Marcel, C., 1996. Clay mineral signature of the NW Atlantic Boundary Undercurrent. Marine Geology, **130**(1): 19-28.

Farmer, G. L., Barber, D., & Andrews, J., 2003. Provenance of Late Quaternary ice-proximal sediments in the North Atlantic: Nd, Sr and Pb isotopic evidence. Earth and Planetary Science Letters, **209**(1): 227-243.

Gross, T. F., Williams, A. J., & Newell, A. R. M., 1988. A deep-sea sediment transport storm. Nature, **331**: 515-521

Hagen, S., & Keigwin, L. D., 2002. Sea-surface temperature variability and deep water reorganisation in the subtropical North Atlantic during Isotope Stage 2–4. Marine Geology, **189**(1): 145-162.

Heinrich, H., 1988. Origin and consequences of cyclic ice rafting in the northeast Atlantic Ocean during the past 130,000 years. Quaternary Research, **29**(2): 142-152.

Heslop, D., Dekkers, M.J., Langereis, C.G., 2002. Timing and structure of the mid-Pleistocene transition: records from the loess deposits of northern China. Palaeogeogr. Palaeoclimatol. Palaeoecol. **185**: 133– 143.

Hillaire-Marcel C., Vernal, A. D., Bilodeau, G., & Wu, G., 1994. Isotope stratigraphy, sedimentation rates, deep circulation and carbonate events in the Labrador Sea during the last 200 ka. Canadian Journal of Earth Sciences, **31**: 63-89.

Horn, D. R., Ewing, M., Horn, B. M., & Delach, M. N., 1971.Turbidites of the Hatteras and Sohm abyssal plains, western North Atlantic. Marine Geology, **11**(5): 287-323.

Jenner, K.A., Piper, D.J., Campbell, D.C., & Mosher, D C., 2010. Piston cores and supporting high-resolution seismic data, Scotian Slope, Eastern Canada: data and interpretations. Geological Survey of Canada, Open File 6558

Keigwin, L. D., & Boyle, E. A., 1999. Surface and deep ocean variability in the northern Sargasso Sea during marine isotope stage 3.Paleoceanography, **14**(2), 164-170.

Lewis, C. F. M., Miller, A. A. L., Levac, E., Piper, D. J. W., & Sonnichsen, G.V., 2012. Lake Agassiz outburst age and routing by Labrador Current and the 8.2 cal ka cold event. Quaternary International **260**: 83-97.

Louden K.E., Tucholke, B. E., & Oakey, G. N., 2004: Regional anomalies of sediment thickness, basement depth and isostatic crustal thickness in the North Atlantic Ocean. Earth and Planetary Science Letters **244**(1): 193-211.

Mao, L., Piper, D. J.W., Saint-Ange, F., Andrews, J. T., & Kienast, M., 2014. Provenance of sediment in the Labrador Current: a record of hinterland glaciation over the past 125 ka. Journal of Quaternary Science **29**(7): 650-660.

Marshall, N.R., Piper, D. J., Saint-Ange, F., & Campbell, D. C., 2014. Late Quaternary history of contourite drifts and variations in Labrador Current flow, Flemish Pass, offshore eastern Canada. Geo-Marine Letters **34**(5): 457-470.

McCave, I. N., Manighetti, B., & Robinson, S. G., 1995. Sortable silt and fine sediment size/composition slicing: Parameters for palaeocurrent speed and palaeoceanography. Paleoceanography, **10**(3): 593-610.

Mosher, D.C., Piper, D. J., Campbell, D. C., & Jenner, K. A., 2004. Near-surface geology and sediment-failure geohazards of the central Scotian Slope." AAPG Bulletin, **88**(6): 703-723.

Mueller-Michaelis, A., & Uenzelmann-Neben, G. 2013. The development of the Western Boundary Undercurrent (WBUC) in a changing climate since the beginning of the Miocene. Kolloquium Freiberg

Nowell, A.R., & Hollister, C.D., 1985. The objectives and rationale of HEBBLE, Deep Ocean Sediment Transport - Preliminary Results of the High Energy Benthic Boundary Layer Experiment. Marine Geology **66**: 1-11.

Piper D.J.W. & Gould K., 2004. Late Quaternary geological history of the continental slope, South Whale Basin, and implications for hydrocarbon development. Geological Survey of Canada, Current Research 2004-D1, 13 pp.

Piper D.J.W., 1988: Glaciomarine sediments on the continental slope off eastern Canada. Geoscience Canada 15, 23-28.

Piper, D. J. W., & Stow, D. A. V., 1991. Fine-grained turbidites. Cycles and events in stratigraphy, Springer. 360-376.

Piper, D. J., & Slatt, R. M., 1977. Late Quaternary clay-mineral distribution on the eastern continental margin of Canada. Geological Society of America Bulletin, **88**(2): 267-272.

Piper, D.J.W., 2005 Late Cenozoic evolution of the continental margin of eastern Canada. Norwegian Journal of Geology, **85**: 231-244.

Reimer, P.J., Bard, E., Bayliss, A., Beck, J. W., Blackwell, P. G., Ramsey, C. B., ... & Grootes, P. M., 2013. IntCal13 and Marine13 radiocarbon age calibration curves 0–50,000 years cal BP. Radiocarbon, **55**(4): 1869-1887

Rebesco, M., Hernández-Molina, F. J., Van Rooij, D., & Wåhlin, A., 2014. Contourites and associated sediments controlled by deep-water circulation processes: State-of-the-art and future considerations. Marine Geology, **352**: 111-154.

Shimeld, J., 2004. A comparison of salt tectonic subprovinces beneath the Scotian Slope and Laurentian Fan. In 24th Annual GCS-SEPM Foundation Bob F. Perkins Research Conference, Houston, pp. 291-306.

Skene, K. I., & Piper, D. J., 2003. Late Quaternary stratigraphy of Laurentian Fan: a record of events off the eastern Canadian continental margin during the last deglacial period. Quaternary International, **99**: 135-152.

Smith, P.C., Petrie, B.D., Elliott, J.A., Oakey, N.S., & Bugden, G.L, 2014. Coastal Ocean Circulation Studies. Voyage of Discovery **17**: 149-157

Stea, R.R., Piper, D. J. W., Fader, G. B. J., & Boyd, R., 1998. Wisconsinan glacial and sea-level history of Maritime Canada and the adjacent continental shelf: a correlation of land and sea events. Geological Society of America Bulletin **110**(7): 821-845.

Stuiver, M., Reimer, P.J., 1993. Extended 14C database and revised CALIB radiocarbon calibration program. Radiocarbon, **35**, 315e330.

Uchupi, E., & Austin Jr, J. A., 1979. The stratigraphy and structure of the Laurentian Cone region. Canadian Journal of Earth Sciences, **16**(9): 1726-1752.

Weitzman, J., Ledger-Piercey, S., Stacey, C., Strathdee, G., Piper, D. J. W., Jarrett, K. A., & Higgins, J., 2014. Logs of short push cores, deep-water margin of Flemish Cap and the eastern Grand Banks of Newfoundland; Geological Survey of Canada, Open File 7148, 389 pp

White, D.C., 2014. Variation in style of overpressure in Scotian Shelf wells, Scotian Basin. (B.Sc Honours thesis) Saint Mary's University, Halifax, Nova Scotia

Zimmerman, H. B., 1972. Sediments of the New England continental rise. Geological Society of America Bulletin, **83**(12), 3709-3724.

Appendix A

Correlations between 35 PC and 37 PC in core photography
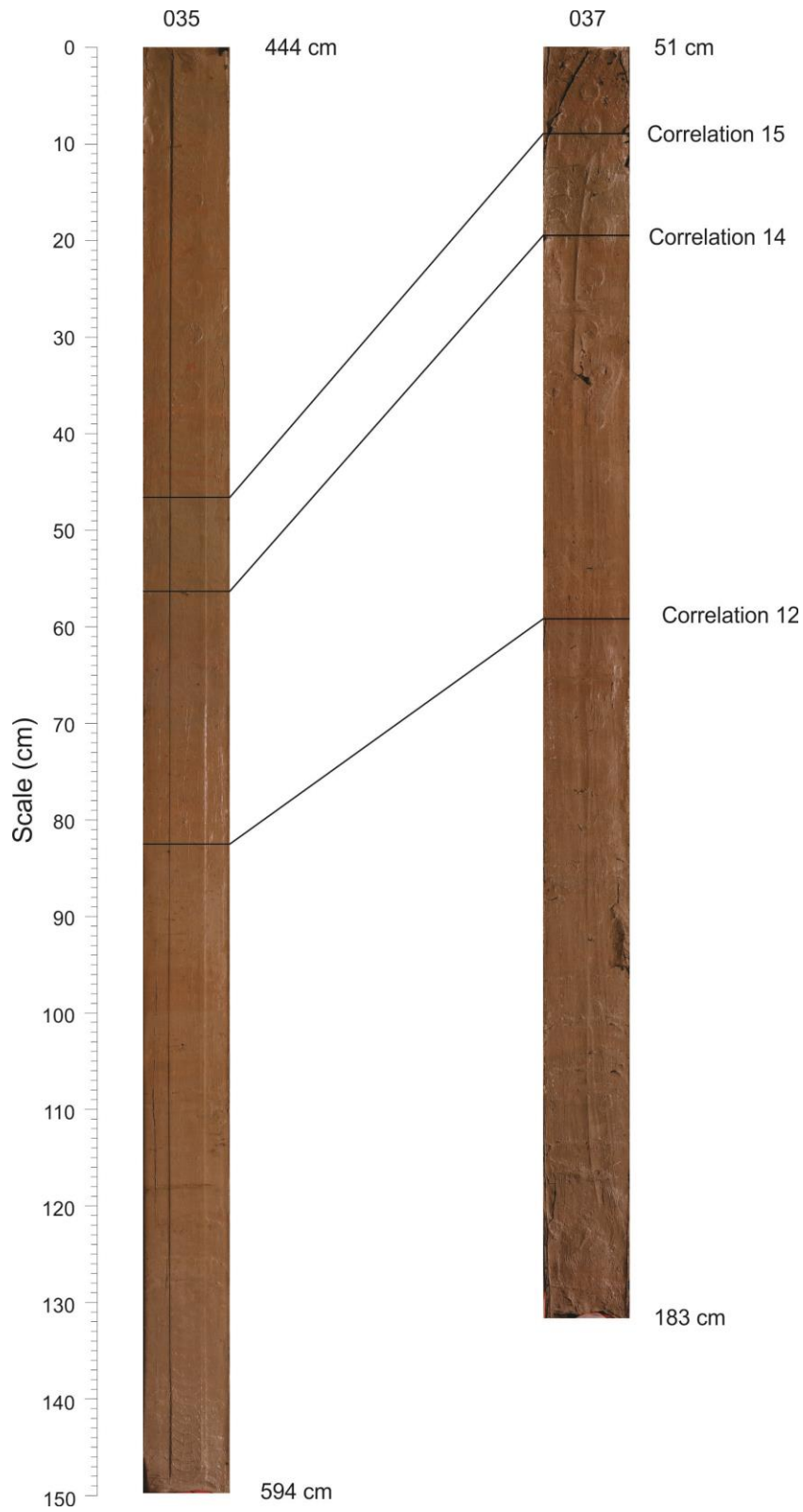
Fig. A-1 – Correlations 12, 14 and 15 between piston cores 35 and 37 depicted on core photography
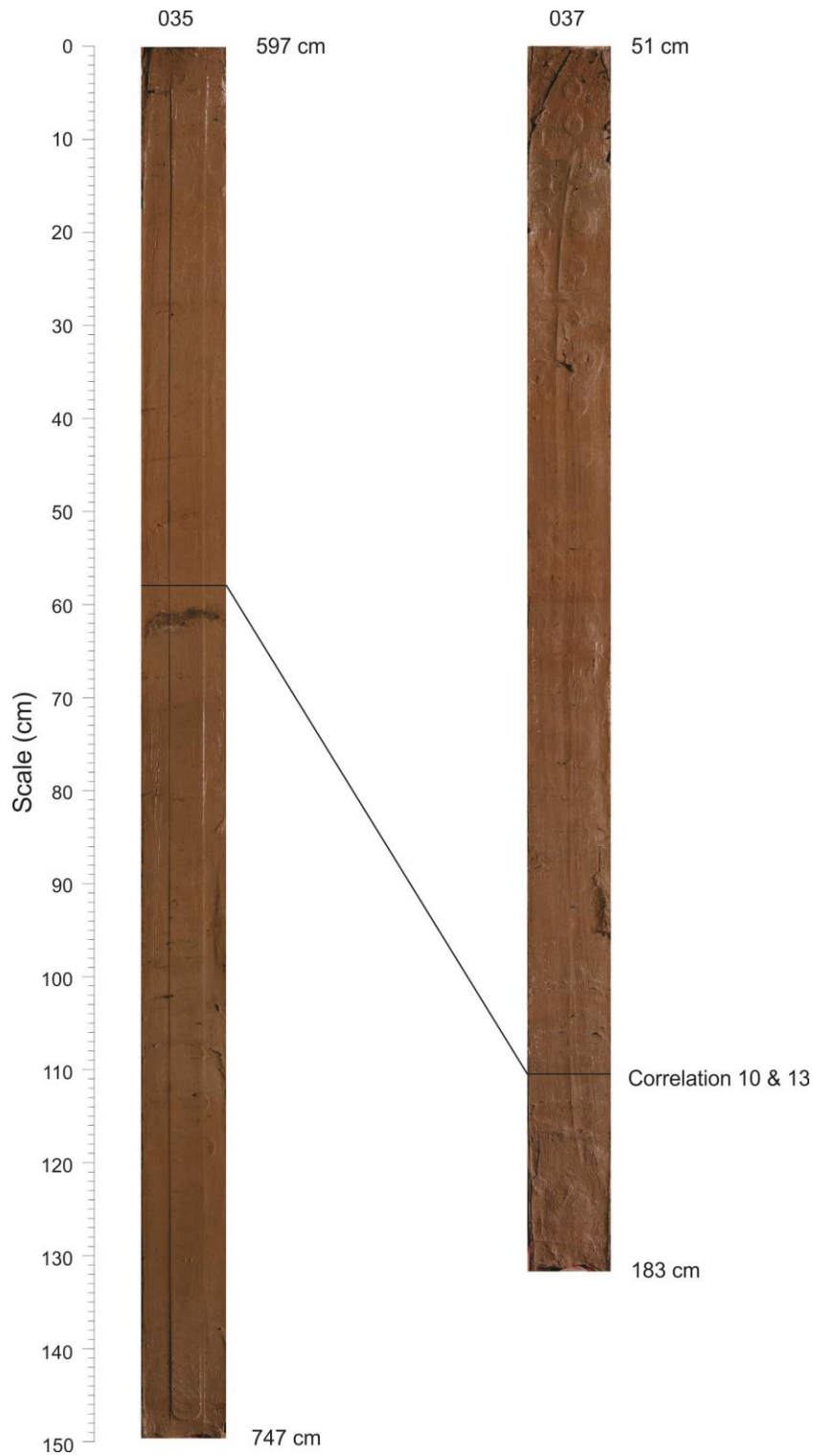
Fig. A-2 – Correlations 10 and 13 between piston cores 35 and 37 depicted on core photography
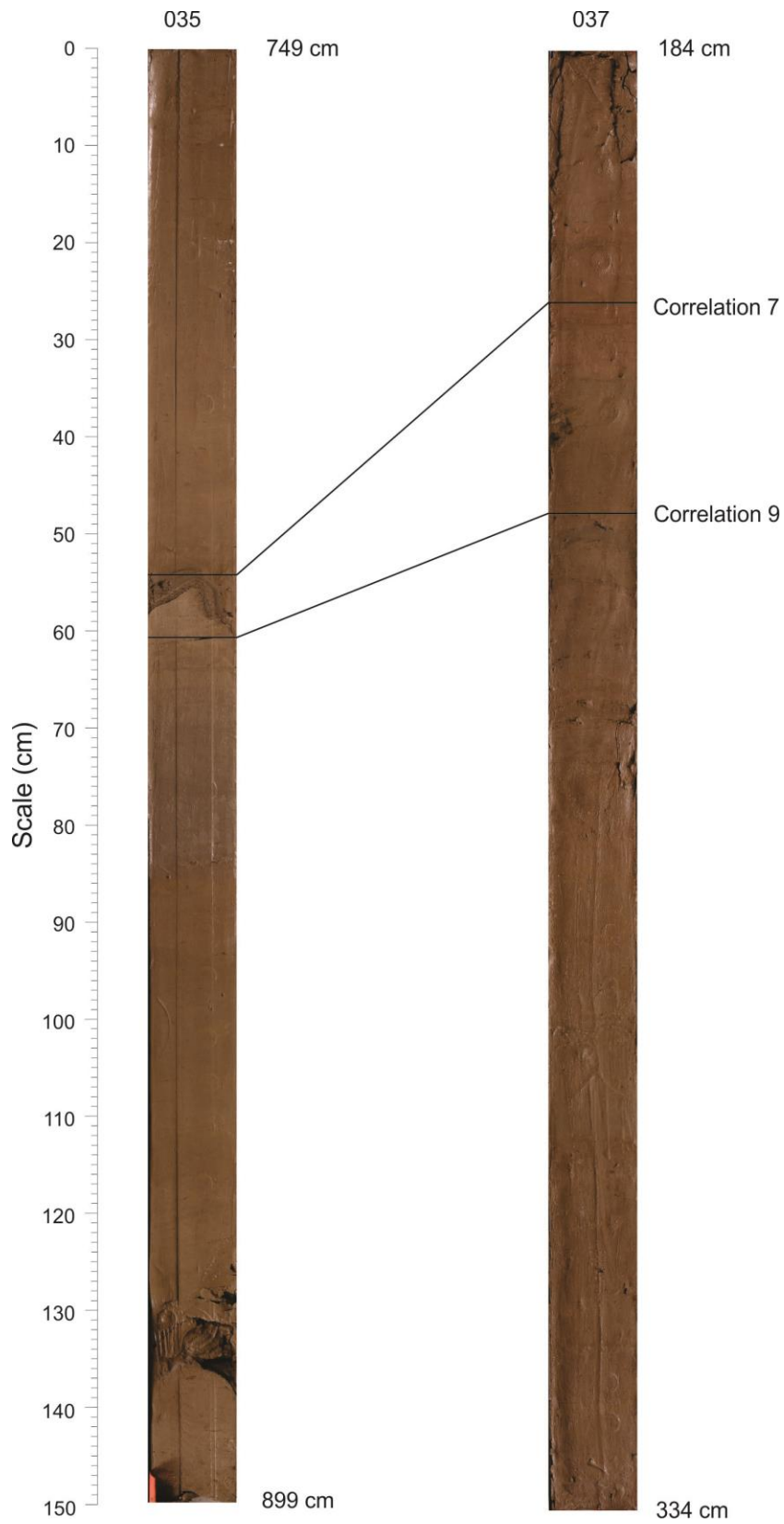
Fig. A-3 – Correlations 7 and 9 between piston cores 35 and 37 depicted on core photography
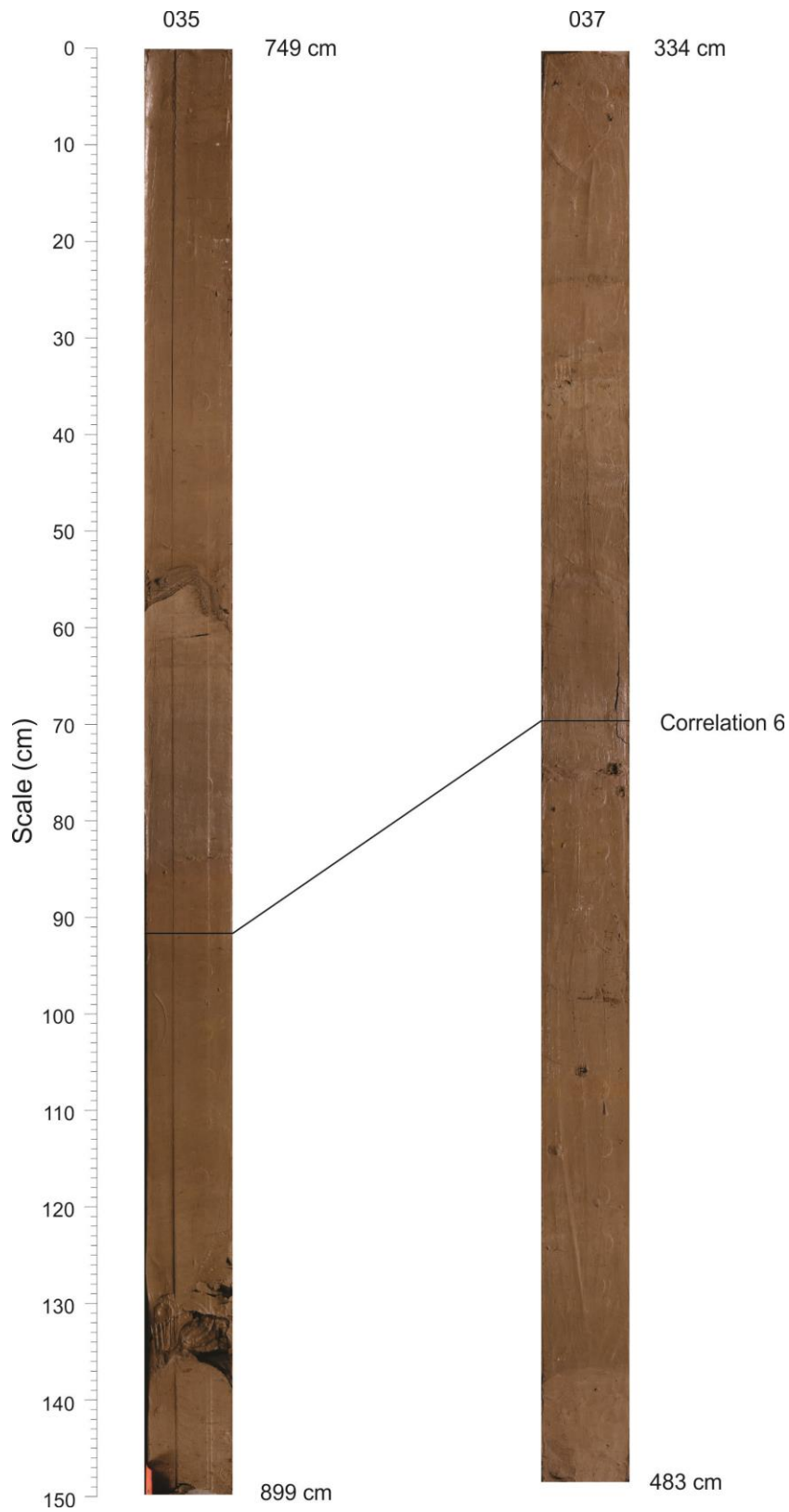
Fig. A-4 – Correlation 6 between piston cores 35 and 37 depicted on core photography

Fig. A-5 – Correlation 8 between piston cores 35 and 37 depicted on core photography
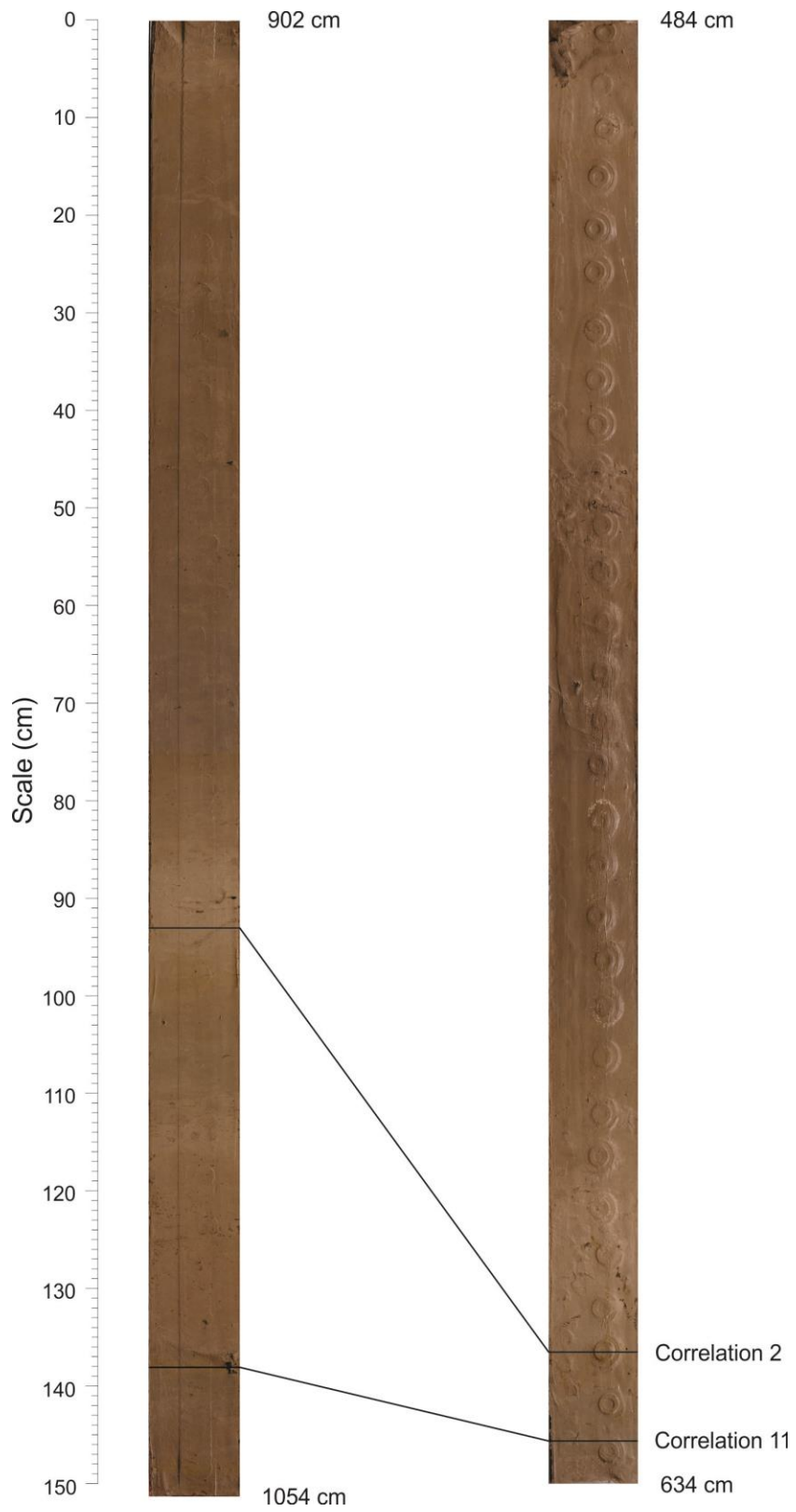
Fig. A-6 – Correlations 2 and 11 between piston cores 35 and 37 depicted on core photography
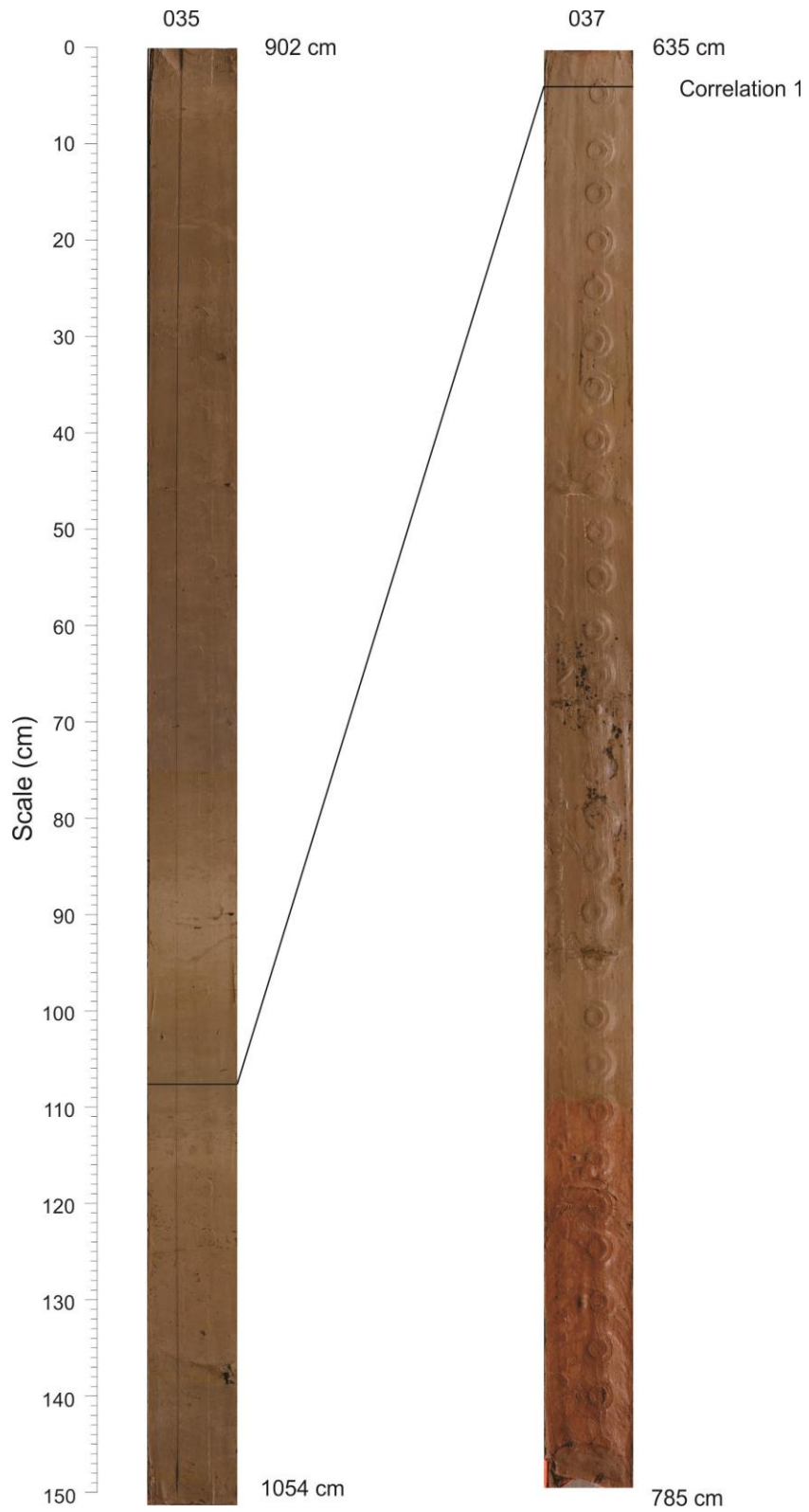
Fig. A-7 – Correlation 1 between piston cores 35 and 37 depicted on core photography
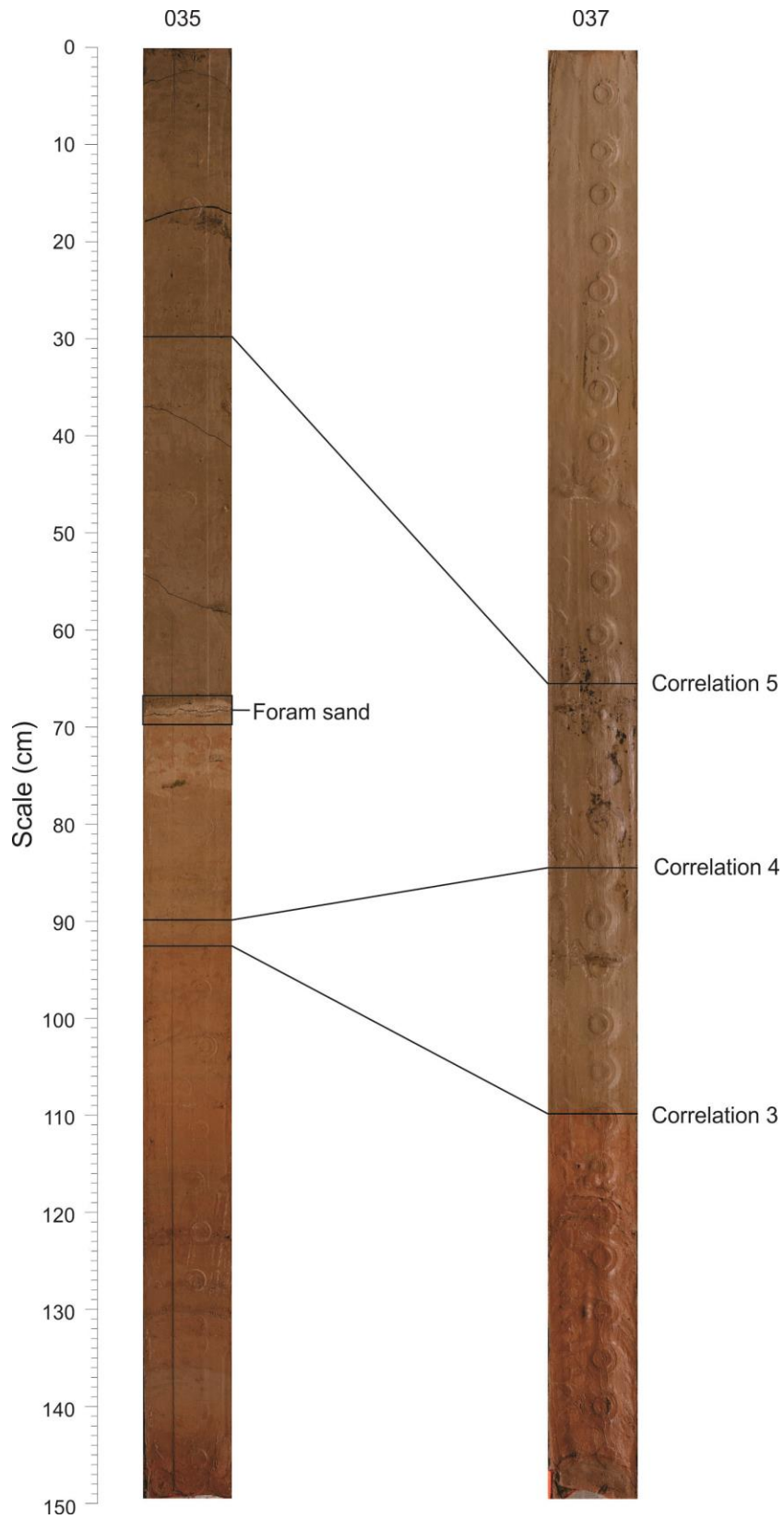
Fig. A-8 – Correlations 3, 4 and 5 between piston cores 35 and 37 depicted on core photography
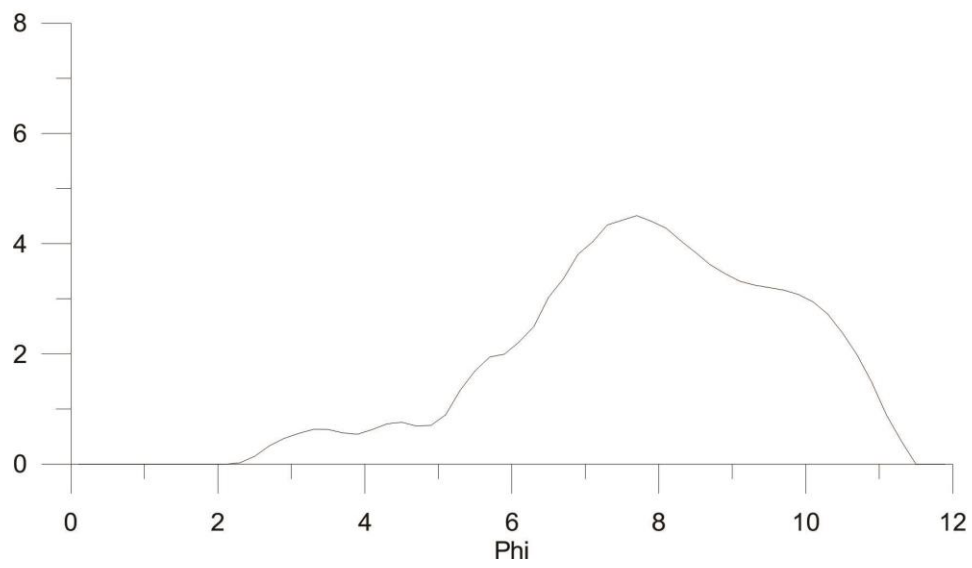
Appendix B

X-Radiographs and grain size analyses
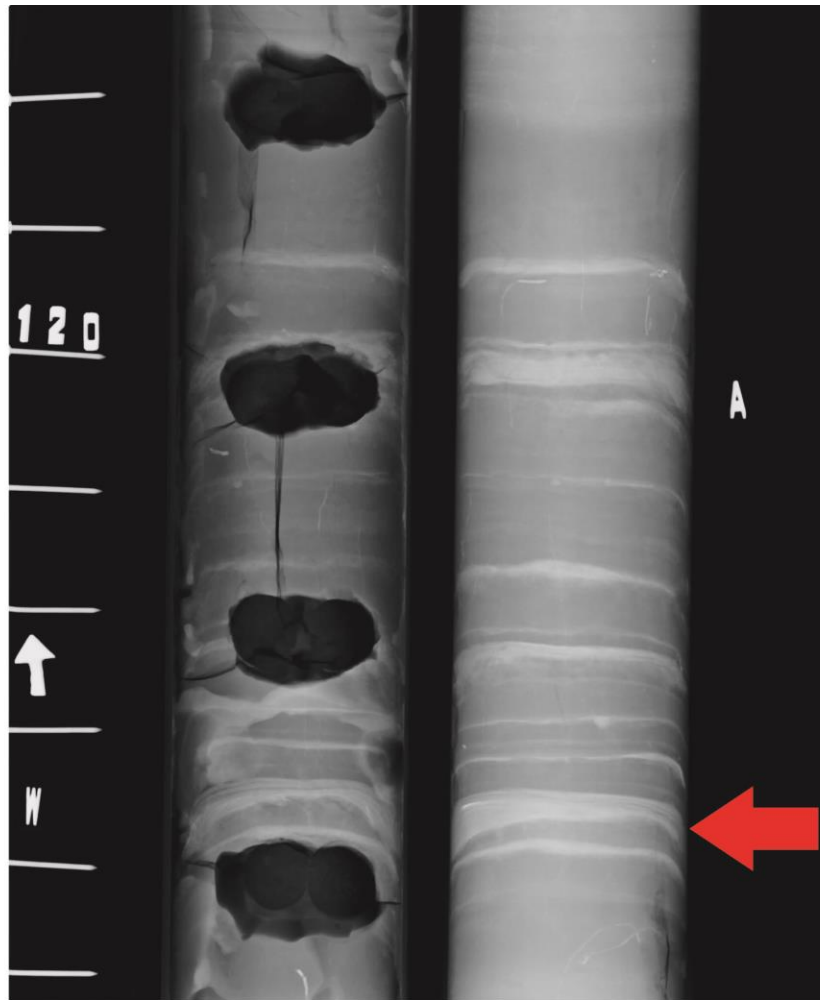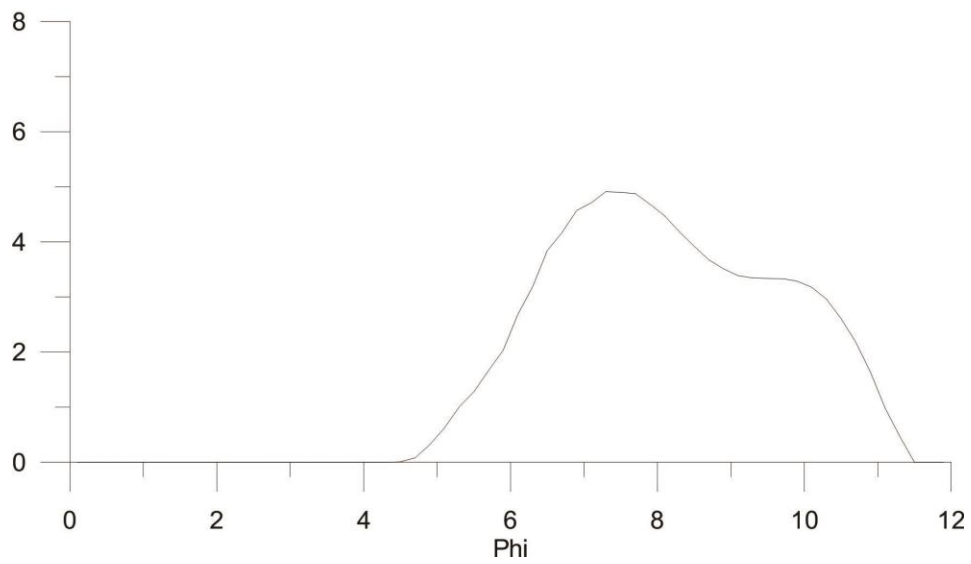
Fig. B-1 - X-Radiograph vs. Grain size at 138 cm in Piston core 37
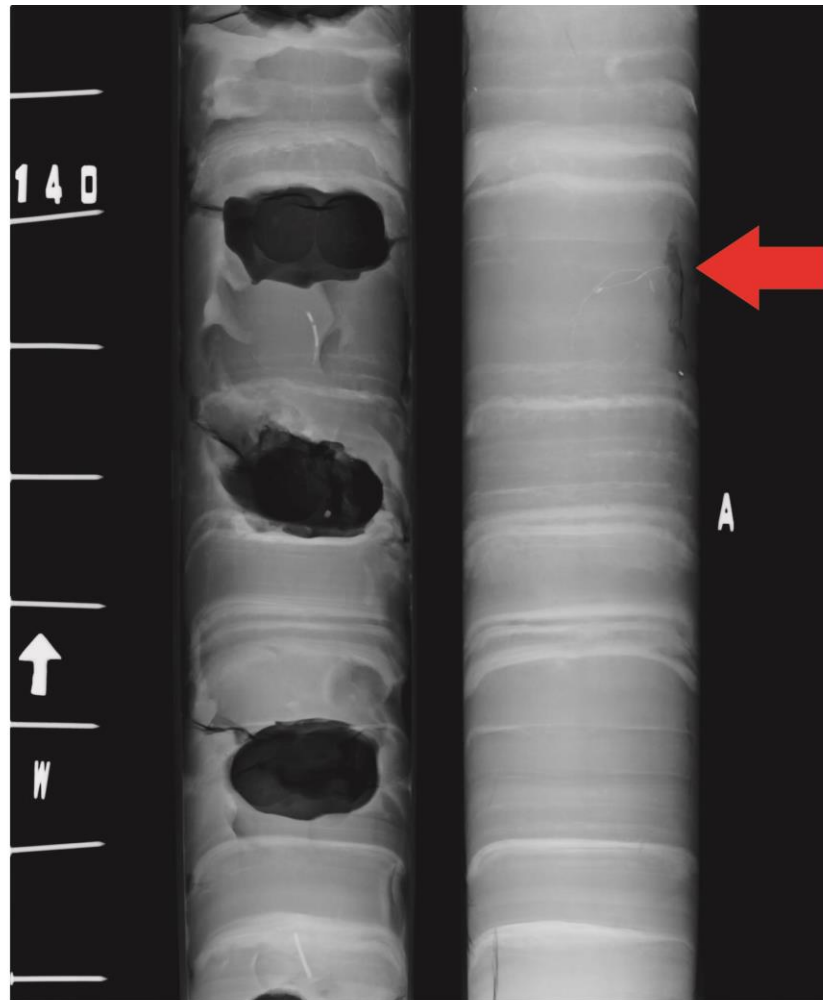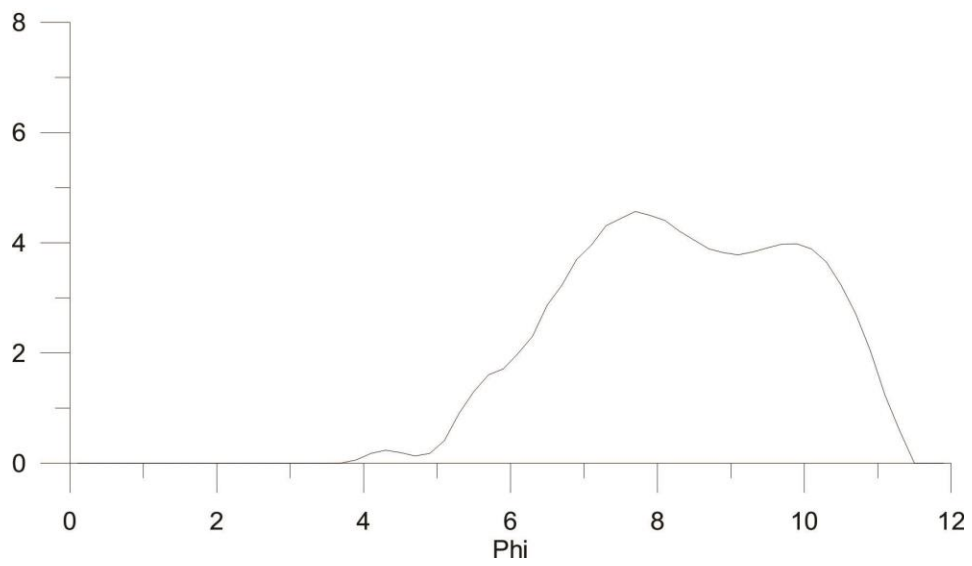
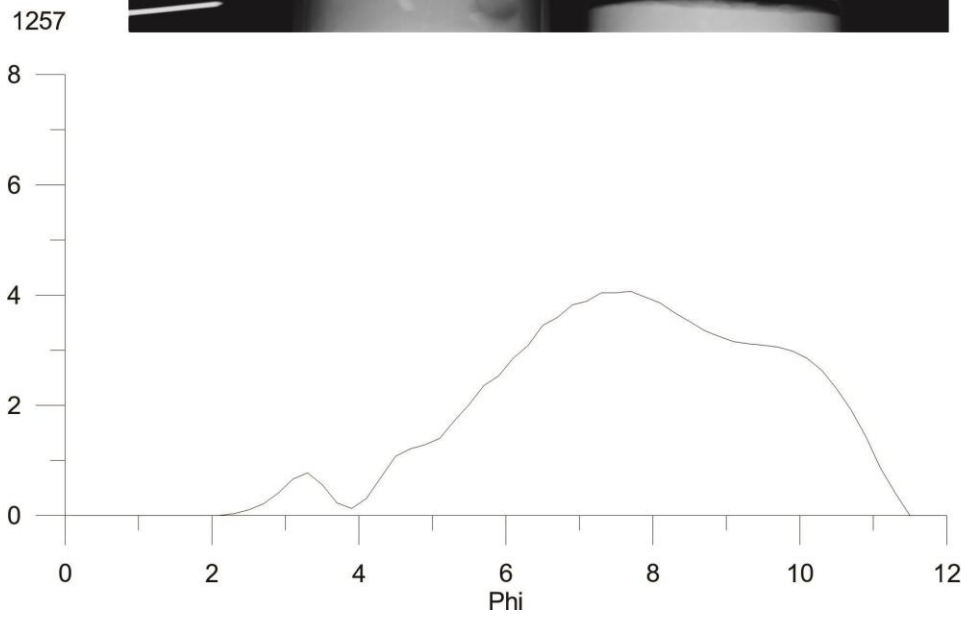Fig. B-2 - X-Radiograph vs. Grain size at 143 cm in Piston core 37
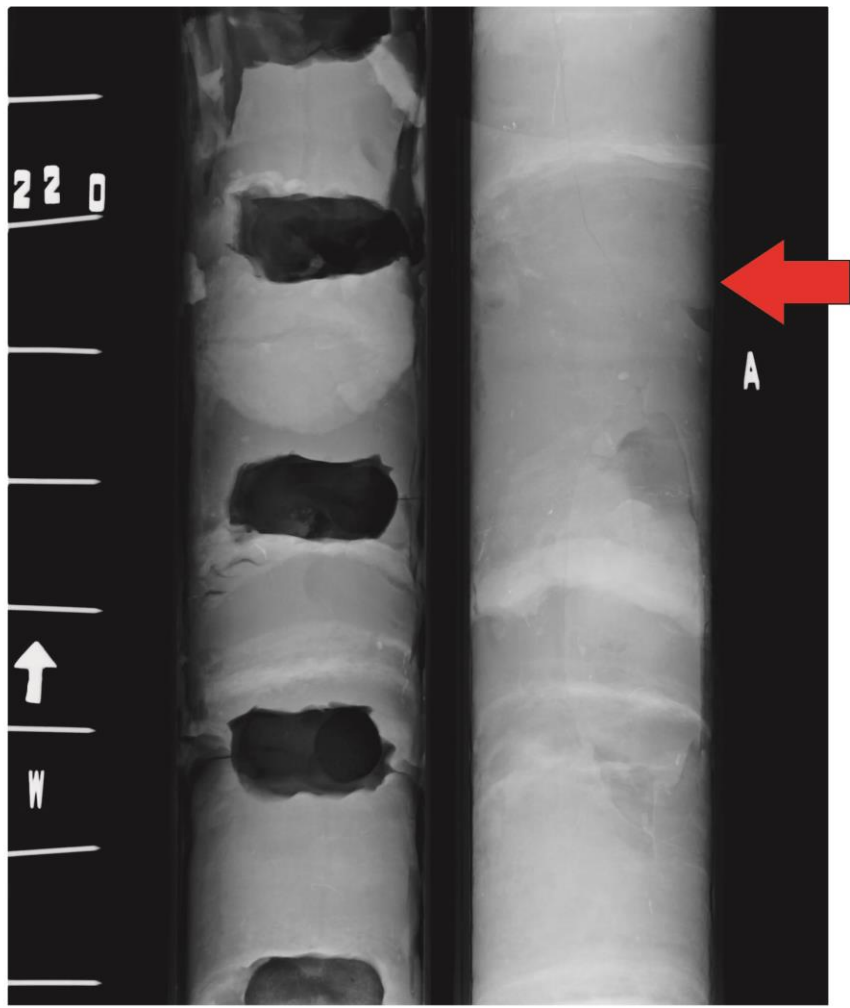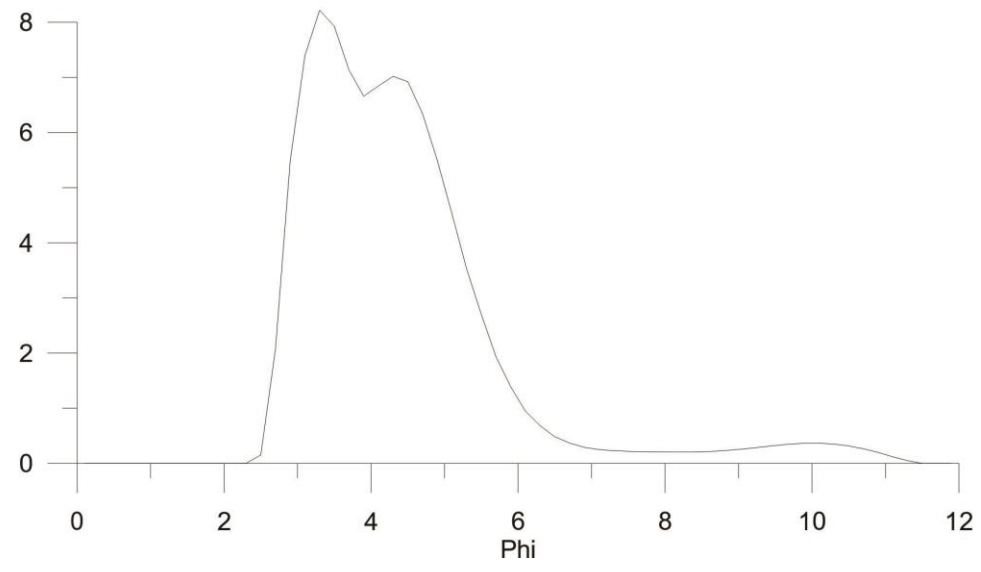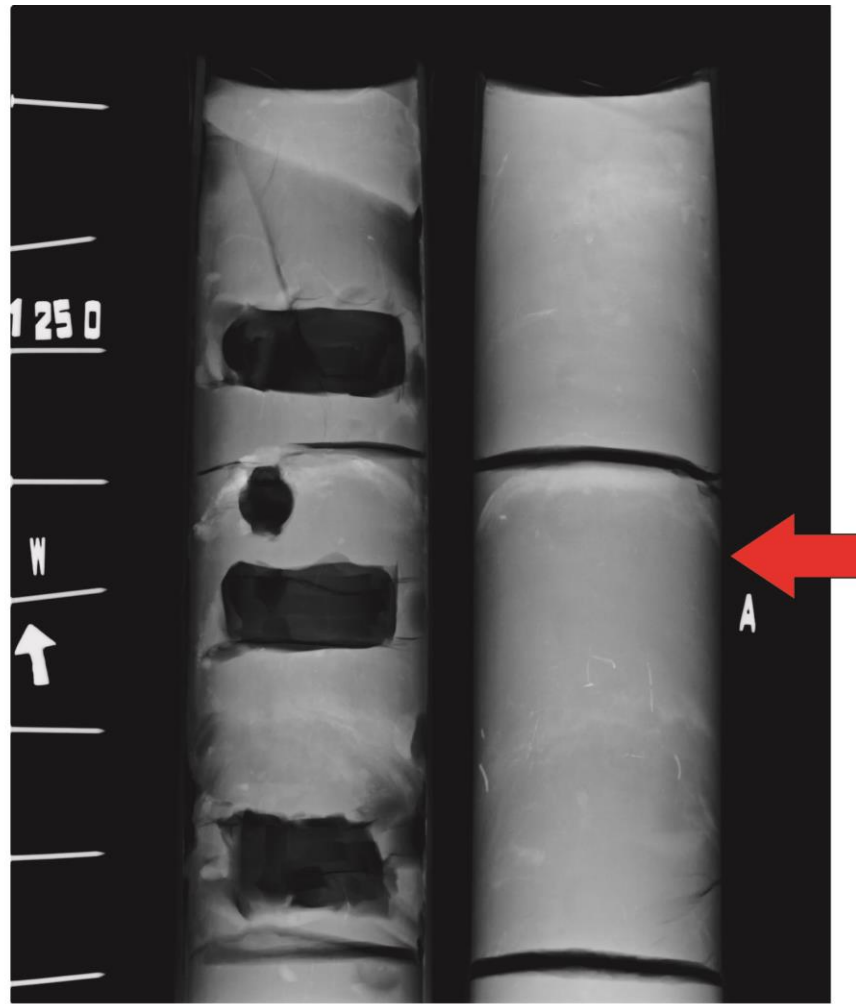
Fig. B-3 - X-Radiograph vs. Grain size at 222 cm in Piston core 37
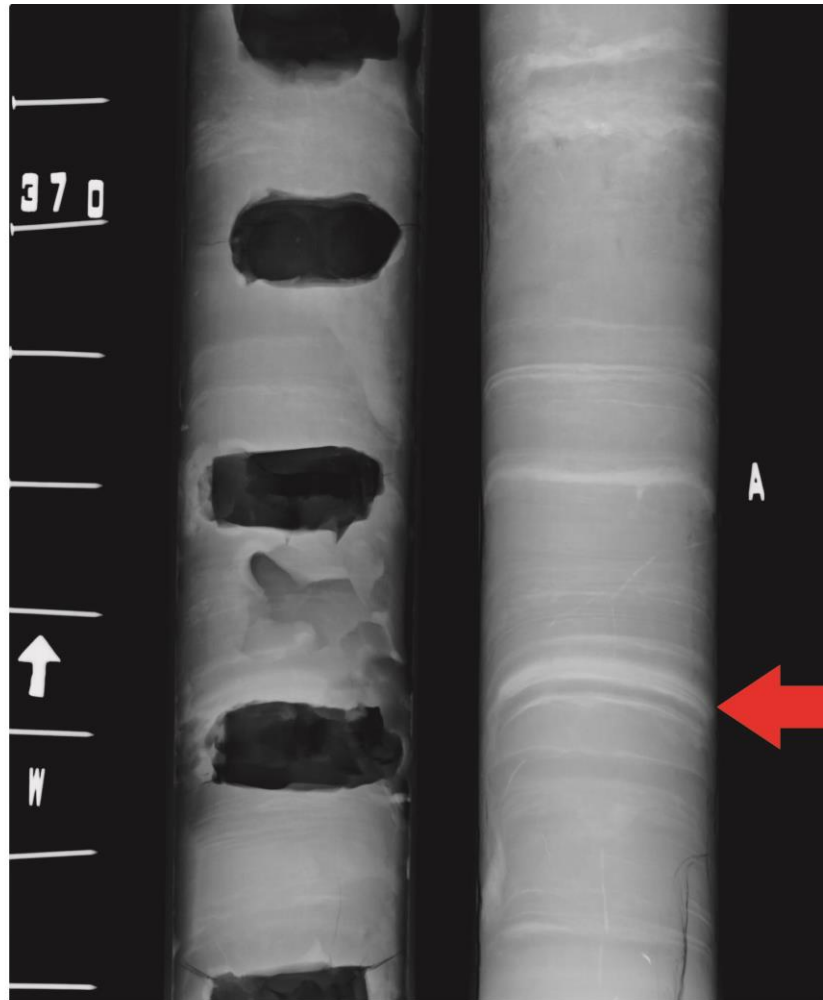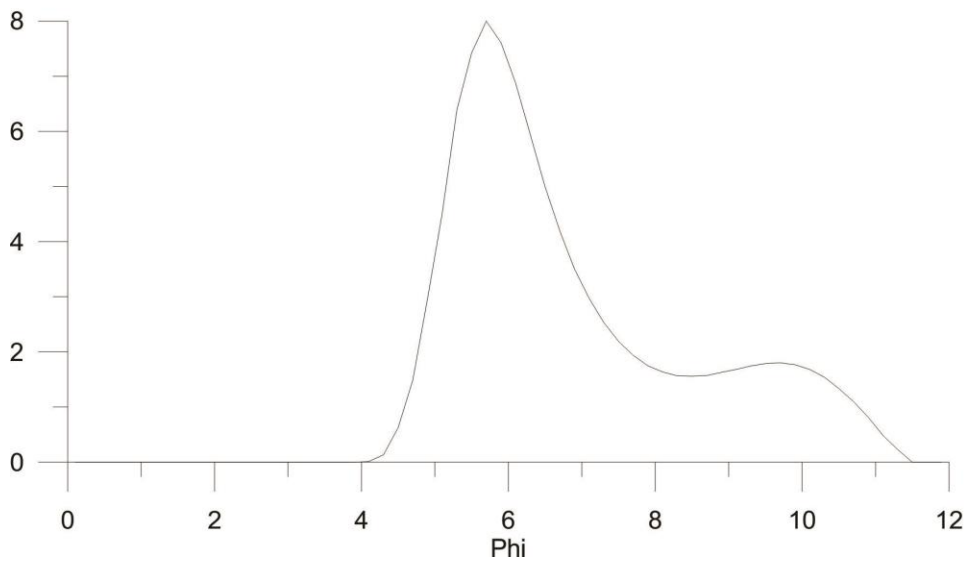
Fig. B-4 - X-Radiograph vs. Grain size at 388 cm in Piston core 37
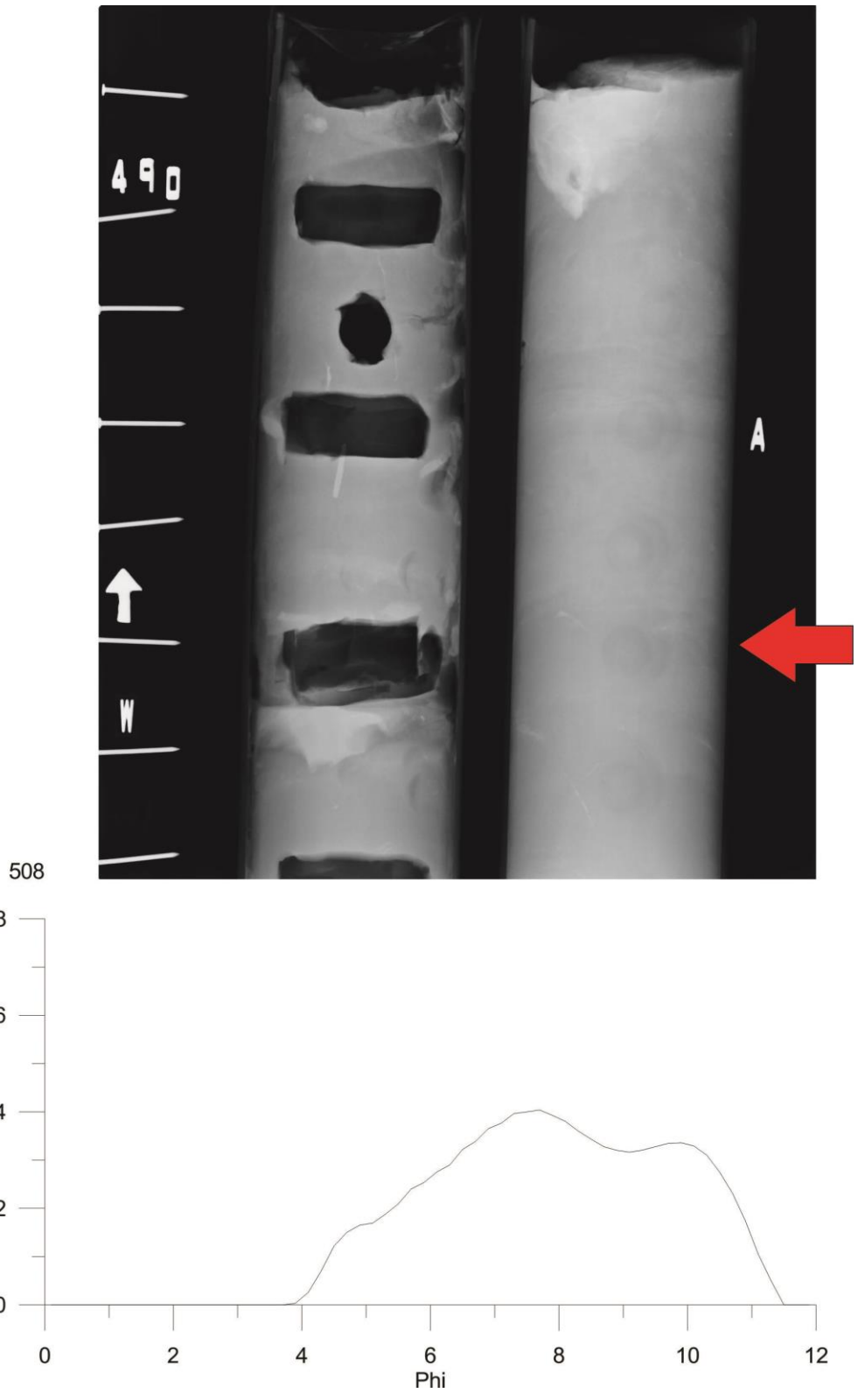
Fig. B-5 - X-Radiograph vs. Grain size at 508 cm in Piston core 37
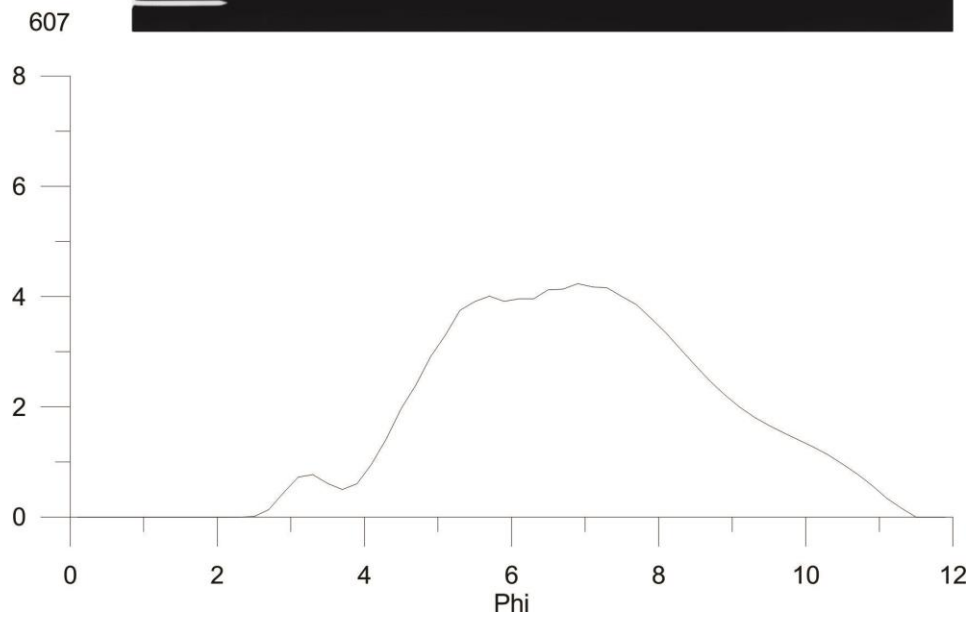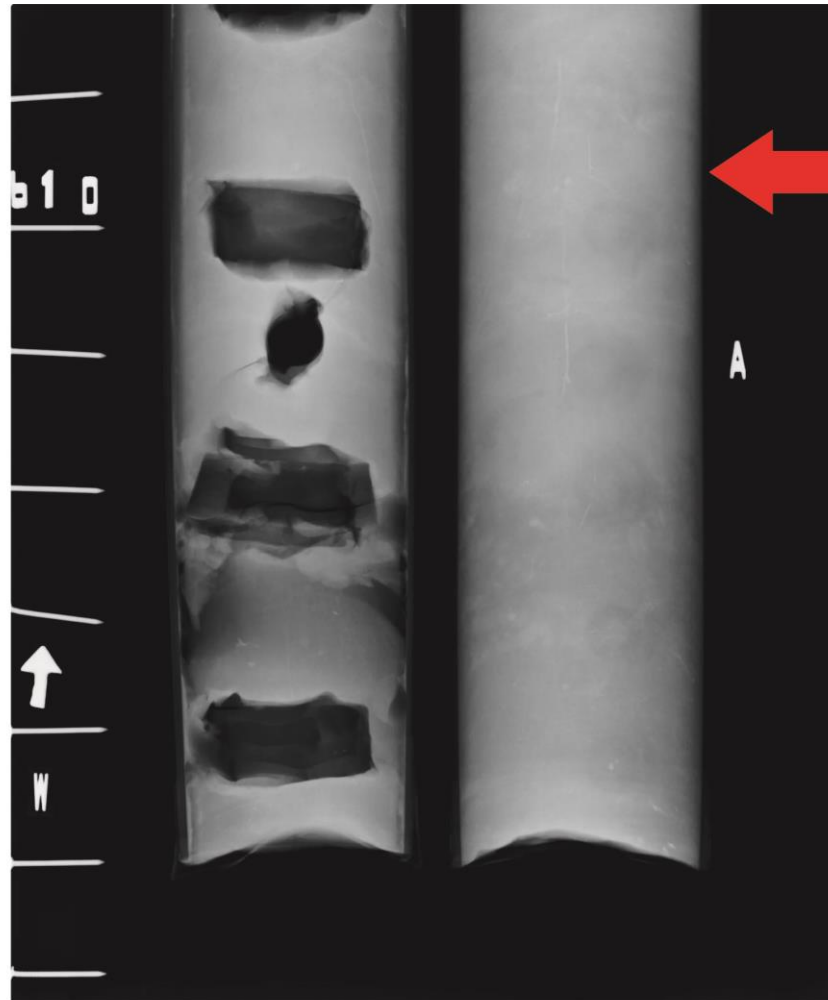
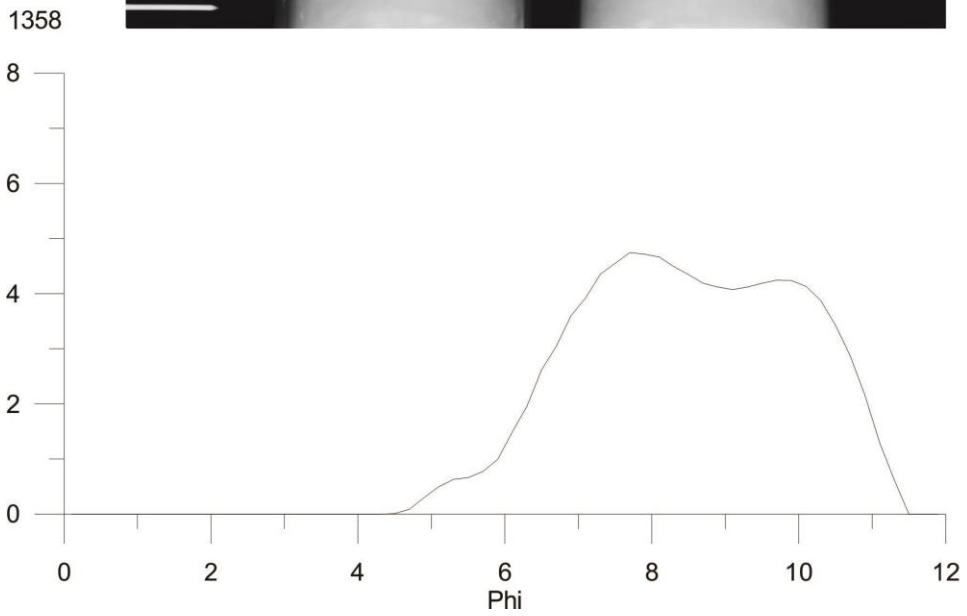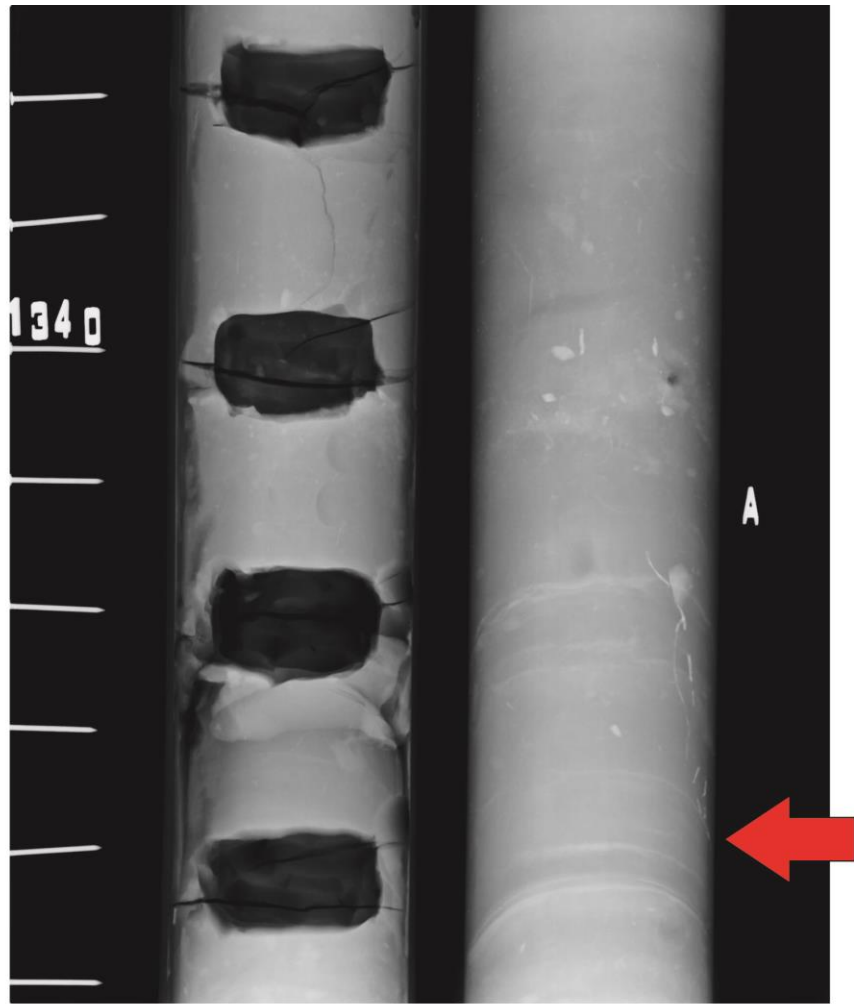Fig. B-6 - X-Radiograph vs. Grain size at 607 cm in Piston core 37
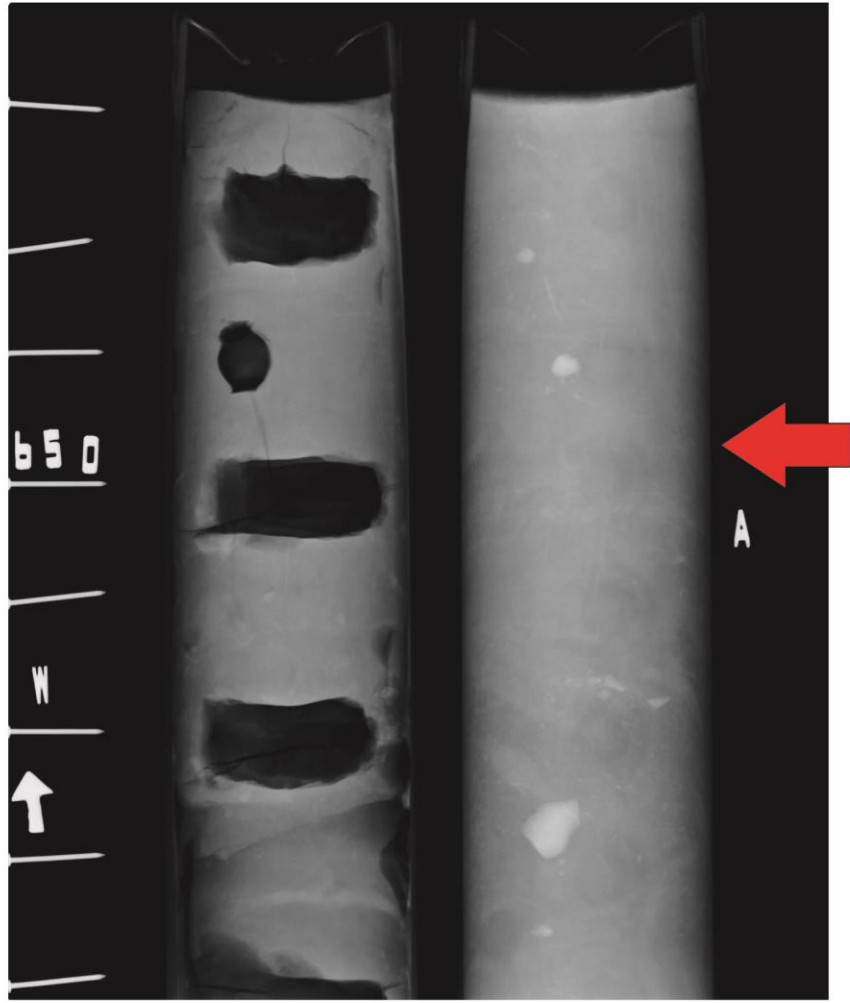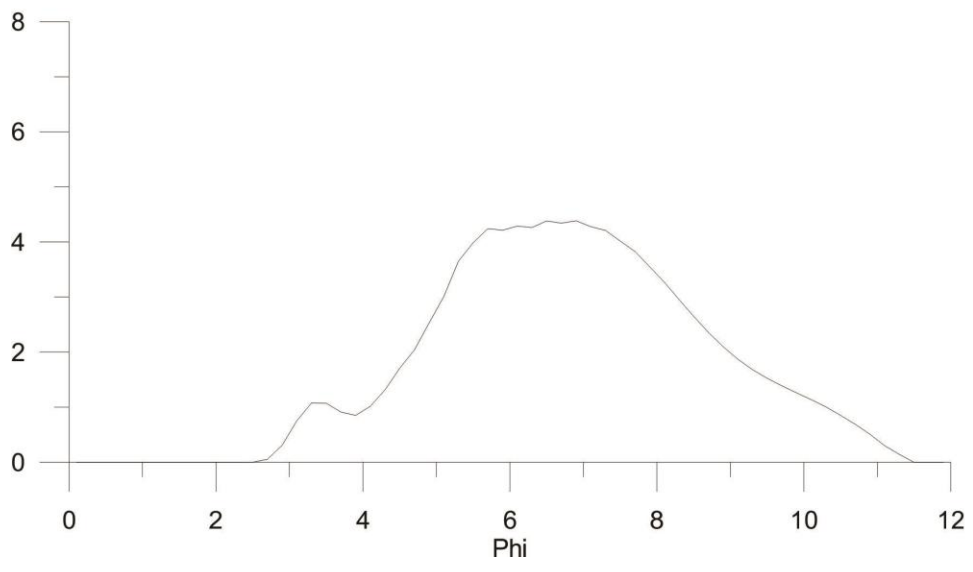
Fig. B-7 - X-Radiograph vs. Grain size at 138 cm in Piston core 37
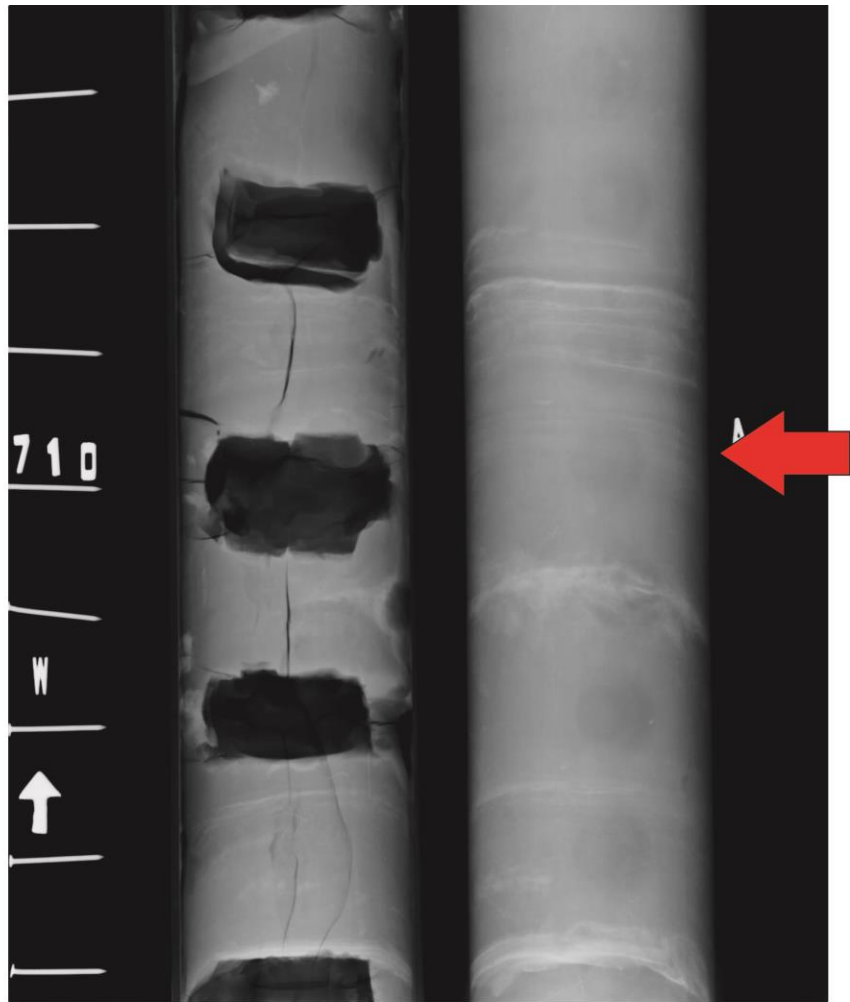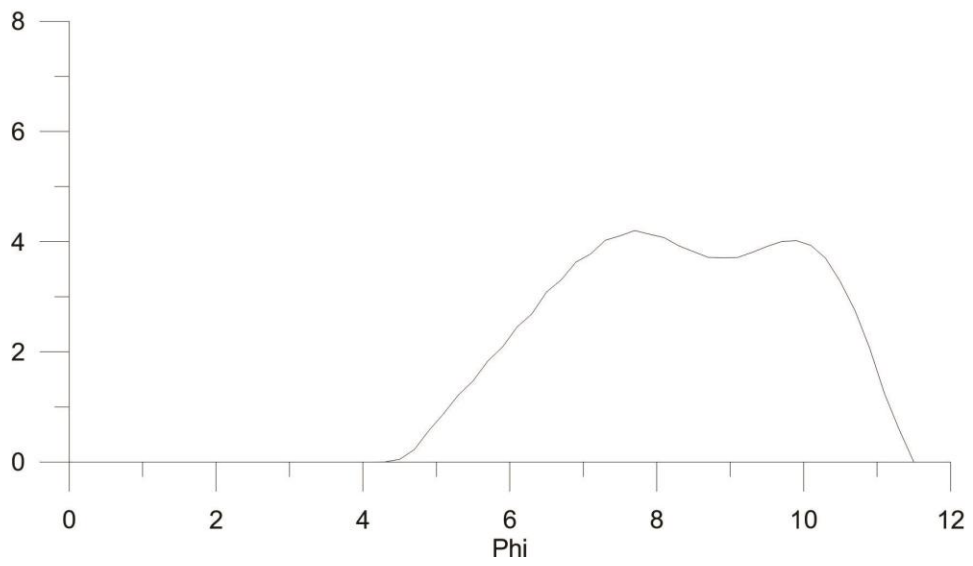
Fig. B-8 - X-Radiograph vs. Grain size at 708 cm in Piston core 37
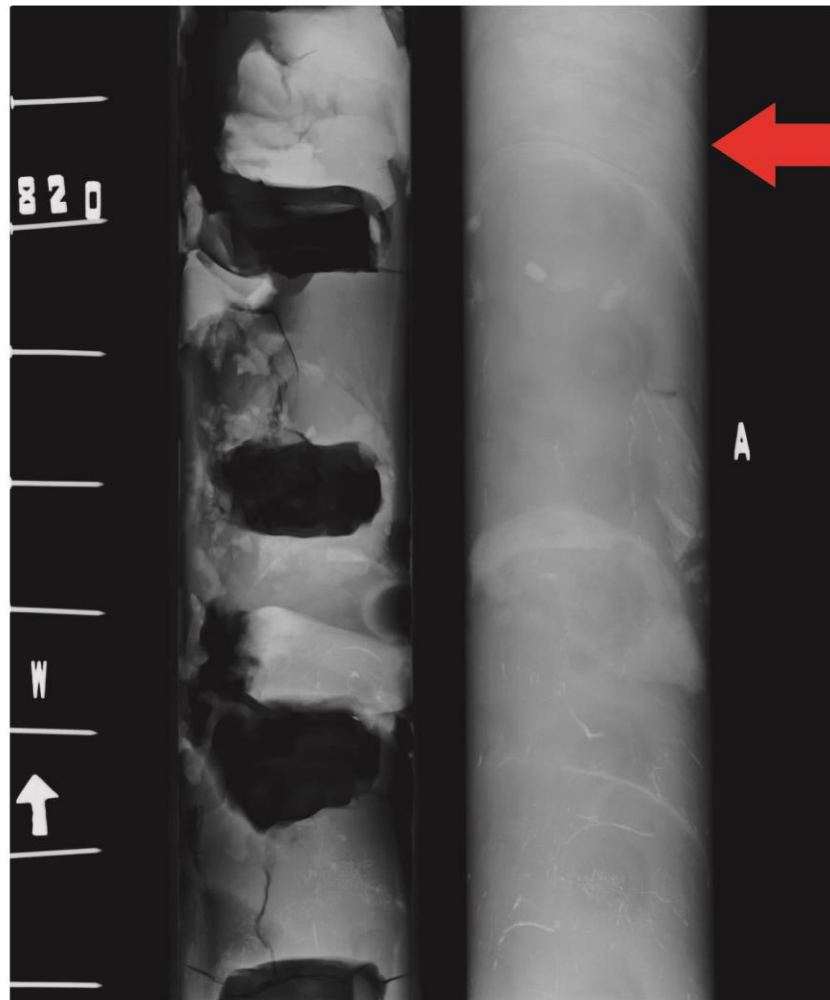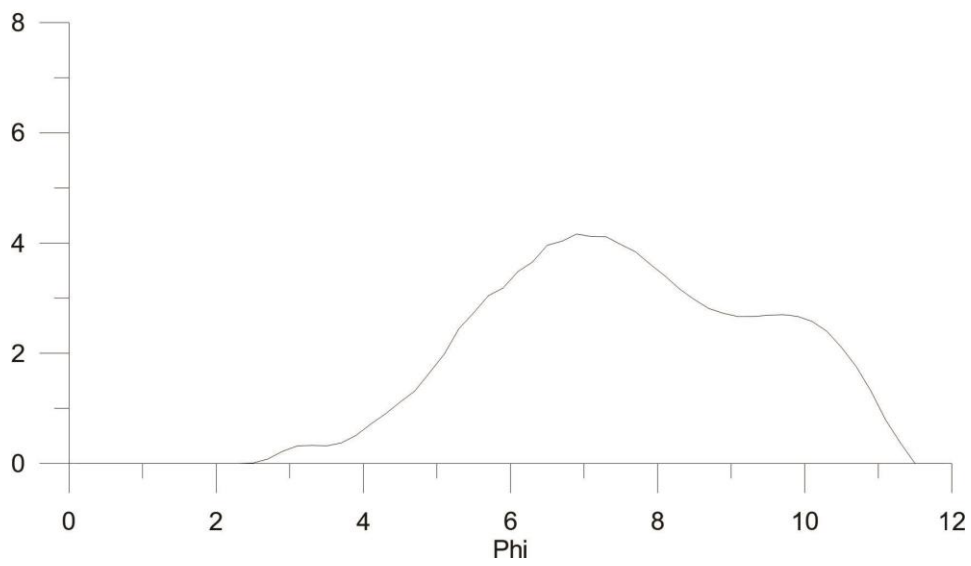
Fig. B-9 - X-Radiograph vs. Grain size at 816 cm in Piston core 37
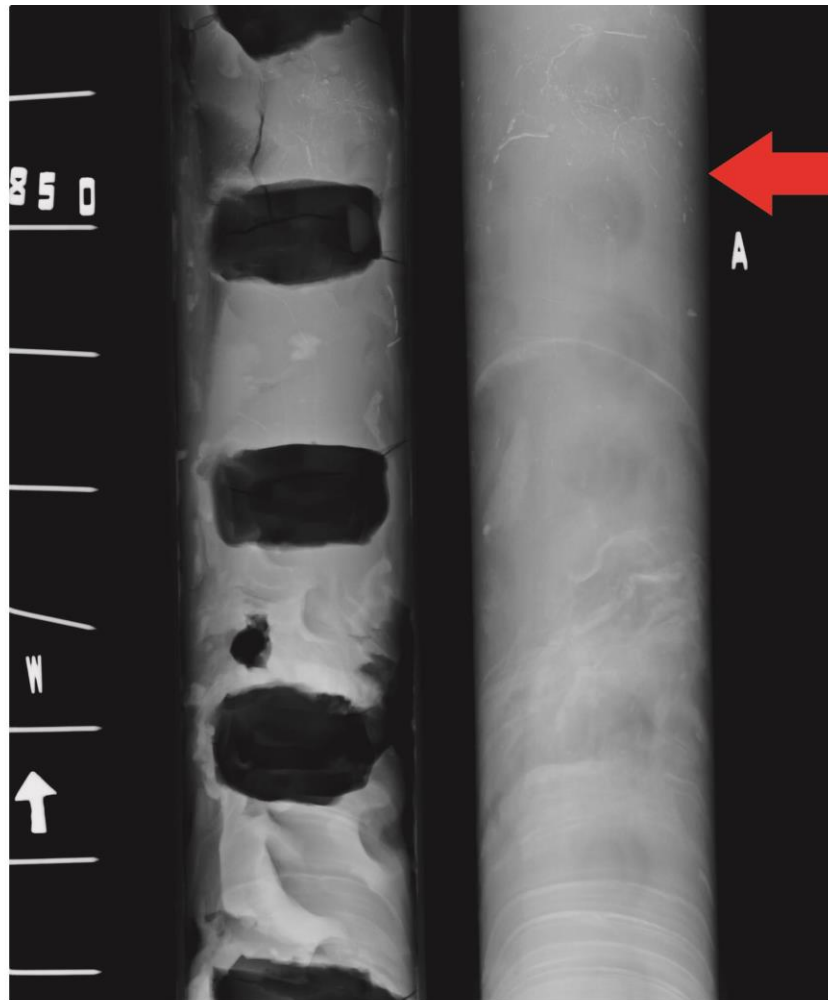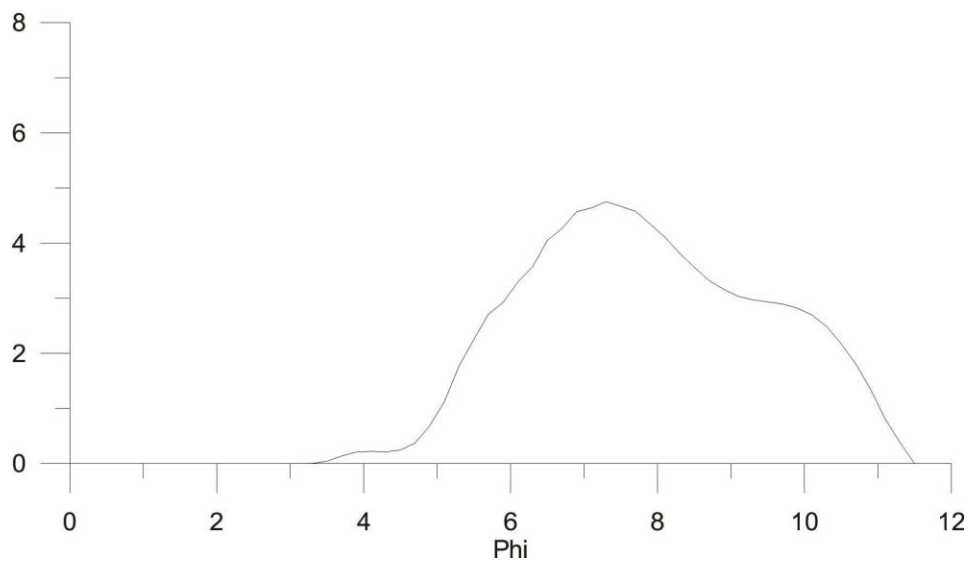
Fig. B-10 - X-Radiograph vs. Grain size at 848 cm in Piston core 37
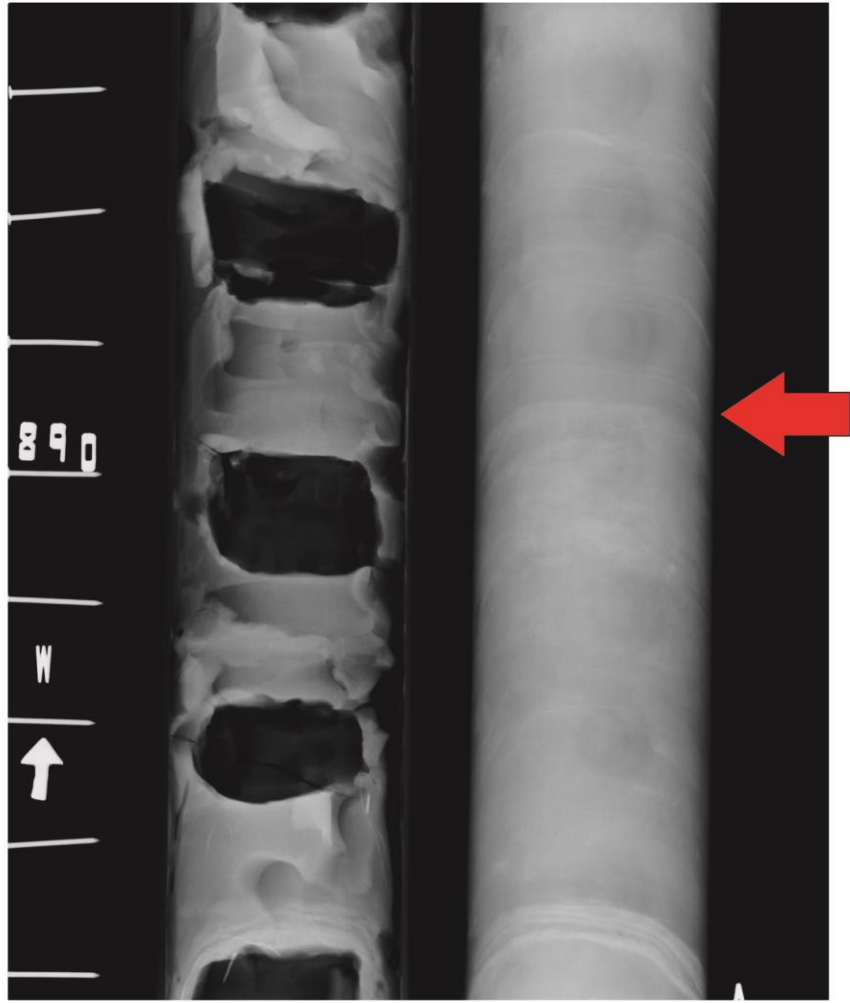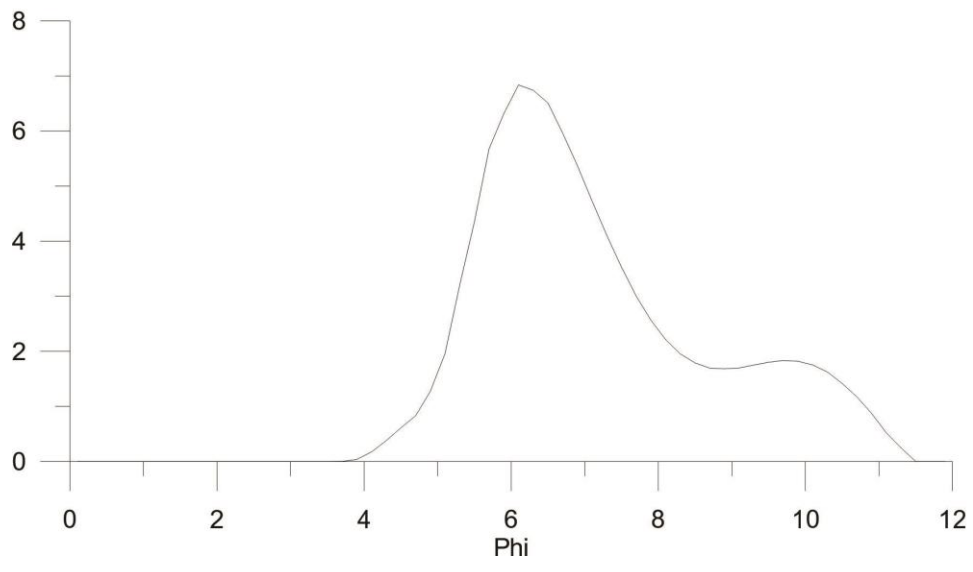
Fig. B-11 - X-Radiograph vs. Grain size at 888 cm in Piston core 37
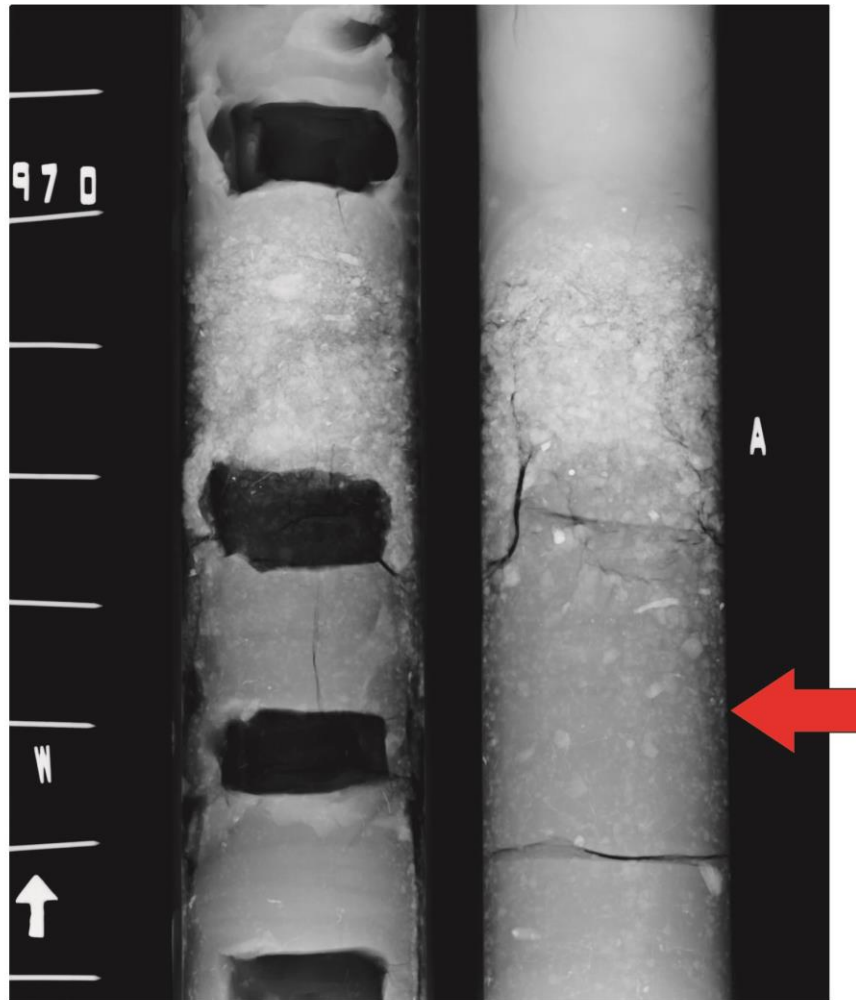
Fig. B-12 - X-Radiograph vs. Grain size at 970 cm in Piston core 37

Fig. B-13 - X-Radiograph vs. Grain size at 1257 cm in Piston core 37

Fig. B-14 - X-Radiograph vs. Grain size at 1358 cm in Piston core 37

Fig. B-15 – X-radiograph at 30 cm showing bioturbated interval as described in text

Fig. B-16 – X-radiograph showing iron monosulphides as described in text

Appendix C

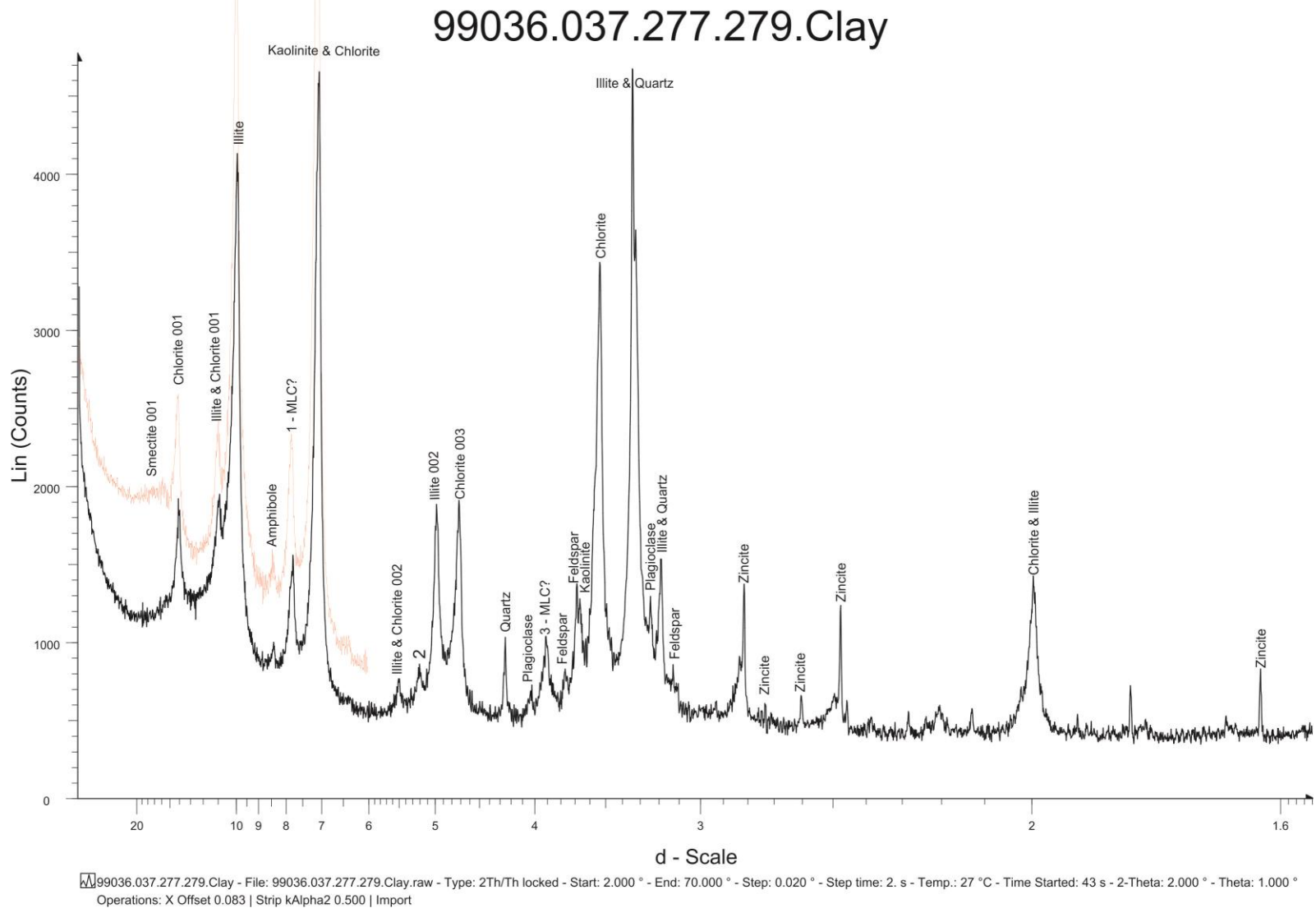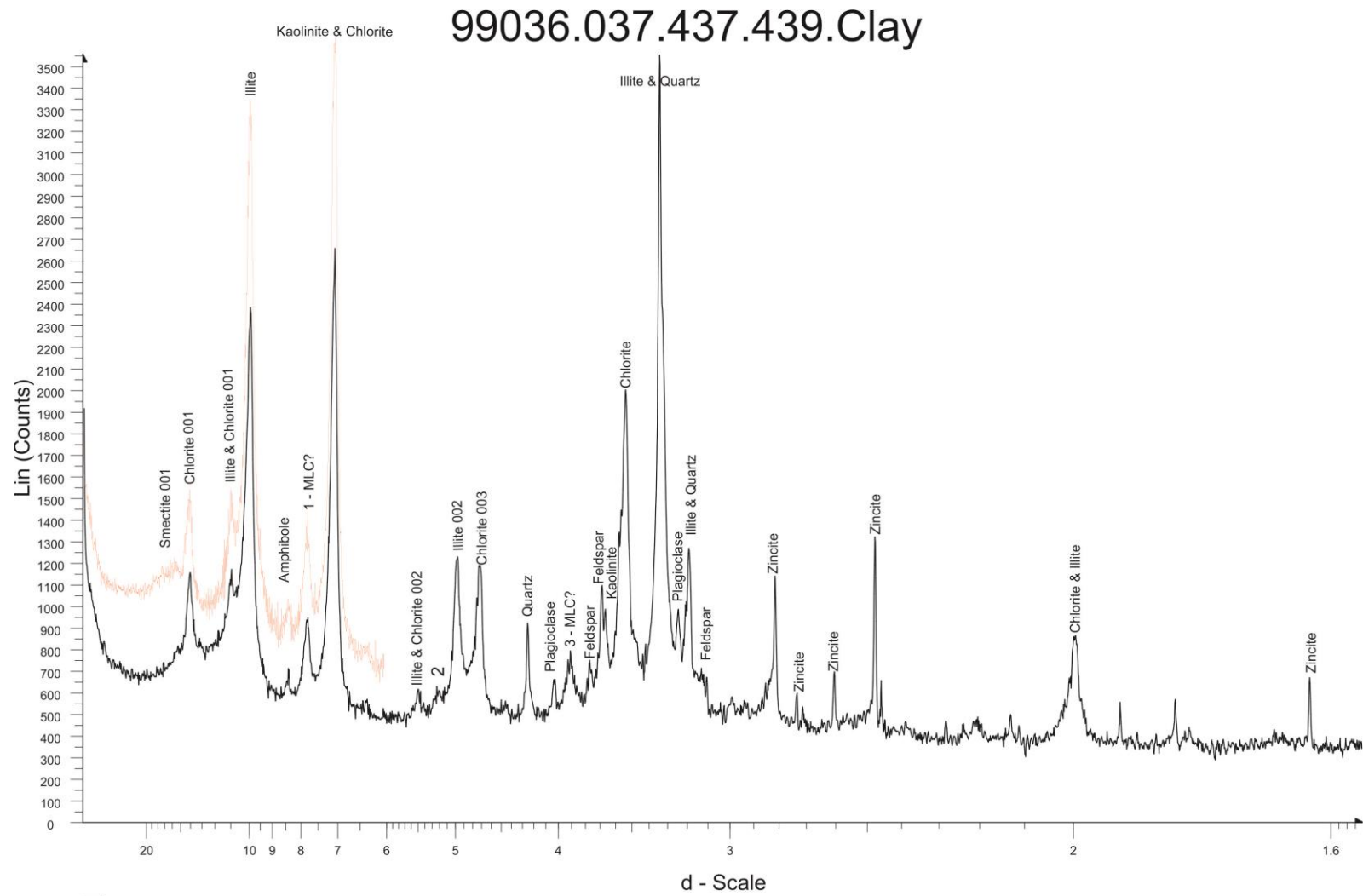X-ray diffractograms of < 2 μm fraction
(Others shown in Fig 4 A - D)

Fig. C-1 - Diffractogram of air dried (black) and glycolated (red) clay at 277 - 279 cm (Type I clay assemblage)

Fig. C -2 - Diffractogram of air dried (black) and glycolated (red) clay at 437 - 439 cm (Type I clay assemblage)

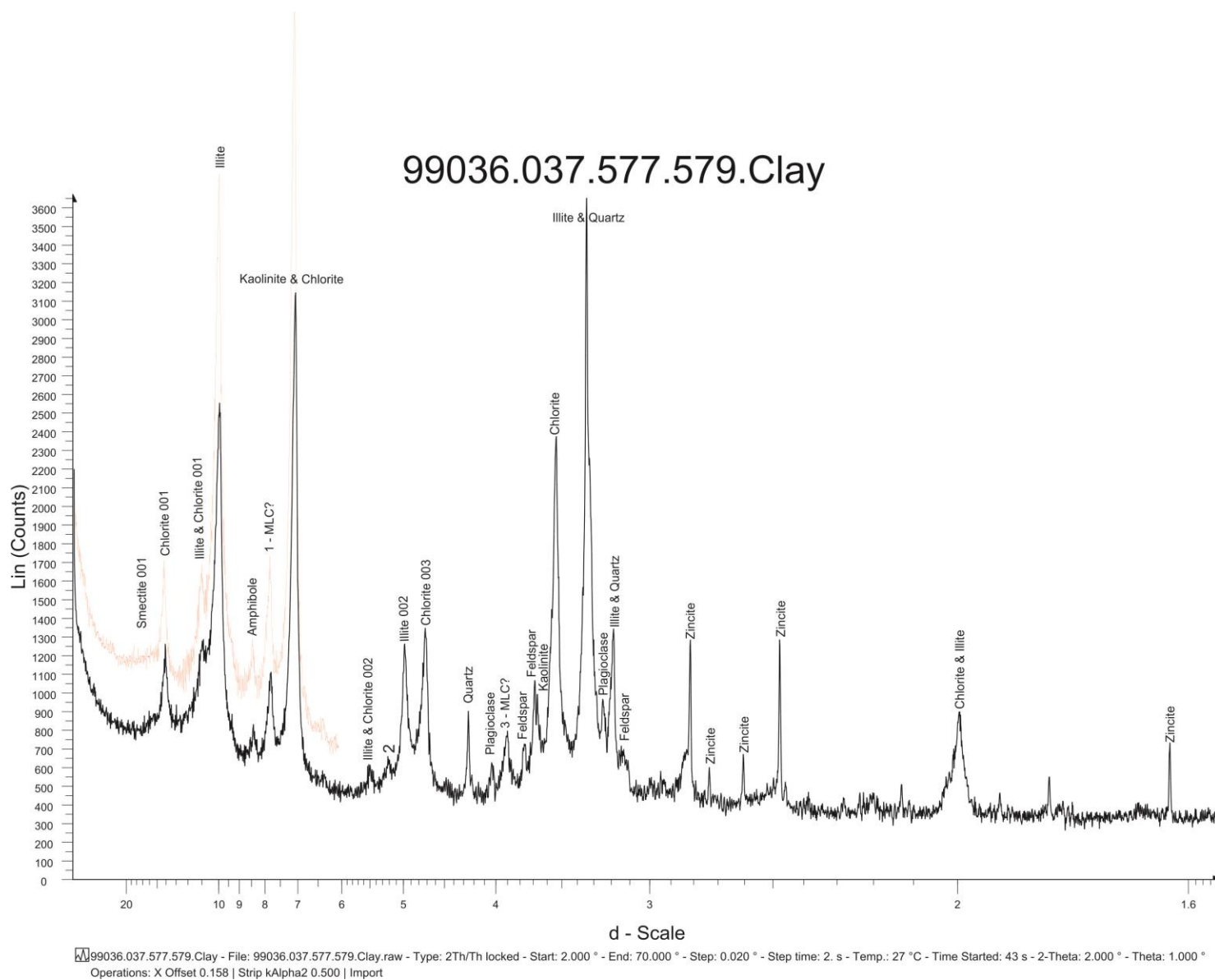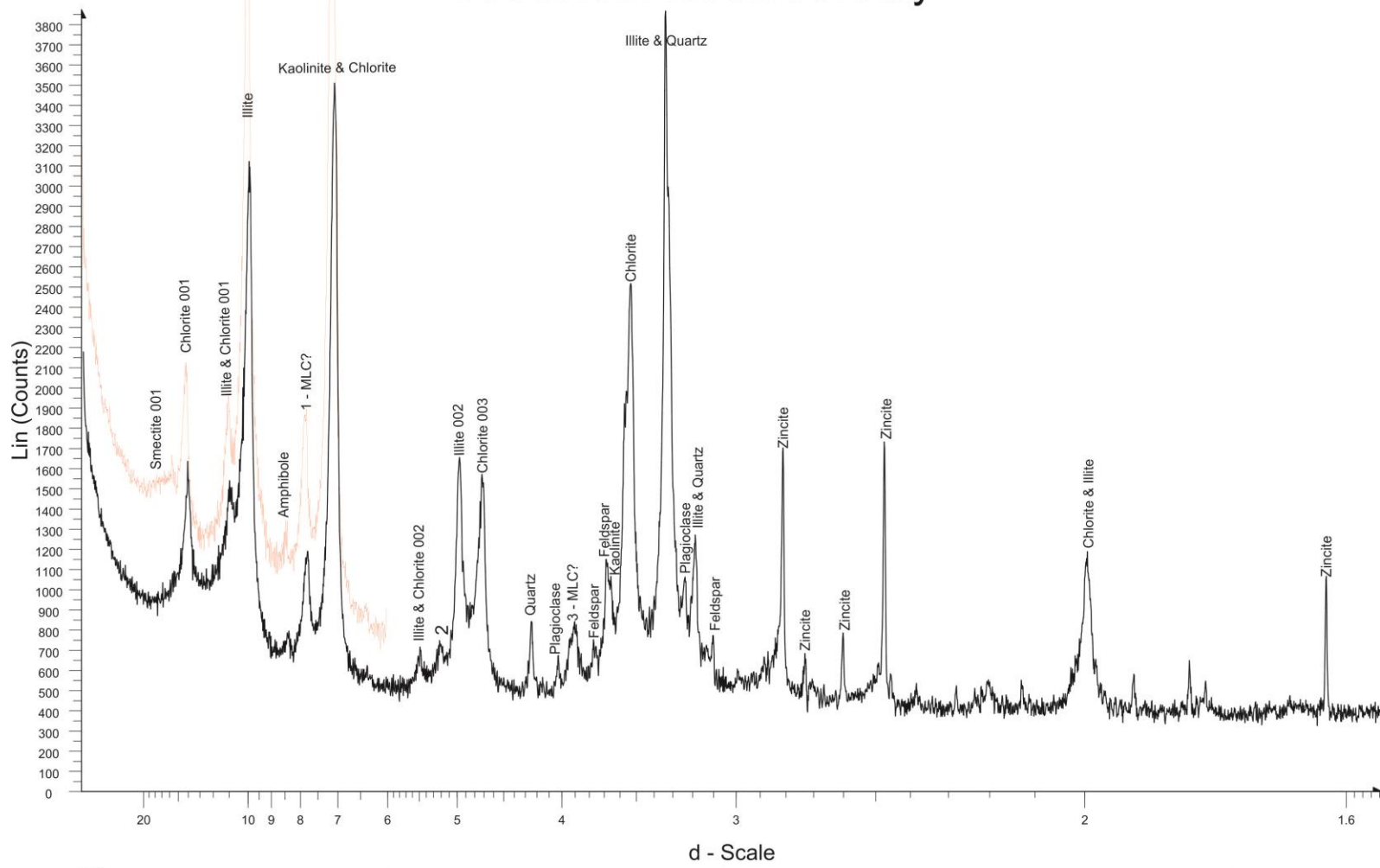Fig. C -3 - Diffractogram of air dried (black) and glycolated (red) clay at 577 - 579 cm (Type I clay assemblage)

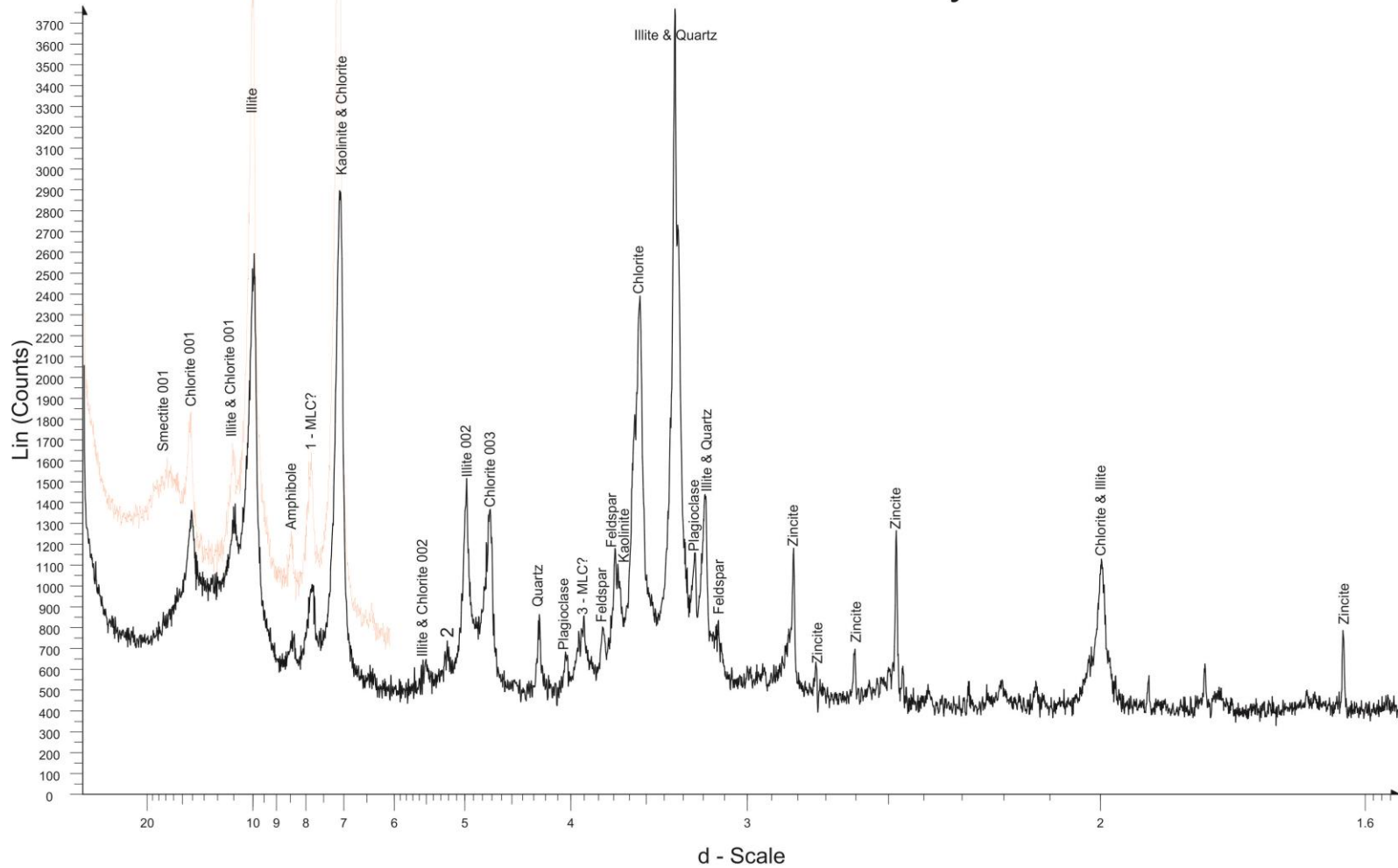Fig. C -4 - Diffractogram of air dried (black) and glycolated (red) clay at 903 - 905cm (Type IV clay assemblage)

Fig. C -5 - Diffractogram of air dried (black) and glycolated (red) clay at 604 - 608 cm (Type IV clay assemblage

Permissions

ELSEVIER LICENSE
TERMS AND CONDITIONS

Mar 30, 2016

This is an Agreement between Jeremy Bentley ("You") and Elsevier ("Elsevier"). It consists of your order details, the terms and conditions provided by Elsevier, and the payment terms and conditions.

All payments must be made in full to CCC. For payment instructions, please see information listed at the bottom of this form.

Supplier	Elsevier Limited The Boulevard,Langford Lane Kidlington,Oxford,OX5 1GB,UK
Registered Company Number	1982084
Customer name	Jeremy Bentley
Customer address	42 Tamarack Drive Halifax, NS B3N3G4
License number	3830220679975
License date	Mar 15, 2016
Licensed content publisher	Elsevier
Licensed content publication	Earth and Planetary Science Letters
Licensed content title	Provenance of Late Quaternary ice-proximal sediments in the North Atlantic: Nd, Sr and Pb isotopic evidence
Licensed content author	G.Lang Farmer,Donald Barber,John Andrews
Licensed content date	15 April 2003
Licensed content volume number	209
Licensed content issue number	1-2
Number of pages	17
Start Page	227
End Page	243
Type of Use	reuse in a thesis/dissertation
Intended publisher of new work	other
Portion	figures/tables/illustrations
Number of figures/tables/illustrations	1
Format	both print and electronic
Are you the author of this Elsevier article?	No
Will you be translating?	No
Original figure numbers	Fig. 6
Title of your thesis/dissertation	The role of downslope versus alongslope sediment transport over the last glacial cycle on the Scotian Rise
Expected completion date	Mar 2016

104

ELSEVIER LICENSE
TERMS AND CONDITIONS

Mar 30, 2016

This is an Agreement between Jeremy Bentley ("You") and Elsevier ("Elsevier"). It consists of your order details, the terms and conditions provided by Elsevier, and the payment terms and conditions.

All payments must be made in full to CCC. For payment instructions, please see information listed at the bottom of this form.

Supplier	Elsevier Limited
	The Boulevard,Langford Lane
	Kidlington,Oxford,OX5 1GB,UK
Registered Company Number	1982084
Customer name	Jeremy Bentley
Customer address	42 Tamarack Drive
	Halifax, NS B3N3G4
License number	3830220382214
License date	Mar 15, 2016
Licensed content publisher	Elsevier
Licensed content publication	Earth and Planetary Science Letters
Licensed content title	A 750-kyr detrital-layer stratigraphy for the North Atlantic (IODP Sites U1302–U1303, Orphan Knoll, Labrador Sea)
Licensed content author	J.E.T. Channell,D.A. Hodell,O. Romero,C. Hillaire-Marcel,A. de Vernal,J.S. Stoner,A. Mazaud,U. Röhl
Licensed content date	1 February 2012
Licensed content volume number	317
Licensed content issue number	n/a
Number of pages	13
Start Page	218
End Page	230
Type of Use	reuse in a thesis/dissertation
Portion	figures/tables/illustrations
Number of figures/tables/illustrations	1
Format	both print and electronic
Are you the author of this Elsevier article?	No
Will you be translating?	No
Original figure numbers	Fig. 5.
Title of your thesis/dissertation	The role of downslope versus alongslope sediment transport over the last glacial cycle on the Scotian Rise
Expected completion date	Mar 2016
Estimated size (number	113

105

Geological Society of America LICENSE
TERMS AND CONDITIONS

Mar 17, 2016

This is a License Agreement between Jeremy Bentley ("You") and Geological Society of America ("Geological Society of America") provided by Copyright Clearance Center ("CCC"). The license consists of your order details, the terms and conditions provided by Geological Society of America, and the payment terms and conditions.

All payments must be made in full to CCC. For payment instructions, please see information listed at the bottom of this form.

License Number	3831321133044
License date	Mar 15, 2016
Licensed content publisher	Geological Society of America
Licensed content title	Geological Society of America bulletin
Licensed content date	Jan 1, 1888
Type of Use	Thesis/Dissertation
Requestor type	Academic institution
Format	Print, Electronic
Portion	chart/graph/table/figure
Number of charts/graphs/tables/figures	1
Title or numeric reference of the portion(s)	Figure 7 (images 1,2,3 and 6 in figure 7)
Title of the article or chapter the portion is from	N/A
Editor of portion(s)	N/A
Author of portion(s)	N/A
Volume of serial or monograph.	N/A
Page range of the portion	831
Publication date of portion	1998
Rights for	Main product
Duration of use	Life of current edition
Creation of copies for the disabled	no
With minor editing privileges	yes
For distribution to	Worldwide
In the following language(s)	Original language of publication
With incidental promotional use	no

106